



**WORKSPACE EVALUATION  
AND KINEMATIC CALIBRATION  
OF STEWART PLATFORM**

by  
Jian Wang

A Dissertation Submitted to the Faculty of the  
College of Engineering  
in Partial Fulfillment of the Requirements for the Degree of  
Doctor of Philosophy in Engineering

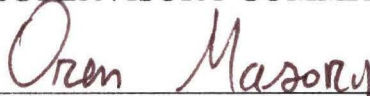
Florida Atlantic University  
Boca Raton, Florida  
December 1992

# WORKSPACE EVALUATION AND KINEMATIC CALIBRATION OF STEWART PLATFORM

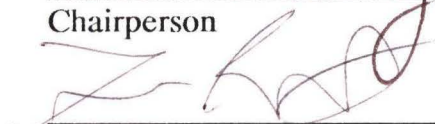
by  
Jian Wang

This dissertation was prepared under the direction of the candidate's dissertation advisor Dr. Oren Masory, Department of Mechanical Engineering, and co-advisor Dr. Zvi Roth, Department of Electrical Engineering. It was submitted to the faculty of the College of Engineering and was accepted in partial fulfillment of the requirements for the degree of Doctor of Philosophy in Engineering.

## SUPERVISORY COMMITTEE:

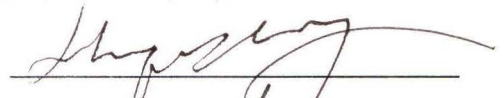
  
\_\_\_\_\_

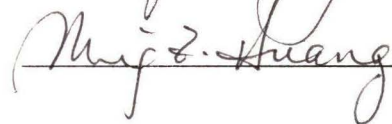
Chairperson

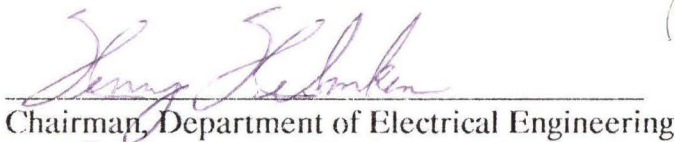
  
\_\_\_\_\_

Dissertation Co-Advisor

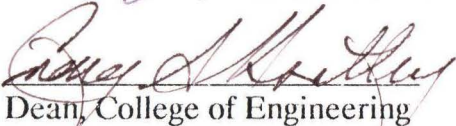
  
\_\_\_\_\_

  
\_\_\_\_\_

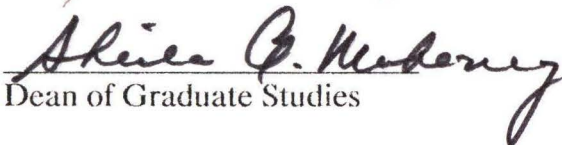
  
\_\_\_\_\_

  
\_\_\_\_\_

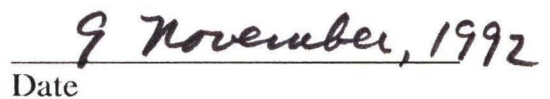
Chairman, Department of Electrical Engineering

  
\_\_\_\_\_

Dean, College of Engineering

  
\_\_\_\_\_

Dean of Graduate Studies

  
\_\_\_\_\_

Date

## ACKNOWLEDGEMENTS

The research reported in this dissertation was supported by the Robotics Center at Florida Atlantic University.

The author would like to express his sincere gratitude to his advisor, Dr. Oren Masory and co-advisor, Dr. Zvi Roth for their excellent guidance and detailed helps toward the preparation of this dissertation. The gratitudes extended to Dr. Hanqi Zhuang and Dr. Ming Huang for their valuable instructions and support. He also wishes to thank Dr. Daniel Raviv for serving on the dissertation committee and providing valuable comments.

Special thanks to Mr. Roy Smollett in the Robotics Center for his great help and support. Helpful discussions with Mr. Kuanchih Wang are gratefully acknowledged.

The author will never forget the great encouragements from his wife and parents.

## **ABSTRACT**

Author: Jian Wang  
Title: **Workspace Evaluation And Kinematic Calibration of Stewart Platform**  
Institution: Florida Atlantic University  
Thesis Advisors: Dr. Oren Masory and Dr. Zvi Roth  
Degree: Doctor of Philosophy  
Year: December, 1992

Parallel manipulators have their special characteristics in contrast to the traditional serial type of robots. Stewart platform is a typical six degree of freedom fully parallel robot manipulator. The goal of this research is to enhance the accuracy and the restricted workspace of the Stewart platform.

The first part of the dissertation discusses the effect of three kinematic constraints: link length limitation, joint angle limitation and link interference, and kinematic parameters on the workspace of the platform. An algorithm considering the above constraints for the determination of the volume and the envelop of Stewart platform workspace is developed. The workspace volume is used as a criterion to evaluate the effects of the platform dimensions and kinematic constraints on the workspace and the dexterity of the Stewart platform. The analysis

and algorithm can be used as a design tool to select dimensions, actuators and joints in order to maximize the workspace.

The remaining parts of the dissertation focus on the accuracy enhancement. Manufacturing tolerances, installation errors and link offsets cause deviations with respect to the nominal parameters of the platform. As a result, if nominal parameters are being used, the resulting platform pose will be inaccurate. An accurate kinematic model of Stewart platform which accommodates all manufacturing and installation errors is developed. In order to evaluate the effects of the above factors on the accuracy, algorithms for the forward and inverse kinematics solutions of the accurate model are developed. The effects of different manufacturing tolerances and installation errors on the platform accuracy are investigated based on this model. Simulation results provide insight into the expected accuracy and indicate the major factors contributing to the inaccuracies.

In order to enhance the accuracy, there is a need to calibrate the platform, or to determine the actual values of the kinematic parameters (Parameter Identification) and to incorporate these into the inverse kinematic solution (Accuracy Compensation). An error-model based algorithm for the parameter identification is developed. Procedures for the formulation of the identification Jacobian and for accuracy compensation are presented. The algorithms are tested using simulated measurements in which the realistic measurement noise is included. As a result, pose error of the platform are significantly reduced.

# TABLE OF CONTENTS

ACKNOWLEDGEMENTS .....	iii
ABSTRACT .....	iv
LIST OF TABLES .....	viii
LIST OF ILLUSTRATIONS .....	ix
CHAPTER 1 INTRODUCTION .....	1
1.1 Introduction to Parallel Manipulators and Stewart Platform .....	1
1.2 Background .....	2
1.2.1 Workspace of Stewart Platform .....	2
1.2.2 Accuracy and Calibration of Stewart Platform .....	4
1.3 Research Objective and Overview of the Dissertation .....	5
CHAPTER 2 WORKSPACE EVALUATION .....	9
2.1 Geometric Parameters and Kinematic Constraints .....	9
2.1.1 Coordinate System and Geometric Parameters .....	9
2.1.2 Kinematic Constraints .....	11
2.2 Workspace Criterion and Determination .....	19
2.3 Effects of Different Parameters and Constraints .....	23
2.3.1 Workspace of a "Standard Platform" .....	23
2.3.2 Effects of Kinematic Constraints .....	27
2.3.3 Effects of Geometric Parameters .....	32
2.4 Concluding Remarks .....	34
CHAPTER 3 ACCURATE MODELING OF STEWART PLATFORM .....	36
3.1 Why Accurate Model .....	36
3.2 Modeling of Multi-Axis Joints .....	38
3.3 Modeling of Joints-Link Trains .....	40

3.4 Complete Model of Stewart Platform .....	44
CHAPTER 4 STEWART PLATFORM ACCURACY .....	47
4.1 Kinematic Analysis of the Accurate Model .....	47
4.1.1 Forward Kinematics .....	47
4.1.2 Inverse Kinematics .....	50
4.2 Effect of Manufacturing Tolerances on the Platform Accuracy .....	55
4.3 Concluding Remarks .....	62
CHAPTER 5 KINEMATIC CALIBRATION .....	64
5.1 Introduction to Calibration of Stewart Platform .....	64
5.2 Parameter Identification .....	66
5.2.1 Problem Statement .....	66
5.2.2 Error Model Based Approach And Identification Procedure .....	67
5.2.3 Jacobian formulation .....	71
5.3 Simulation Studies .....	74
5.4 Computational Issues .....	81
5.5 Concluding Remarks .....	82
CHAPTER 6 ACCURACY COMPENSATION .....	83
6.1 Compensation Procedure .....	83
6.2 Accuracy Improvement After Compensation .....	86
CHAPTER 7 CONCLUSIONS .....	90
APPENDICES .....	93
APPENDIX A Computation of the Coordinates of the Intersections of Link Vectors and Their Common Normal .....	93
APPENDIX B Flow Chart of the Program to Compute Workspace Volume And Boundary .....	96
APPENDIX C Nominal, Actual and Identified Parameters Used in .....	
the Simulation Studies.....	99
REFERENCES .....	101



## LIST OF TABLES

Table 3.1	Nominal D-H parameters of a joint-link train .....	42
Table 3.2	Modeling of errors by kinematic parameters .....	43
Table 3.3	Nominal D-H parameters of ${}^B\mathbf{T}_{0j}$ of Stewart platform .....	45
Table C.1	Nominal, actual and identified parameters and the errors .....	100

## LIST OF ILLUSTRATIONS

Figure 2.1	Stewart platform and coordinate systems .....	10
Figure 2.2	Ball joint rotational angle definition .....	13
Figure 2.3	Joint angle constraints .....	14
Figure 2.4	Different cases of link interference <sup>1</sup> .....	17
Figure 2.5	Workspace slicing .....	20
Figure 2.6	Fast search for workspace boundaries .....	21
Figure 2.7	An example of multi-connected domain .....	22
Figure 2.8	Workspace of a " Standard Platform" .....	24
Figure 2.9	Workspace volume versus joint angle constraint .....	28
Figure 2.10	Workspace boundaries for different join angle constraints .....	28
Figure 2.11	Workspace volume of the modified platform .....	30
Figure 2.12	Workspace boundaries of the modified platform .....	30
Figure 2.13	Workspace volume versus stroke .....	31
Figure 2.14	Platform constraints versus roll angle .....	31
Figure 2.15	Workspace volume versus joint location .....	33
Figure 2.16	Workspace volume versus plate-base radii ratio .....	33
Figure 3.1	U joint and its coordinate frames .....	39
Figure 3.2	Ball joint and its coordinate frames .....	39
Figure 3.3	A joint-link train and its coordinate frames .....	41
Figure 3.4	An example of the closed loop constraint .....	46
Figure 4.1	Range of a rotary joint .....	51
Figure 4.2	Platform maximum position error due to different manufacturing errors .....	57
Figure 4.3	Platform pose error due to base tolerance .....	58
Figure 4.4	Platform pose error due to all manufacturing errors .....	60
Figure 5.1	Flowchart of kinematic identification procedure for serial manipulators .....	68

Figure 5.2	Flowchart of the kinematic parameter identification procedure for Stewart platform .....	70
Figure 5.3	Convergence of the pose error vector norm versus iteration number .....	75
Figure 5.4	Convergence of the parameters error vector norm (Case 2) .....	77
Figure 5.5	Initial and final values of the kinematic parameter errors (Case 2) .....	77
Figure 5.6	Convergence of the parameters error vector norm (Case 3) .....	79
Figure 5.7	Initial and final values of the kinematic parameters errors (Case 3) .....	79
Figure 5.8	Convergence of the parameters error vector (Case 4) .....	80
Figure 5.9	Convergence of the pose error vector (Case 4) .....	80
Figure 6.1	Comparison of the translation error before and after compensation .....	87
Figure 6.2	Comparison of the position error components before and after compensation .....	88
Figure 6.3	Comparison of the orientation error components before and after compensation .....	89
Figure A.1	Intersections of link vectors and their common normal .....	95
Figure B.1	Flow chart for workspace computation .....	97
Figure B.2	Flow chart of the fast search algorithm .....	98

# CHAPTER 1

## INTRODUCTION

### 1.1 Introduction to Parallel Manipulators and Stewart Platform

Most industrial robots are open-chain mechanisms which are constructed with consecutive links connected by rotational or prismatic one degree of freedom joints. These serial manipulators have large workspace, high dexterity and maneuverability. However, due to their serial structure they exhibit low stiffness and poor positioning accuracy. As a result, their use in applications that require large loads (e.g. machining) and high accuracy is limited. In recent years, therefore, there has been increasing interest in the research and applications of parallel manipulators. In a parallel manipulator, the end effector is attached to a moveable plate that is supported in-parallel by a numbers of actuated links, or prismatic joints. It has been recognized that this kind of manipulators possess the following advantages compared with serial manipulators: 1) High force/torque capacity since the load is distributed to several in-parallel actuators; 2) High structural rigidity; and 3) High accuracy due to the noncumulative joints' errors. Therefore, these are suitable for applications in which high speed, high positioning accuracy and fast

dynamic response are required. However, despite these advantages, this type of manipulators do have a major drawback, that is, their restricted workspace.

The first parallel actuated mechanism was originally proposed by D. Stewart in 1965 as an aircraft simulator, hence so called "Stewart platform". Later, many articles have been published and the topics included inverse and forward kinematics analysis [Fichter 1986; Hunt,1983; Nguyen and Boron,1989; Nanua et al, 1990; Huang, 1991], workspace analysis [Yang and Lee,1983; Lee and Shah, 1988; Nguyen and Poor, 1989; Gosselin,1990], practical design/construction considerations [Fichter, 1986], dynamics [Sugimoto, 1987; Lee et al, 1989], and calibration [Zhuang and Roth, 1991]. Studies have also been conducted for its applications that included using it as an aircraft simulator [Hoffman and Hoffman, 1979], in mechanical assembly [McCallion and Truong, 1979], as a compliance device [McCallion et al, 1979], as an end-effector of a telerobotic assembly [Nguyen and Boron, 1989], as a vehicle emulation system [Durfee et al, 1991] and as robot arms [Fichter and McDowell, 1980; Powell, 1982; Landsburger and Sheridan, 1985; Sheridan, 1986; Dagalakis et al, 1988]. In addition, some new structural design based on the Stewart platform were proposed [Fichter and McDowell, 1980].

## **1.2 Background**

### **1.2.1. Workspace of Stewart Platform**

The workspace of a Stewart platform can be defined as a reachable region of the origin of a coordinate system attached to the center of the moving plate. Since its major drawback is a restricted workspace, it is of primary importance to develop

algorithms by which the workspace can be determined and the effect of different designs on the workspace can be evaluated. The workspace determination of a parallel manipulator is not straightforward, due to: 1) An analytic solution of its forward kinematics problem, which involves the solution of a set of highly non-linear simultaneous equations, is not available; and 2) The workspace depends also on constraints introduced by joint angle limitations, link length limitations and interference between the links. Few published reports have been concerned with this issue. The workspace of a special case platform, where all joints are evenly distributed and the payload platform is allowed to rotate only about one axis, was analyzed by Yang and Lee [1983]. The workspace of a three degree of freedom parallel manipulator was simulated by Lee and Shah [1988]. Algorithms for the determination of the workspace of a Stewart platform, based on numerical discretization of Cartesian space and integration of all workspace blocks, were proposed by Fichter [1986] and by Nguyen and Boron [1989]. A method based on the geometric properties of the workspace was suggested by Gosselin [1990]. It leads to a graphical representation of the region of the three dimensional Cartesian space that is attainable by the manipulator with a given orientation of the platform. In the above references, however, physical constraints such as joint angle limitations and link interference, which exist in practical system, were not considered. In the related literature so far, there have been little investigations on the effects of different constraints and geometric parameters on the workspace. However, this kind of evaluation is important for expanding and utilizing the workspace in design and applications of parallel manipulators.

### 1.2.2 Accuracy And Calibration of Stewart Platform

The accuracy problem of robot manipulators has long been one of the principal concerns in robot design and control. A large number of publications dealing with the accuracy of the serial manipulators appeared. These include such topics as error modeling [Wu, 1984; Veischegger and Wu; 1985, Mooring et al 1991], effects of manufacturing tolerance on pose accuracy [Mooring, 1983; Sugimoto and Okata, 1985] and the effect of the different level of complexity of kinematic models on the manipulator accuracy [Mooring and Padavala, 1989]. However, very few publications addressing the same issue as related to parallel manipulators can be found in the literature although high accuracy is generally believed to be one of their advantages compared to that of serial manipulators [Lee and Shah, 1988; Nguyen and Boron, 1989]. Moreover, almost all of the kinematic modeling and analysis methods for Stewart platform in the literature so far use an "ideal" kinematic model, or conventional model, in which the joints connecting actuators to both plates are treated as points. Therefore, the accuracy problems of Stewart platform, including how to establish an accurate kinematic model which accommodates the manufacturing and installation errors, how these errors effect the platform accuracy, and how to evaluate the accuracy of a practical Stewart platform, need to be further explored.

An effective way of improving the accuracy of robot manipulators is robot calibration. Robot calibration is a process by which the effects of robot kinematic errors on its accuracy are calibrated by proper corrections to the joint commands through modification of the robot control software without changing its hardware structure. Similar to the accuracy problem, while there have been numerous reports

dealing with the calibration issues of serial robot manipulators [Wu, 1984; Roth et al, 1987; Hayati et al, 1988; Everett et al, 1989; Huang and Masory, 1990; Zhuang and Roth, 1991], little attention has been given to parallel ones. Zhuang and Roth [1991] presented a calibration method of Stewart platform based on the following approach: by fixing one link at a time and moving the other five links during measurement process, one is able to compute kinematic parameters one link at a time. The approach requires relatively little computation, however, the approach has following problems: 1) It is difficult to implement since the link lengths can not be arbitrarily specified or driven (forward kinematics solution may not exist); 2) The measurable workspace is small because of the restricted motion pattern of the robot; 3) Kinematic parameters of individual links are computed separately, therefore, the coupling effects among the legs are not fully explored and the solution may not be global optimal; and 4) The model used is a simplified one and it did not include all the kinematic parameters of the platform (it was assumed that the joints used to connect the links between the base and the platform are perfect). New approaches for the calibration and accuracy compensation of Stewart platform and parallel manipulators need to be developed.

### **1.3 Research Objective and Overview of the Dissertation**

In order to enhance the advantages and to minimize the drawbacks of parallel manipulators in general, and Stewart platform in particular, the following work is conducted in this dissertation:



1. Evaluation and analysis of the platform workspace taking all constraints into account. The results will provide a tool by which the platform dimensions, joints and actuators can be selected.
2. Development of an accurate model and procedure by which the platform can be calibrated, and its accuracy can thus be enhanced.

The dissertation is organized as follows:

Chapter 2 discusses the workspace of the Stewart platform. First, all the kinematic constraints related to the workspace problem of Stewart platform are analyzed and their explicit equations are derived. Second, the algorithms for determination of the Stewart platform workspace envelopes and volumes considering all the constraints are developed. Third, a workspace criterion is proposed and used in the analysis of the effect of the platform dimensions, actuator's strokes, and the kinematic constraints on the workspace and dexterity of Stewart platform. The results and the algorithms can be used as a design tool for the selection of dimensions, joints and actuators so that the maximum platform workspace could be obtained.

The remaining part of the dissertation deals with the issue of the accuracy enhancement. In Chapter 3, a new accurate model of Stewart platform, which accommodates all manufacturing tolerances and installation errors, is proposed. The proposed model consists of six serial joint-link trains, each of which will be modeled by eight transformations from the base frame to the end-effector frame. The joints are modeled by two or three transformations. Thus the manufacturing and assembly errors related to joints and links can be modeled adequately.

In Chapter 4, the relationship between the pose of the end-effector and the joint variables is established for the proposed accurate model. Algorithms for

solving general forward and general inverse kinematics problems of the accurate model are developed. These algorithms with a set of typical tolerances are used to compute pose errors of a particular platform, which means that the accuracy of a Stewart platform with known manufacturing tolerances and assembly errors can be evaluated.

Chapter 5 presents an error-model based approach for the kinematic calibration of Stewart platform. The method is adopted from serial manipulator calibration methodology. As a result, the procedure and the algorithm can be easily understood, and implemented. The chapter focuses on the error model construction that is the central issue in adopting this method. Due to the inherent difficulty of analytical solution of the forward kinematics of the Stewart platform, it is inevitable to use a numerical method to compute the identification Jacobian matrix that relates robot pose errors to robot kinematic parameter errors. The detailed algorithm for the computation of the identification Jacobian matrix is presented. Simulated measurements, which will include realistic noise, are provided to show the effectiveness of the proposed calibration approach.

Chapter 6 discusses the accuracy compensation problem of the Stewart platform. The details of the compensation procedure for the accurate model is given and the simulation results show that great improvement in the accuracy of the platform can be achieved after compensation.

Chapter 7 concludes the dissertation with a summary and future research topics.

Before beginning a more detailed discussion of workspace analysis, accurate modeling and calibration, it is appropriate to establish a consistent notation that will be used in this dissertation. The following widely used notation is chosen:

- 1) Scalars are represented by uppercase or lowercase characters that are not shown as boldface.
- 2) Vectors are represented by boldface, lowercase characters.
- 3) Matrices are represented by boldface, uppercase characters.
- 4) Superscripts and subscripts are used and their meanings will be defined in each individual case.

# CHAPTER 2

## WORKSPACE EVALUATION

This chapter discusses the workspace problem of Stewart platform. Geometric parameters and kinematic constraints which affect the workspace of Stewart platform are analyzed in Section 2.1. Three kinds of constraints: link length, joint angle and link interference are defined and the constraint equations are derived. In Section 2.2, the workspace volume is selected as a criterion for workspace evaluation and optimization. Then an algorithm which can be used to systematically compute the workspace volume is developed. Section 2.3 investigates the effects of geometric parameters and kinematic constraints on the workspace. Concluding remarks are given in Section 2.4.

### 2.1 Geometric Parameters and Kinematic Constraints

#### 2.1.1 Coordinate System And Geometric Parameters

The Stewart platform, illustrated in Figure 2.1, is composed of six variable length links, a fixed base and a movable plate to which the tool is attached. It is assumed that the base and the plate are circular with radii  $R_b$  and  $R_p$  respectively.

A base coordinate system  $\{B\}$  is placed at the base center  $O_b$  with its  $Z$  axis perpendicular to the base plane. Similarly, the coordinate system  $\{P\}$  is located at the center of the moving plate. The joints pairs attached to the plate and the base are denoted by  $P_1$  to  $P_6$  and  $B_1$  to  $B_6$  respectively. The joints connected to the base are two degrees of freedom Universal joints (U-joints) and to the top plate are three degrees of freedom ball joints such that the platform has six degrees of freedom. If U-joints are replaced by ball joints, the links will have redundant rotary motion. This should be avoided. One may switch the top ball joints and the bottom U-joints.

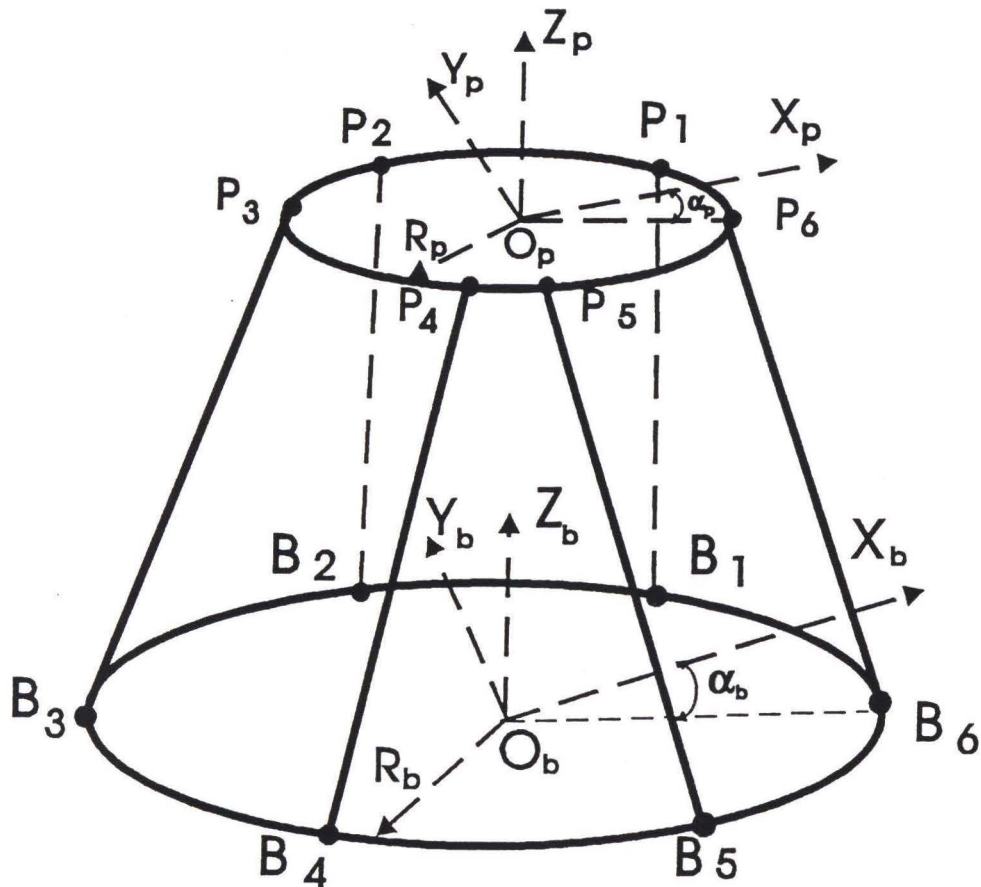


Figure 2.1 Stewart platform and coordinate systems

The coordinates of  $B_i$ ,  $i=1\dots6$  with respect to  $\{B\}$  denoted as  $\mathbf{b}_i$ , and those of  $P_i$  with respect to  $\{P\}$  as  $\mathbf{p}_i$ . The X axis of  $\{B\}$  is selected along the line which bisects the angle  $B_1O_bB_6$ , and similarly for the X axis of  $\{P\}$ . Denote half of the angle  $B_1O_bB_6$  as the base angle  $\alpha_b$ , and half of the angle  $P_1O_pP_6$  as the plate angle  $\alpha_p$ . These angles are used to define the location of joints on the base and the plate relative to  $\{B\}$  and  $\{P\}$  respectively:

$$\begin{aligned}\mathbf{b}_i &= R_b (\cos \alpha_{b_i}, \sin \alpha_{b_i}, 0) \\ \mathbf{p}_i &= R_p (\cos \alpha_{p_i}, \sin \alpha_{p_i}, 0)\end{aligned}\tag{2.1}$$

where  $i=1\dots6$ , and

$$\begin{array}{ll}\alpha_{b_1} = \alpha_b & \alpha_{p_1} = \alpha_p \\ \alpha_{b_2} = 120^\circ - \alpha_b & \alpha_{p_2} = 120^\circ - \alpha_p \\ \alpha_{b_3} = 120^\circ + \alpha_b & \alpha_{p_3} = 120^\circ + \alpha_p \\ \alpha_{b_4} = 240^\circ - \alpha_b & \alpha_{p_4} = 240^\circ - \alpha_p \\ \alpha_{b_5} = 240^\circ + \alpha_b & \alpha_{p_5} = 240^\circ + \alpha_p \\ \alpha_{b_6} = 360^\circ - \alpha_b & \alpha_{p_6} = 360^\circ - \alpha_p\end{array}$$

## 2.1.2 Kinematic Constraints

Three types of kinematic constraints affect the available workspace of a Stewart platform: link length limitations, joint angle limitations and link interference.

### 2.1.2.1 Link length limitations

The plate pose can be described by a 3x3 orientation matrix  $\mathbf{R}$  and a translation vector  $\mathbf{q}$  which define  $\{P\}$  with respect to  $\{B\}$ .  $\mathbf{l}_i$ , the vectors connecting  $B_i$  to  $P_i$  expressed in  $\{B\}$ , where  $i=1,2\dots,6$  indicates the link number, are given by:

$$\mathbf{l}_i = \mathbf{R} \mathbf{p}_i + \mathbf{q} - \mathbf{b}_i \quad (2.2)$$

The links length, denoted as  $L_1$  to  $L_6$ , are given by:

$$L_i = |\mathbf{R} \mathbf{p}_i + \mathbf{q} - \mathbf{b}_i| \quad (2.3)$$

The link length constraint is expressed by:

$$L_{\min_i} \leq L_i \leq L_{\max_i} \quad (2.4)$$

where  $L_{\min_i}$  and  $L_{\max_i}$  are the minimum and maximum allowable length of link  $i$ .

### 2.1.2.2 Joint angle constraints

The links are typically attached to the plate by ball joints, and to the base by U-joints. A ball joint is free to rotate about all three axes, however in practice, its motion is restricted by the joint physical construction. As shown in Figure 2.2, the rotational angle of a ball joint,  $\theta$ , defined as the angle between the Z axis of a coordinate system attached to its socket and  $\mathbf{u}$ , a vector along the leg connected to the joint, is physically constrained. The rotation angle of a U-joints is restricted in a

similar way. In other words, every practical joint has its maximum rotational angle  $\theta_{\max}$ .

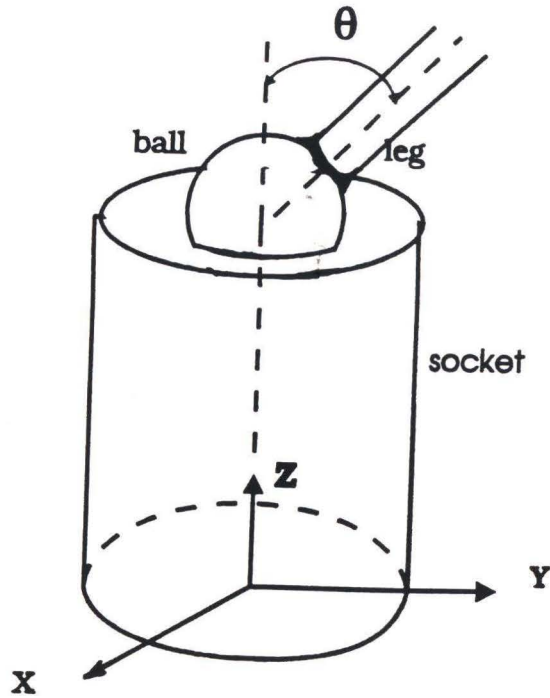


Figure 2.2 Ball joint rotational angle definition

Assume that the socket of a ball joint  $i$  is installed so that a unit vector  $\mathbf{n}_{p_i}$  describes its orientation with respect to  $\{P\}$ . The rotational angle of a ball joint in the plate,  $\theta_{p_i}$ , and its constraint can be computed by:

$$\theta_{p_i} = \cos^{-1} \frac{\mathbf{l}_i \cdot \mathbf{R} \mathbf{n}_{p_i}}{|\mathbf{l}_i|} \leq \theta_{p_{\max}} \quad (2.5a)$$



Similarly, the rotational angle of a U-joint in the base,  $\theta_{b_i}$ , is given by (see Figure 2.3):

$$\theta_{b_i} = \cos^{-1} \frac{\mathbf{l}_i \cdot \mathbf{n}_b}{|\mathbf{l}_i|} \leq \theta_{b_{\max}} \quad (2.5b)$$

where  $\mathbf{n}_b$  is the unit vector which describes the U-joint orientation with respect to  $\{B\}$ ,  $\theta_{p_{\max}}$  and  $\theta_{b_{\max}}$  are the maximum allowable rotational angles of the ball and the U-joints respectively.

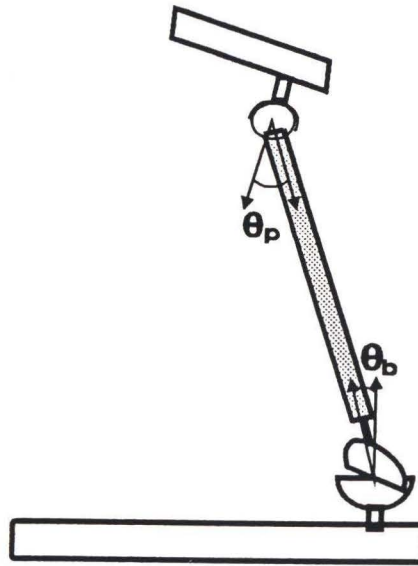


Figure 2.3 Joint angle constraints

The joints can also be installed along particular directions. If each joint is installed along its nominal direction  $\mathbf{l}_{n_i}$ , which is the direction of vector  $\mathbf{l}_i$  when each link length is equal to  $0.5(L_{\min_i} + L_{\max_i})$  and the plate has no rotation with respect to the base, then the rotational angles are given by:

$$\theta_{p_i} = \cos^{-1} \frac{\mathbf{I}_i \cdot \mathbf{R} \mathbf{I}_{n_i}}{|\mathbf{I}_i| |\mathbf{I}_{n_i}|} \quad (2.6a)$$

and

$$\theta_{b_i} = \cos^{-1} \frac{\mathbf{I}_i \cdot \mathbf{I}_{n_i}}{|\mathbf{I}_i| |\mathbf{I}_{n_i}|} \quad (2.6b)$$

With such installation, it is possible to substantially increase the platform workspace as will be shown in the simulation results in Section 2.3.

### 2.1.2.3 Link interference constraints

Since links have physical dimensions, interference might occur. For the sake of analysis assume that each link is cylindrical with a diameter  $D$ . Let  $D_i$  ( $i=1-6$ ) be the shortest distance between the center lines of two adjacent links, the interference constraint can be expressed by:

$$D_i \geq D \quad (2.7)$$

Let  $\mathbf{n}_i$  be a unit vector in the direction of the common normal between two consecutive link vectors  $\mathbf{I}_i$  and  $\mathbf{I}_{i+1}$ :

$$\mathbf{n}_i = \frac{\mathbf{I}_i \times \mathbf{I}_{i+1}}{|\mathbf{I}_i \times \mathbf{I}_{i+1}|} \quad (2.8)$$

The shortest distance between the two lines defined by the vectors  $\mathbf{l}_i$  and  $\mathbf{l}_{i+1}$ ,  $\Delta_i$ , as shown in Figure 2.4, is given by:

$$\Delta_i = |\mathbf{n}_i \cdot (\mathbf{b}_{i+1} - \mathbf{b}_i)| \quad (2.9)$$

It should be stressed that in general the shortest distance between links ( $D_i$ ) is not necessarily equal to the shortest distance between the link vectors ( $\Delta_i$ ). The relationship between the two depends on the location of the intersection points ( $C_i$  and  $C_{i+1}$ ) of the link vectors  $\mathbf{l}_i, \mathbf{l}_{i+1}$  with their common normal  $\mathbf{n}_i$ . The coordinates  $\mathbf{c}_i$  of  $C_i$  can be computed by (see Appendix A for derivation):

$$\frac{\mathbf{c}_i - \mathbf{b}_i}{{}^B\mathbf{p}_i - \mathbf{b}_i} = \frac{(\mathbf{b}_{i+1} - \mathbf{b}_i) \cdot \mathbf{m}_i}{({}^B\mathbf{p}_i - \mathbf{b}_i) \cdot \mathbf{m}_i} \quad (2.10)$$

where  ${}^B\mathbf{p}_i$  are the coordinates of  $P_i$  with respect to the  $\{B\}$ , and  $\mathbf{m}_i$  is a vector defined by :

$$\mathbf{m}_i = \mathbf{n}_i \times ({}^B\mathbf{p}_{i+1} - \mathbf{b}_{i+1}) \quad (2.11)$$

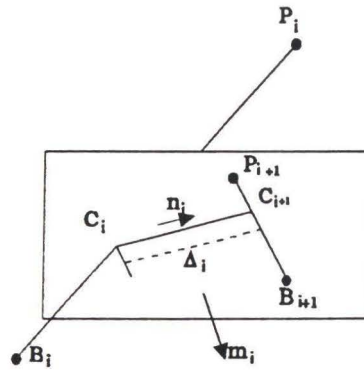
Similarly for  $\mathbf{c}_{i+1}$ . According to the location of  $C_i$  and  $C_{i+1}$ , three different cases need to be distinguished:

**Case 1: Both intersection points are on the links**

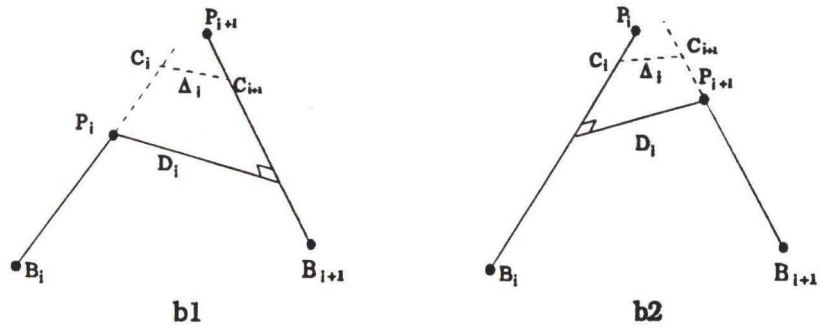
In this case, as shown in Figure 2.4a,  $D_i = \Delta_i$ , and interference occurs if  $D > \Delta_i$ .

**Case 2: One of the intersection points is outside the link**

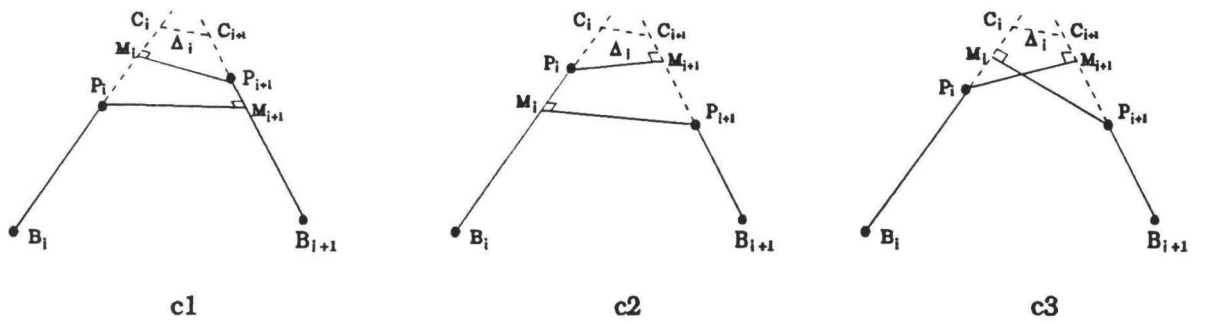
In this case, as shown in Figure 2.4b, the distance  $D_i$  can be determined according to the positions of the two intersection points. As shown in Figure 2.4b1, if



(A)



(B)



(C)

Figure 2.4 Different cases of link interference

$C_i$  is located beyond  $P_i$ , but  $C_{i+1}$  is on the  $i+1^{\text{th}}$  link, then  $D_i$ , which is the distance from  $P_i$  to the  $i+1^{\text{th}}$  link, is given by:

$$D_i = \frac{|(\mathbf{p}_i^B - \mathbf{b}_{i+1}) \times \mathbf{l}_{i+1}|}{|\mathbf{l}_{i+1}|} \quad (2.12)$$

if  $C_{i+1}$  is located beyond  $P_{i+1}$ , but  $C_i$  is on the  $i^{\text{th}}$  link as shown in Figure 2.4b2, then  $D_i$ , which is the distance from  $P_{i+1}$  to the  $i^{\text{th}}$  link, is given by:

$$D_i = \frac{|(\mathbf{p}_{i+1}^B - \mathbf{b}_i) \times \mathbf{l}_i|}{|\mathbf{l}_i|} \quad (2.13)$$

### Case 3: Both intersection points are not on the links

In this case, as shown in Figure 2.4c,  $D_i$  depends on the location of  $M_i$ , which is the intersection point between  $\mathbf{l}_{i+1}$  and the normal from point  $P_i$  to vector  $\mathbf{l}_{i+1}$ , and the location of  $M_{i+1}$ , which is the intersection point between  $\mathbf{l}_i$  and the normal from  $P_{i+1}$  to vector  $\mathbf{l}_i$ . There are three possibilities:

1. If  $M_{i+1}$  is located on the link  $P_{i+1}B_{i+1}$  while  $M_i$  is out of the link  $P_iB_i$ , as shown in Figure 2.4c1, then  $D_i$  is given by Equation (2.12).
2. If  $M_i$  is located on the link  $P_iB_i$  while  $M_{i+1}$  is out of the link  $P_{i+1}B_{i+1}$ , as shown in Figure 2.4c2, then  $D_i$  is given by Equation (2.13).
3. If both  $M_i$  and  $M_{i+1}$  are located out of the links, as shown in Figure 2.4c3, then  $D_i$  is the distance between two joints  $P_i$  and  $P_{i+1}$ .

## 2.2 Workspace Criterion and Determination

The workspace of the Stewart platform can be defined as the 3D Cartesian space which is reachable by the center of the moving plate, namely, the origin of  $\{P\}$ . Since the workspace of a Stewart platform is closed, the volume of the workspace can be used as a criterion for workspace evaluation and optimization. Furthermore, the volume of the workspace for different platform orientations can be used as a measure for the platform dexterity. The workspace volume is a function of the geometric parameters as well as the kinematic constraints of the platform. Therefore, the volume criterion can also be used to evaluate the effect of different geometric parameters and kinematic constraints on the workspace.

For every pose (position and orientation) of  $\{P\}$ , the links length  $L_i$ , joint rotational angle  $\theta_{p_i}$ ,  $\theta_{b_i}$  and the distance between link pairs,  $D_i$ , can be determined as described in the preceding section. These values are then compared with a given set of physical constraints  $L_{\max}$ ,  $L_{\min}$ ,  $\theta_{p_{\max}}$ ,  $\theta_{b_{\max}}$  and  $D$ . If any of the constraints is violated, the particular pose is not reachable and therefore is out of the workspace. Similarly, if all of the constraints are satisfied, the pose is reachable and is within the workspace.

The workspace volume,  $V$ , is computed as follows:

1. The workspace was divided into slices of thickness  $\Delta Z$  parallel to the X-Y plane, as shown in Figure 2.5.
2. The boundaries of each slice are found and the volume of each slice is calculated.
3. The volume of the platform workspace is computed by summing all slices' volumes.

A program that calculates the workspace volume according to the above procedure was written. In this regard, few points should be emphasized:

1. The search for a pose, which is within the workspace, starts at the plane  $Z=Z_0$  which lies well below (does not intersect) the workspace. Note that  $Z_0$  is not necessarily defined by the plane where all links are at minimum length ( $L_i=L_{min}$ ) and therefore  $Z_0$  should be less than  $Z_{min}$ .
2. The search ends at the plane  $Z_{max}$  which contains only one feasible pose.

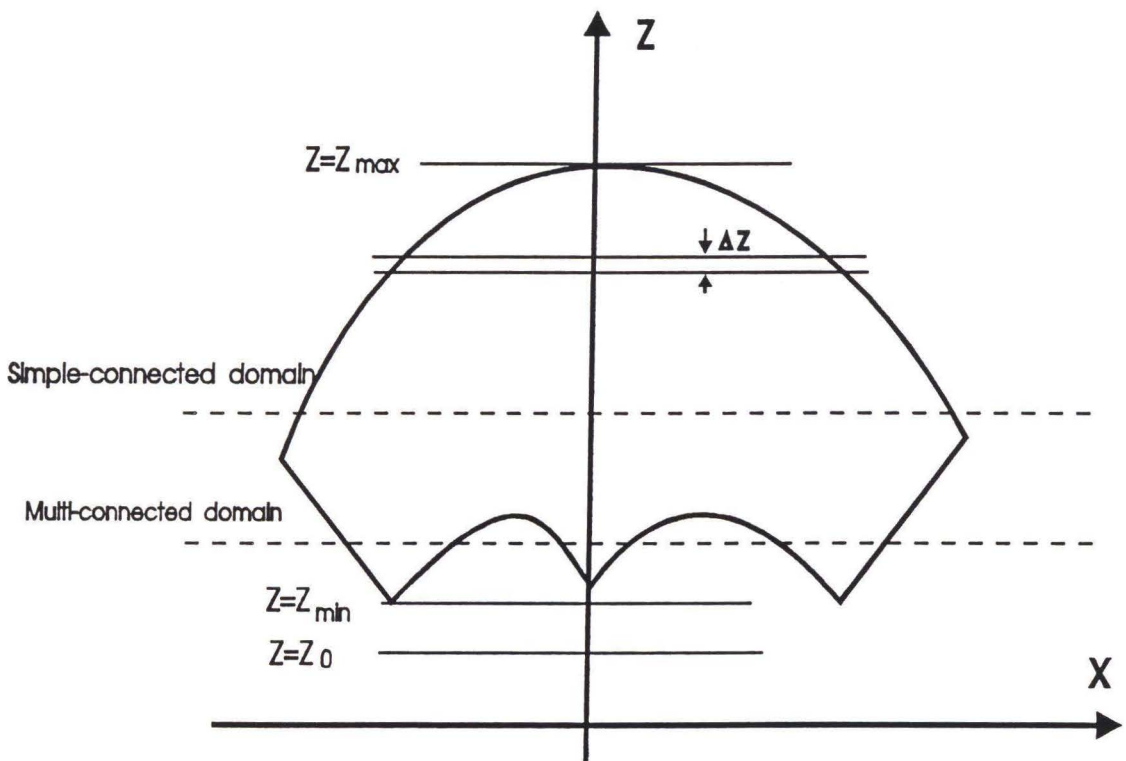


Figure 2.5 Workspace slicing

3. The intersection of the workspace with a plane parallel to the XY plane is in most cases a simply-connected domain. In this case, the boundary of the slice is found using a fast search method illustrated in Figure 2.6. Assume that a point  $A_1$  on the boundary was obtained by increasing radius  $\rho$  until one constraint is violated. Then the angle  $\gamma$  is increased by  $\Delta\gamma$  and the coordinates of the point  $T_1$  are calculated using the values  $\gamma_i + \Delta\gamma$  and  $\rho_i$ . If the point is within the workspace,  $\rho$  is increased gradually until a constraint is violated and a new boundary point ( $A_2$  in Figure 2.6) is found. Otherwise, if the new point is out of the workspace ( $T_2$  in Figure 2.6),  $\rho$  is decreased gradually until a new boundary point is found. ( $A_3$  in Figure 2.6). Once all boundary points are registered, the volume of the slice is determined by:

$$V_i = \frac{1}{2} \sum_j \rho_j^2 \Delta\gamma \Delta Z \quad (2.14)$$

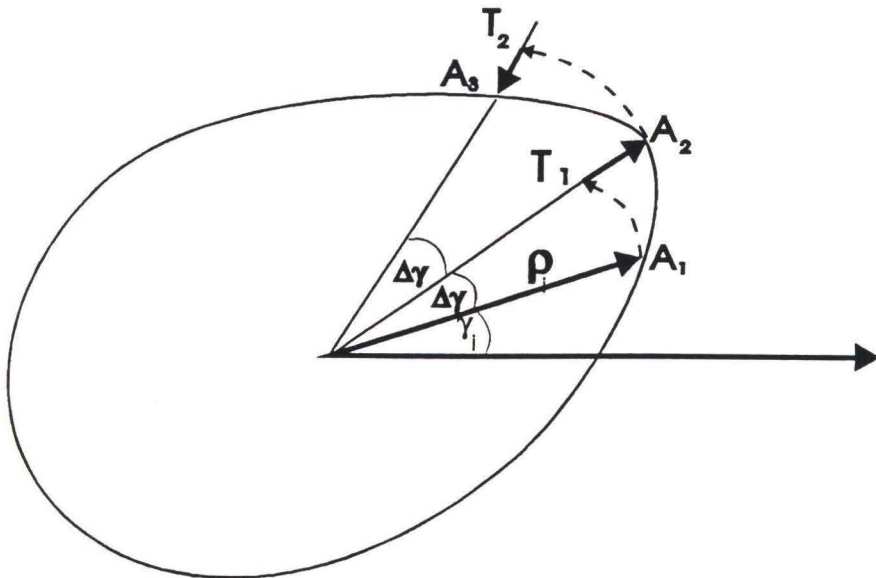


Figure 2.6 Fast search for workspace boundaries



4. In some cases, as shown in Figure 2.7, the intersection is not a simply-connected domain, which often happens in the lower part of the platform workspace. In this figure, the hatched area is within workspace. Therefore, the search radius  $\rho_{\max}$  should be large enough to cover the whole region. In this case the volume of the slice is given by:

$$V_i = \frac{1}{2} \sum_j (\rho_{j_1}^2 + \rho_{j_2}^2 - \rho_{j_3}^2) \Delta\gamma \Delta Z \quad (2.15)$$

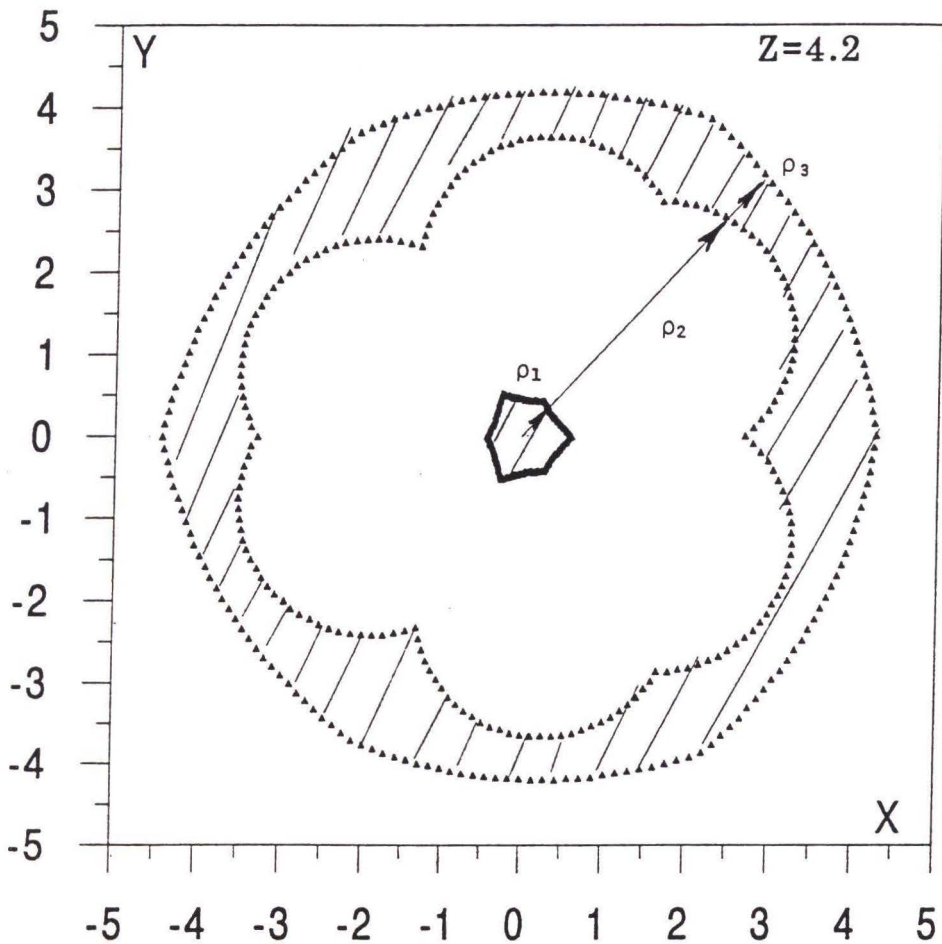


Figure 2.7 An example of multi-connected domain

5. The workspace volume,  $V$ , is computed by summing up the volumes of all slices.

The flow chart of the program (written in Fortran) is given in Appendix B.

## 2.3 Effects of Different Parameters and Constraints

The effects of different geometric parameters and kinematic constraints on the workspace and dexterity of a Stewart platform are presented in this section. The results obtained by changing a particular parameter of a platform while keeping all others constant.

### 2.3.1 Workspace of a "Standard Platform"

A "Standard Platform", in which all dimensions were normalized with respect to  $R_p$ , was used in this study. Its dimensions, joints' location and kinematic constraints are defined by:

$$R_p=1 \quad R_b=3 \quad \alpha_p = 15^\circ \quad \alpha_b = 30^\circ$$

$$\theta_{p_{\max}} = \theta_{b_{\max}} = 45^\circ$$

$$L_{\min}=4.5 \quad L_{\max}=7.5$$

$$D=0.1$$

A Stewart platform, with the above parameters and constraints, was simulated and its workspace is shown in Figure 2.8. Figures 2.8 (a) and 2.8 (b) illustrate the platform workspace for the case where the plate orientation, defined by Roll, Pitch and Yaw angles, was constrained to move parallel to its base (Roll=Pitch=Yaw=0) while in Figures 2.8 (c) and 2.8 (d) the plate all three angles

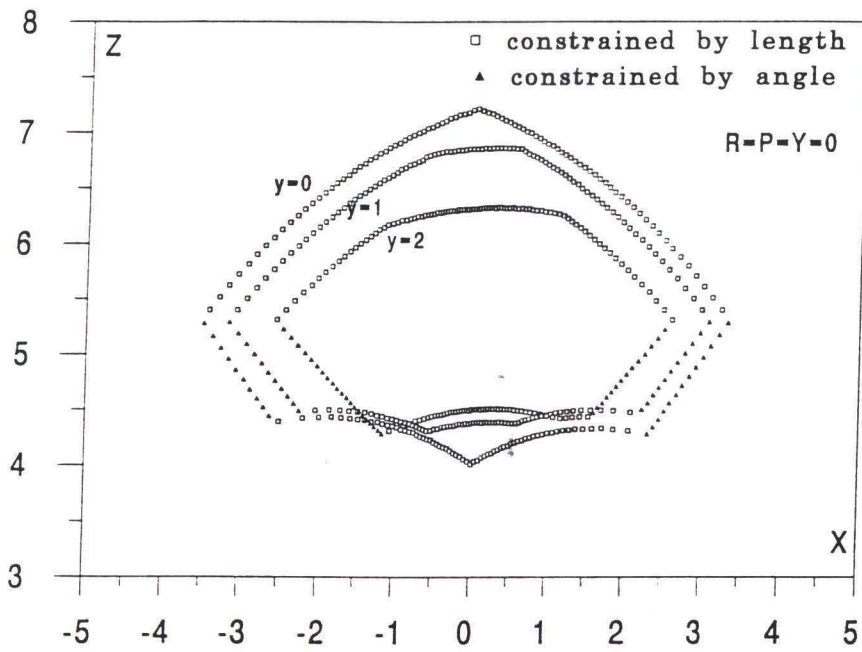


Figure 2.8 (a)

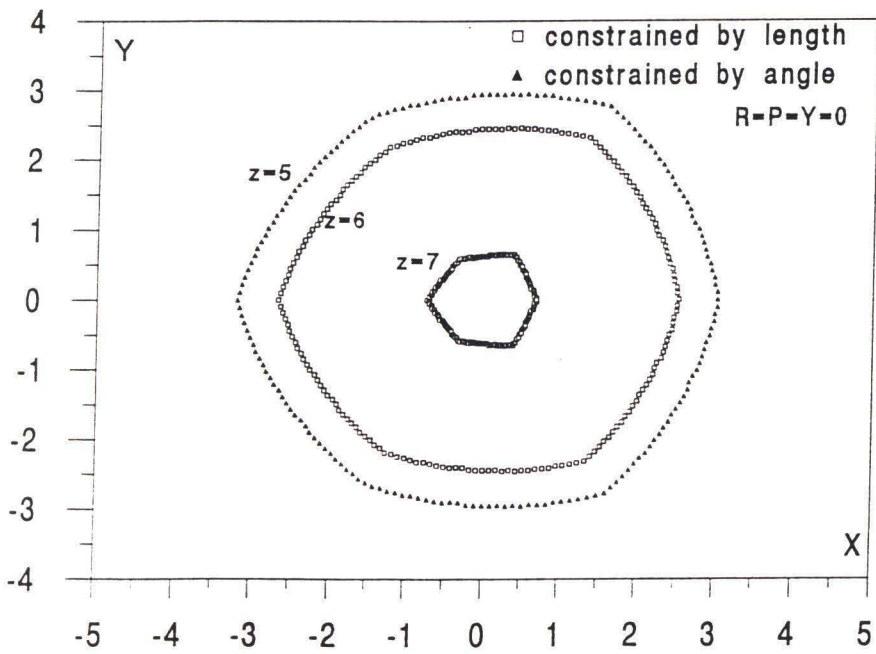


Figure 2.8 (b)

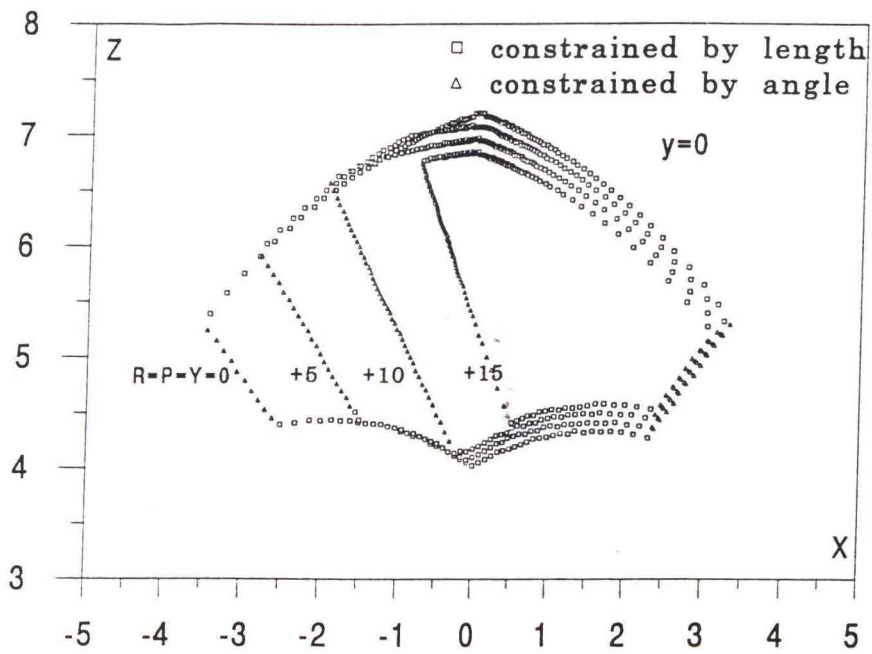


Figure 2.8 (c)

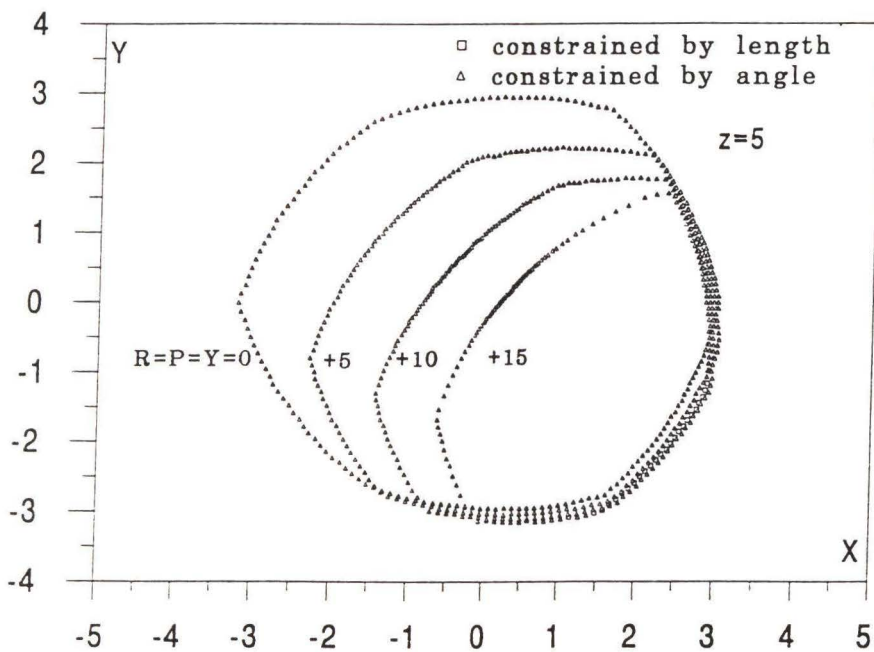


Figure 2.8 (d)

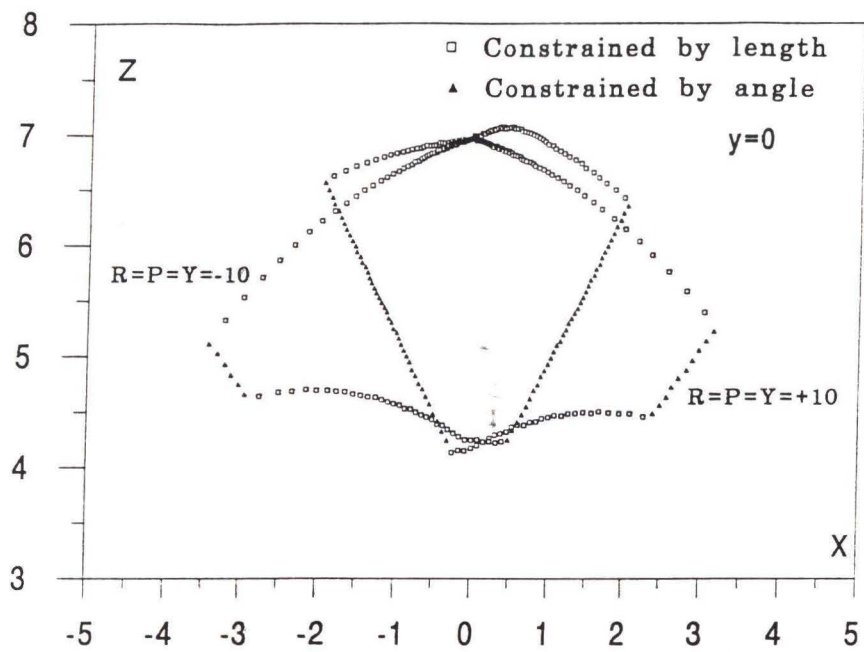


Figure 2.8 (e)

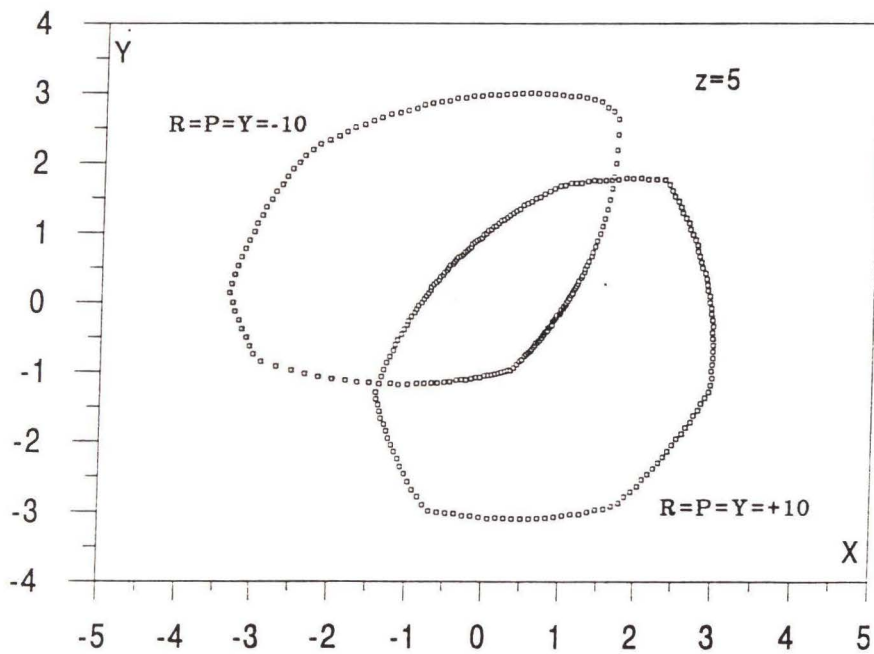


Figure 2.8 (f)

Figure 2.8 Workspace of a "Standard Platform"

could vary from  $0^\circ$  to  $+5^\circ$ ,  $+10^\circ$ , and  $+15^\circ$ . In Figures 2.8 (e) and 2.8 (f), the plate orientation was varied in the range of  $0^\circ$  to  $+10^\circ$  and  $0^\circ$  to  $-10^\circ$ . Observing these figures the following conclusion can be drawn:

1. The surface that contains the workspace is composed of three sections determined by three constraints: a) Upper dome which is constrained by  $L_{\max}$ ; b) Conical surface constrained by the joints' angle limitations; and c) Bottom dome constrained by  $L_{\min}$  (Figures 2.8 (a) and 2.8 (b)).
2. For  $\text{Roll} = \text{Pitch} = \text{Yaw} = 0^\circ$  the platform workspace is symmetrical about the Z axis while for any other orientation it is not.
3. The workspace of the platform is substantially decreased as the orientation requirements increase (Figures 2.8 (c) - (f)).

## 2.3.2 Effects of Kinematic Constraints

### 2.3.2.1 Joint angle constraint

The workspace volume,  $V$ , for different end-effector orientations versus joint angle limitations (all other parameters and constraints are nominal) is illustrated in Figure 2.9 (RPY are the Roll, Pitch and Yaw angles of the plate). As shown, this constraint has significant effect on the workspace volume and for large orientation angles the volume can be zero which means that the platform is locked. The effect of the joints angle is further demonstrated in Figure 2.10.

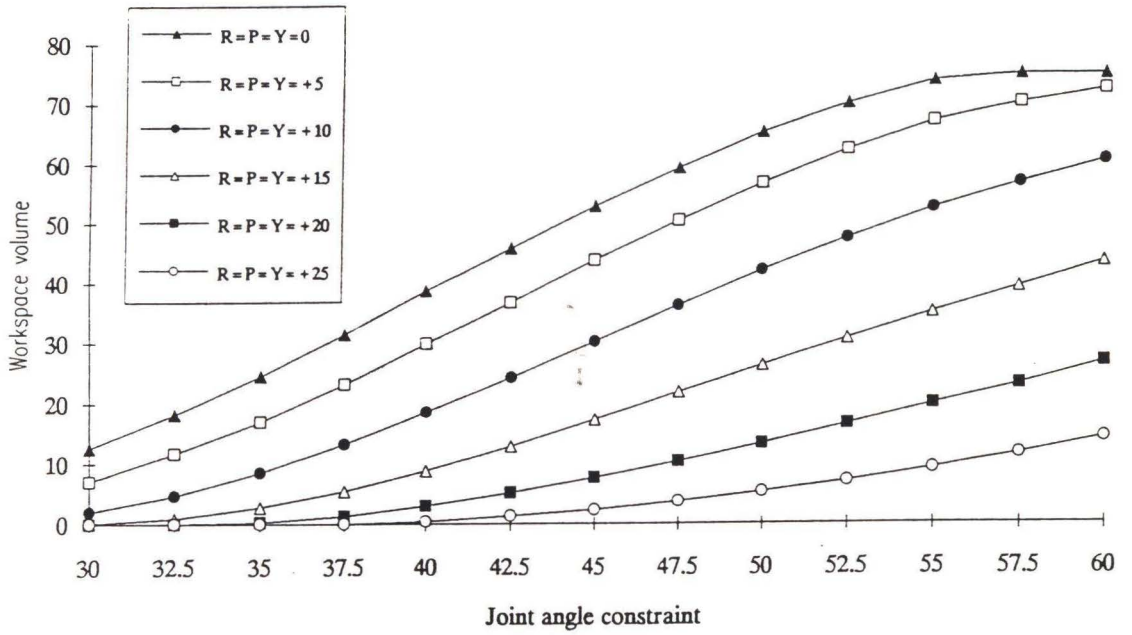


Figure 2.9 Workspace volume versus joint angle constraint

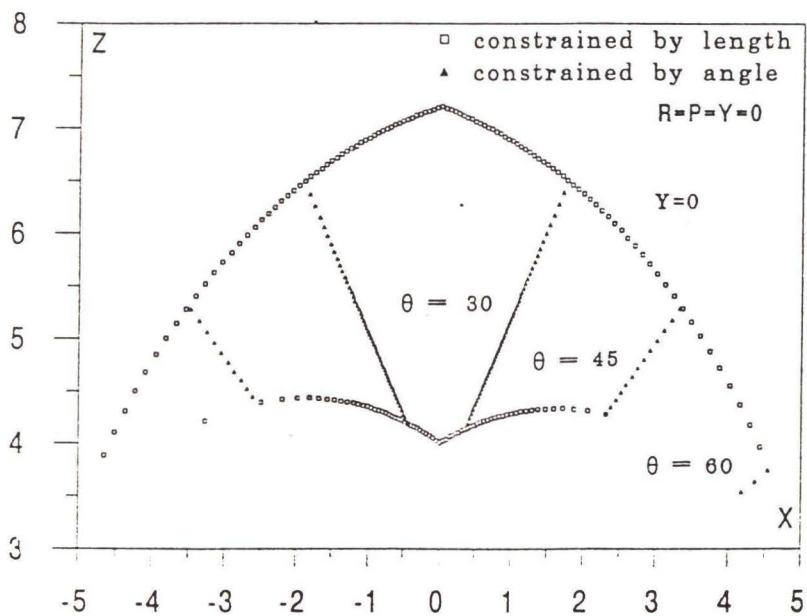


Figure 2.10 Workspace boundaries for different joint angle constraints

Although the maximum rotational angle of the joints cannot be changed once the joints have been selected, it is possible to enlarge the workspace by fully utilizing their range of rotation. Rather than mounting the joints perpendicular to the base and the plate plane, it is advantageous to install each joint along the direction of the respected vector  $I_{n_i}$ . Comparing the results shown in Figure 2.11 to the ones in Figure 2.9, the workspace volume in this case is increased significantly for joints with limited rotational angle. This improvement is also clearly shown in Figure 2.12 when compared with Figure 2.8.

### 2.3.2.2 Link length constraint

In practice,  $L_{\min}$  can be approximated by the travel range of the link,  $S$ , plus a constant,  $C$  (in case of a hydraulic actuator this corresponds to the actuator's stroke plus a constant). Thus,  $L_{\min}$  and  $L_{\max}$  can be expressed by:

$$L_{\min} = S + C \quad (2.16)$$

$$L_{\max} = 2S + C \quad (2.17)$$

The effect of the link travel on the workspace volume is shown in Figure 2.13, where  $C=1.5$  was assumed. The workspace volume approximately increases with the cubic power of the stroke.



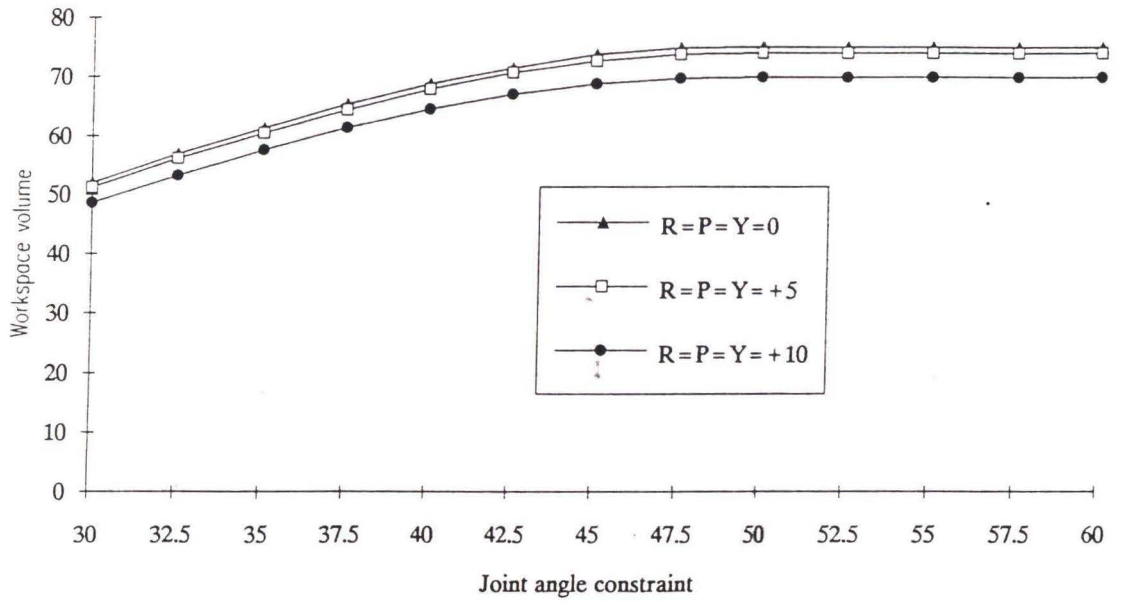


Figure 2.11 Workspace volume of the modified platform

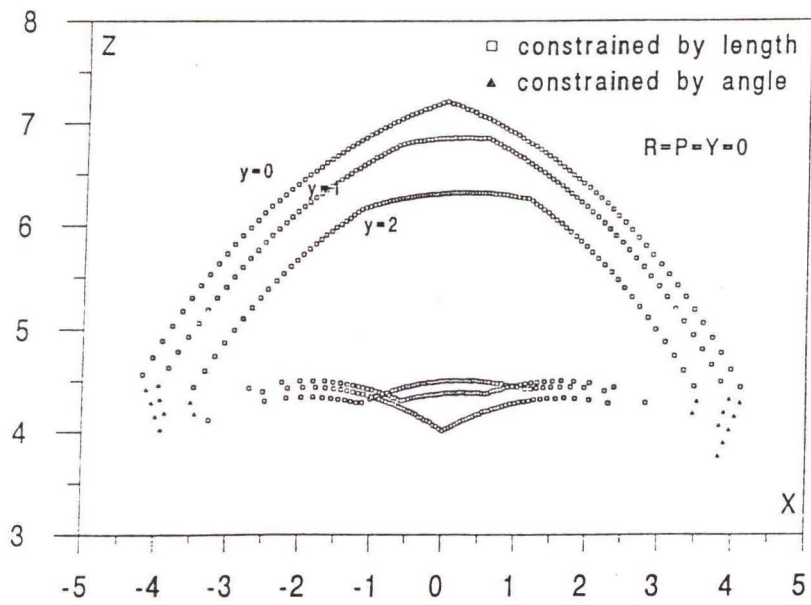


Figure 2.12 Workspace boundaries of the modified platform

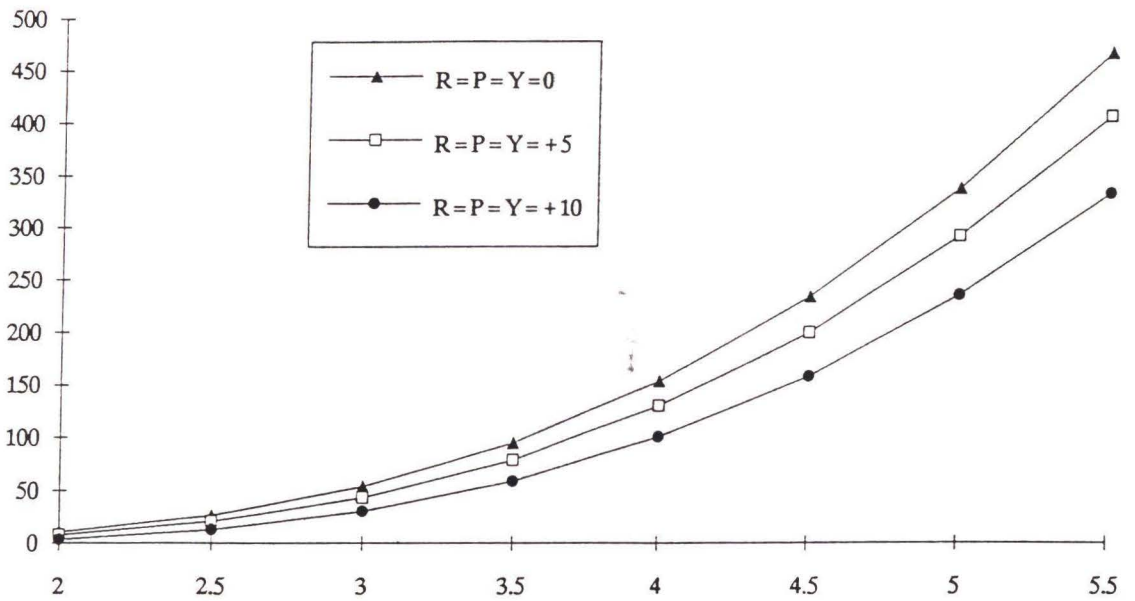


Figure 2.13 Workspace volume versus stroke

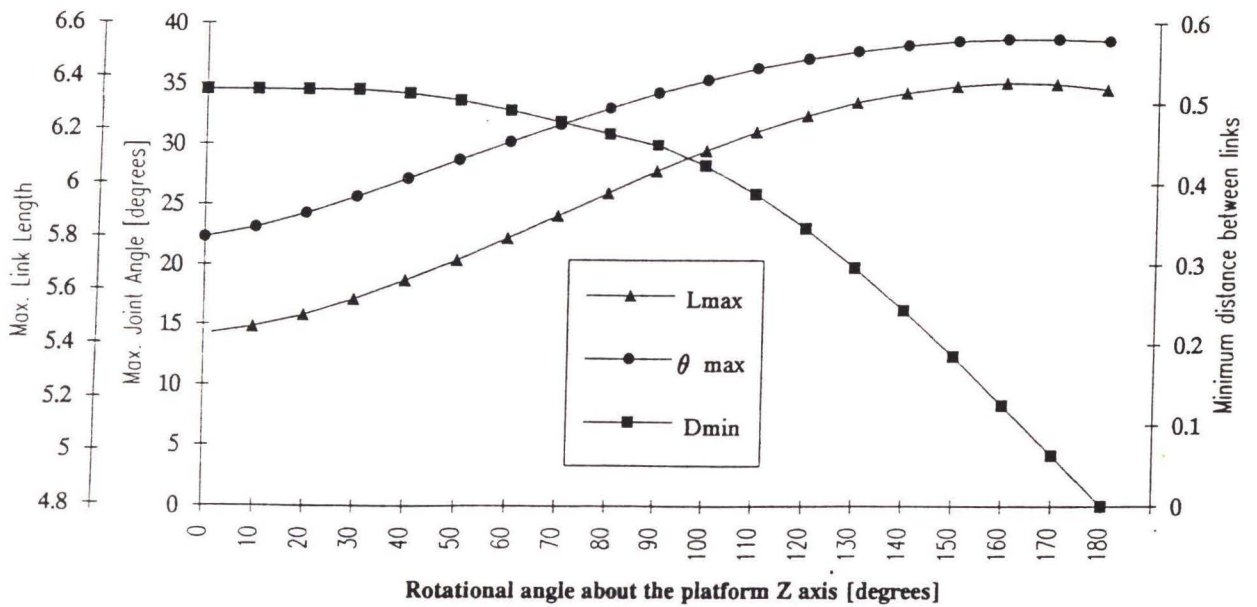


Figure 2.14 Platform constraints versus roll angle

### 2.3.2.3 Link interference

Simulation results show that link interference usually does not affect the workspace of the platform since other constraints are being violated first. However, an example in which the "Standard Platform" is rotated about the Z axis at a constant position defined by  $X=0$ ,  $Y=0$  and  $Z=5$  will be used to demonstrate interference. Figure 2.14 illustrates the values of the  $\min(D_i)$ ,  $\max(L_i)$  and  $\max(\theta_b, \theta_p)$  for this special case as function of the rotation angle. As shown link interference occurs at roll angle of  $165^\circ$  while link length and joints angle constraints were not violated through out the motion. One has to realize that this is an extreme case, and in most cases where the platform is also translated, other constraints are likely to be violated first.

## 2.3.3 Effect of Geometric Parameters

### 2.3.3.1 Joints' locations

The results, shown in Figure 2.15, were obtained by fixing location of the joints on the base, defined by  $R_b=3$  and  $\alpha_b=30^\circ$ , while changing the location of the joints on the platform. It appears that locations of the joints have little effect on the workspace. Although the maximum workspace volume is obtained at  $\alpha_b=\alpha_p$ , this configuration is not recommended since in such a case the Jacobian of the platform is singular [Fichter, 1986].

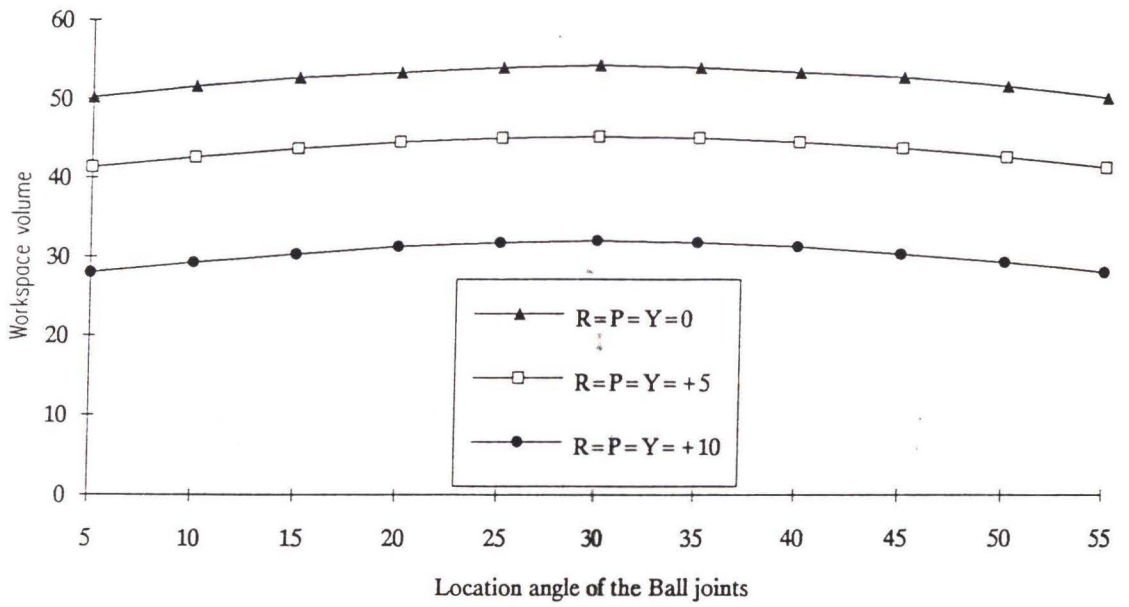


Figure 2.15 Workspace volume versus joint location

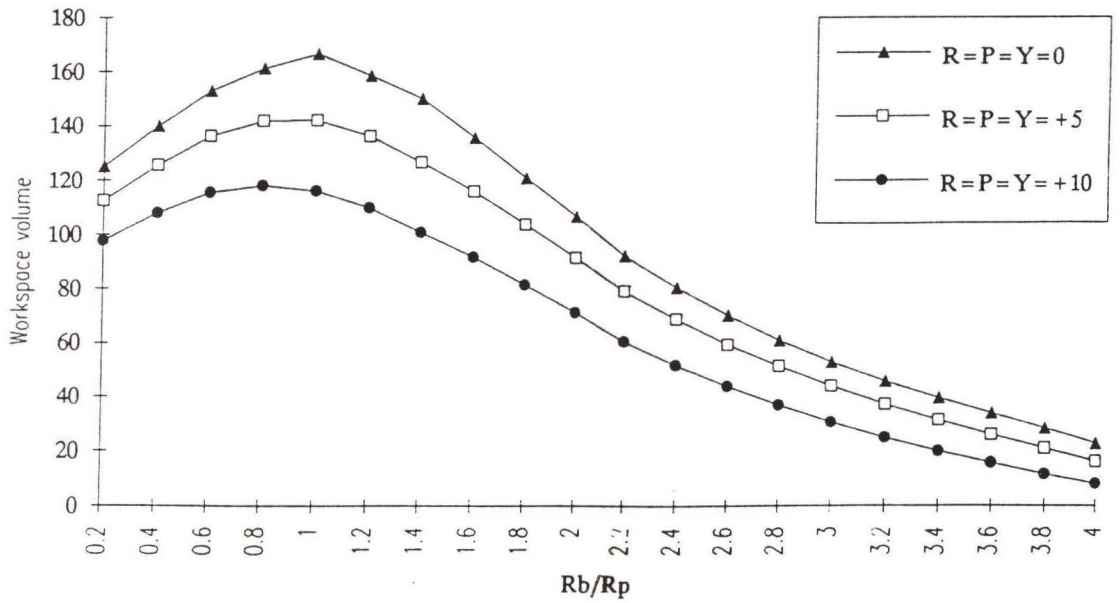


Figure 2.16 Workspace volume versus plate-base radius ratio

### 2.3.3.2. Base and plate dimensions

Figure 2.16 shows how the platform workspace varies as function of the ratio  $R_b/R_p$ . As shown, the volume,  $V$ , reaches its maximum value at about  $R_b/R_p=1$ . For  $R_b/R_p>1.0$  the volume is constrained by links' length and/or joints' angle. For  $R_b/R_p<1$  the volume might be also constrained by link interference. In this particular case the platform will be locked ( $V=0$ ) when  $R_b/R_p$  is close to 0.1.

## 2.4 Concluding Remarks

The analysis of the workspace volume and the dexterity of a Stewart platform, considering all kinematic constraints and platform's dimensions, was presented. The workspace volumes and boundaries for different geometric parameters and kinematic constraints are computed and presented by normalized dimensions. Therefore, the information provided can be used for the selection of dimensions, joints and actuators to maximize the workspace of a Stewart platform.

The following concluding remarks are in order:

1. The proposed algorithm can be used to determine the workspace volume and envelop of a practical Stewart platform given the geometric parameters and the kinematic constraints.
2. The 3D Cartesian workspace of Stewart platform is embedded in a closed space. However, there may be some "holes" within the space, especially in the lower part of the space, to which the manipulator cannot reach. One should check the reachability for specified poses or trajectories during motion planning and control.

3. The workspace of Stewart platform is primarily restricted by the link length constraint and joint angle constraint. In some cases, it is also constrained by the link interference.
4. Joint locations on both plates have little effect on the workspace of Stewart platform.
5. The workspace can be improved by fully utilizing the range of rotation of joints that are installed along the direction of the link vector  $\mathbf{l}_{n_i}$ .
6. The dimension ratio of the top and base plates has important effect on the workspace and needs to be properly selected. In the case of "Standard platform", the ratio should be close to 1 in order to achieve the near maximum workspace.

## CHAPTER 3

### ACCURATE MODELING OF STEWART PLATFORM

An accurate model which accommodates all manufacturing tolerances and installation errors is developed in this chapter. Deficiencies of the conventional or nominal model for the purpose of accuracy analysis are discussed in Section 3.1. In Section 3.2, U-joints or ball joints are modeled in terms of two or three cascaded homogeneous transformations. In Section 3.3, a joint-link train is defined to model one of the six link branches of Stewart platform. The complete model of the Stewart platform is given in Section 3.4. The procedure of model construction of Stewart platform is given step by step and the parameters used in the model are related to error modeling. The accurate model contains all information for the kinematic analysis and accuracy evaluation that is discussed in the next chapter.

#### 3.1 Why Accurate Model

In developing the conventional or nominal kinematic model of Stewart platform with the coordinate frames  $\{B\}$  and  $\{P\}$ , as illustrated in Figure 2.1, the following assumptions are made:

1. All joints are perfect in the sense that their axes are perpendicular one to another and intersect at the same point (referred to as the joint center).
2. The actuators are perfectly assembled to the joints so that each actuator axis passes through the respective joint centers.
3. The extension of each actuator can be measured without any offset.
4. The platform dimension is accurate so that the locations of the joints are precisely known.

Under these assumptions, both U-joints and ball joints can be treated as points and links as straight line segments of known length connected between the respective joints' centers, and the inverse kinematics of the Stewart platform is given by Equation (2.2).

Machining tolerances and assembly errors always exist. As a result, both U-joints and ball joints are not perfect - their axes neither intersect nor are perpendicular to one another. As such, joint centers actually do not exist. Furthermore, when the actuators are connected to both plates by some kind of coupling devices, installation error is also more or less exist. Consequently, the axes of the actuators are skew to the joint's axes. In most cases, such as in workspace evaluation or in applications such as an aircraft simulator where very high platform pose accuracy is not required, these error are certainly negligible. However, for accuracy analysis or applications that require high pose accuracy, this model is improper. Therefore, the accurate model which can accommodate the above errors need to be developed.



### 3.2 Modeling of Multi-Axis Joints

As mentioned above, U-joints and ball joints are used in the construction of the Stewart platform, therefore there is a need to model these multi-axis joints. A U-joint can rotate about two axes  $Z_0$  and  $Z_1$  (Figure 3.1) while a ball joint can rotate about three axes  $Z_0$ ,  $Z_1$  and  $Z_2$  (Figure 3.2). The D-H convention [Denavit and Hartenberg, 1955] is used to model these joints so that the above errors can be included. By the D-H convention,  $T_i$  represents homogeneous a transformation from frame  $\{i-1\}$  to frame  $\{i\}$  and is defined by:

$$T_i = \begin{bmatrix} R_i & q_i \\ 0 & 1 \end{bmatrix} \quad (3.1)$$

where

$$R_i = \begin{bmatrix} \cos \theta_i & -\sin \theta_i \cos \alpha_i & \sin \theta_i \sin \alpha_i \\ \sin \theta_i & \cos \theta_i \cos \alpha_i & -\cos \theta_i \sin \alpha_i \\ 0 & \sin \alpha_i & \cos \alpha_i \end{bmatrix} \quad (3.2)$$

and

$$q_i = [a_i \cos \theta_i, a_i \sin \theta_i, d_i]^T \quad (3.3)$$

In the Equation (3.2) and (3.3), four D-H parameters, namely the link length  $a_i$ , the twist angle  $\alpha_i$ , the link offset  $d_i$ , and the joint angle  $\theta_i$ , are conventionally defined as follows:

$a_i$ : the distance between  $Z_{i-1}$  and  $Z_i$ .

$\alpha_i$  : the angle between  $Z_{i-1}$  and  $Z_i$  .

$d_i$  : the distance from  $X_{i-1}$  to  $X_i$  along  $Z_{i-1}$  .

$\theta_i$  : the angle between  $X_{i-1}$  to  $X_i$  along  $Z_{i-1}$  .

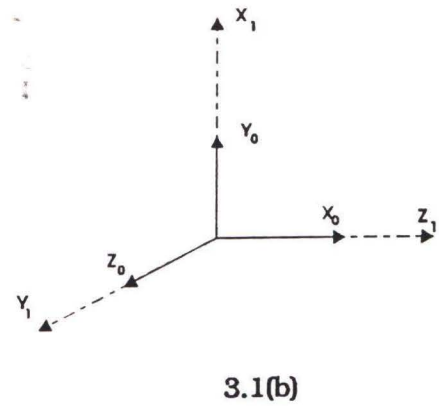
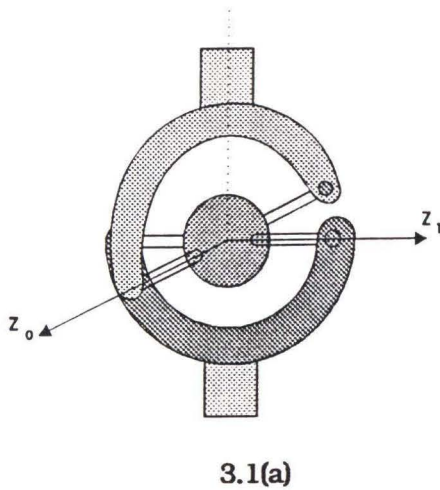


Figure 3.1 U-joint and its coordinate frames

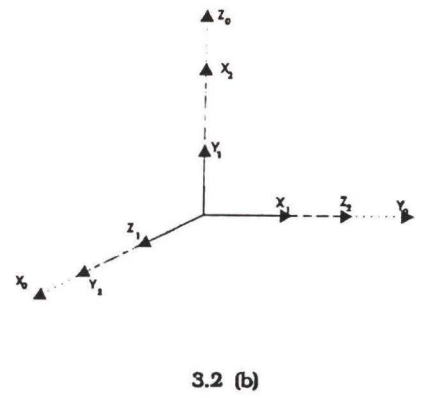
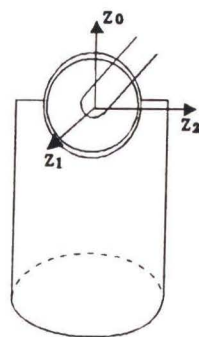
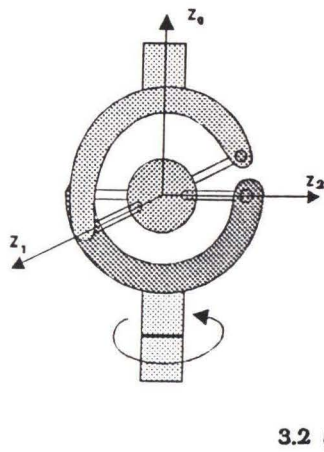


Figure 3.2 Ball joint and its coordinate frames

For a U-joint, the parameters in  $T_1$  can be used to represent the manufacturing tolerance. For example,  $a_1$  and  $d_1$  define the distance between the axes and  $\alpha_1$  the twist angle between them. Similarly, the parameters in the transformation matrices  $T_1$  and  $T_2$ ,  $(a_1, a_2, d_1, d_2, \alpha_1, \alpha_2)$  can be used to model errors of a ball joint. Joint angle  $\theta_i$  are passive joint variables and will be discussed shortly.

### 3.3 Modeling of Joint-Link Trains

A **joint-link train** is defined as the consecutive structure elements starting from the center of the base,  $\{B\}$ , going to the center of the moving plate  $\{P\}$  through one of the links. In modeling the joint-link train, additional manufacturing and installation errors have to be considered: 1) Dimensional errors of the base (or position errors of the U-joints); 2) Dimensional errors of the moving plate (or position errors of the ball joints); 3) Offset errors in the length readings of the prismatic actuator; and 4) Installation errors that occur when connecting the joints to the actuators.

By treating each joint-link train as a serial kinematic chain, the above manufacturing and assembly errors can be accurately modeled. Kinematically, a joint-link train can be modeled by a set of consecutive transformations from frame  $\{B\}$  to frame  $\{P\}$  as illustrated in Figure 3.3. In this figure frames were assigned as follows: frames  $\{0\}$  and  $\{1\}$  to the U-joint; frame  $\{2\}$  to the prismatic joint; and frames  $\{3\}$  to  $\{5\}$  to the ball joint. For convenience, an additional frame  $\{6\}$ , the origin of which coincides with that of frame  $\{5\}$  and its orientation is the same as of

frame  $\{P\}$ , is introduced. Eight transformations are needed to model each joint-link train in order to express the pose of the end-effector with respect to the base:

$${}^B T_P = {}^B T_0 T_1 T_2 T_3 T_4 T_5 T_6 T_P \quad (3.4)$$

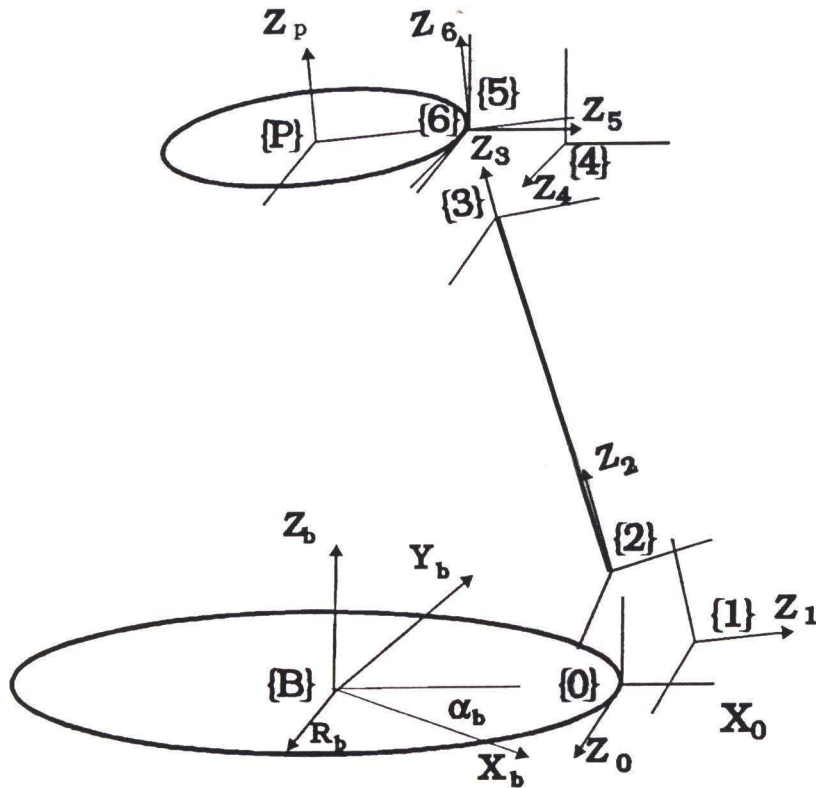


Figure 3.3 A Joint-Link train and its coordinate frames

where  ${}^B T_0$  and  $T_P$  are fixed homogeneous transformations from  $\{B\}$  to  $\{0\}$  and from  $\{6\}$  to  $\{P\}$  respectively. Denote  $T = \{R, q\}$ , then  $T_P = \{R_P, q_P\}$  where  $R_P$  and  $q_P$  are given by:

$$\mathbf{R}_p = \mathbf{I} \quad (3.5)$$

and

$$\mathbf{q}_p = -\mathbf{p} = -\{p_x, p_y, p_z\} \quad (3.6)$$

where  $\mathbf{p}$  is the coordinates of the origin of  $\{6\}$  with respect to  $\{P\}$ .

The nominal D-H parameters for  $T_0, \dots, T_6$  of a joint-link train are listed in Table 3.1. Note that  $\theta_0$  in the table is a geometric parameter.

T	a	d	$\alpha$	$\theta$
0	$R_b$	0	$90^\circ$	$\theta_0$
1	0	0	$90^\circ$	$\theta_1$
2	0	0	$90^\circ$	$\theta_2$
3	0	$d_3$	$0^\circ$	$0^\circ$
4	0	0	$90^\circ$	$\theta_4$
5	0	0	$90^\circ$	$\theta_5$
6	0	0	$90^\circ$	$\theta_6$

Table 3.1: Nominal D-H parameters of a joint-link train

The transformations  $T_1$  to  $T_6$ , describe a 2R-P-3R serial manipulator. However, in this case the revolute joints are passive ones, that is, these have neither actuators nor transducers. Three types of parameters can be distinguished in each joint-link train: 1) Measurable variables,  $d_3$ , which describes extension of the prismatic joints; 2) Unmeasurable variables,  $\theta$ , that describe the joint angles  $\theta_1, \theta_2, \theta_4, \theta_5, \theta_6$ ; and 3) Geometric parameters describing the dimension of the platform.

There are seven constant geometric parameters for each joint-link train:  $a_3=0$  and  $d_4=0$  since joint 3 is a prismatic joint [Mooring et al, 1990; Hsu and Everett, 1987];  $a_6=0$  and  $d_6=0$  since the origin of the additional frame {6} coincides with the origin of frame {5}; and  $\mathbf{R}_p=\mathbf{I}$  due to the fact that the orientation of the frame {6} is same as that of frame {P}. In the following, variables will be referred to as vector  $\mathbf{v}$  and geometric parameters as vector  $\mathbf{u}$ .

The geometric parameter vector,  $\mathbf{u}$ , in the transformations  $\mathbf{T}_0, \dots, \mathbf{T}_6$ , and  $\mathbf{T}_p$  that are used to model the manufacturing and assembly errors mentioned above, for each joint-link train, are summarized in Table 3.2.

Transformation	Parameters	Errors which can be modeled
$\mathbf{T}_0$	$a_0, d_0, \alpha_0, \theta_0$	Dimensional errors of the base
$\mathbf{T}_1$	$a_1, d_1, \alpha_1$	Errors in the U-joint
$\mathbf{T}_2$	$a_2, d_2, \alpha_2$	Installation errors between the actuator and the U-joint
$\mathbf{T}_3$	$\alpha_3, \theta_3$	Installation errors between the actuator and the ball joint
$\mathbf{T}_4$	$a_4, \alpha_4$	Errors in the ball joint
$\mathbf{T}_5$	$a_5, d_5, \alpha_5$	Errors in the ball joint
$\mathbf{T}_6$	$\alpha_6$	Dimensional errors of the moving plate
$\mathbf{T}_p$	$\mathbf{p}$	Dimensional errors of the moving plate

Table 3.2: Modeling of errors by kinematic parameters

There is a joint variable offset for each joint-link train:  $\delta d_3$  which is the difference between the true value of a variable and its transducer reading. All together there are 22 independent geometric parameters in each joint-link train.

### 3.4 Complete Model of the Stewart Platform

A complete model of a Stewart platform is composed of six similar joint-link trains:

$${}^B\mathbf{T}_P = {}^B\mathbf{T}_{0j} \mathbf{T}_{1j} \mathbf{T}_{2j} \mathbf{T}_{3j} \mathbf{T}_{4j} \mathbf{T}_{5j} \mathbf{T}_{6j} \mathbf{T}_{Pj} \quad j=1,2,\dots,6 \quad (3.7)$$

where  $j$  is an index for the joint-link trains.

For a nominal model,  $\mathbf{T}_{1j}$ - $\mathbf{T}_{6j}$  ( $j=1,\dots,6$ ) are given in Table 3.1 as  $\mathbf{T}_1$ - $\mathbf{T}_6$ . The transformation from the frame  $\{6\}$  to the plate center  $\{P\}$ ,  $\mathbf{T}_{Pj}$ , is given by  $\mathbf{T}_{Pj} = \{\mathbf{R}_{Pj}, \mathbf{q}_{Pj}\}$  where  $\mathbf{R}_{Pj} = \mathbf{I}$  and  $\mathbf{q}_{Pj} = -\mathbf{p}_j$ , where  $\mathbf{p}_j$  is given by Equation 2.1.  ${}^B\mathbf{T}_{0j}$  is given by Table 3, in which  $R_b$  is the base radius and  $\alpha_b$  is the base angle.  $R_b$  and  $\alpha_b$  are the same as in Equation 2.1.

Stewart platform is virtually a closed-loop mechanism, or a manipulator that is made of a set of closed kinematic loops. One aspect of modeling of a closed-loop mechanism is the existence of a number of dependent variables [Mooring, Roth and Driels, 1991]. The rotary joint variables in each joint-link train,  $\theta_1, \theta_2, \theta_4, \theta_5, \theta_6$ , are the dependent ones. Each of these joints has neither an actuator nor a transducer and passively moves along the platform. It will be shown in Chapter 4 that these variables are determined uniquely by the platform pose. In other hand, the pose is

not determined by the joints of a single joint-link train but by six joint-link trains, or specifically, by six prismatic actuators.

j	a	d	$\alpha$	$\theta$
1	$R_b$	0	$90^\circ$	$\alpha_b$
2	$R_b$	0	$90^\circ$	$120^\circ - \alpha_b$
3	$R_b$	0	$90^\circ$	$120^\circ + \alpha_b$
4	$R_b$	0	$90^\circ$	$240^\circ - \alpha_b$
5	$R_b$	0	$90^\circ$	$240^\circ + \alpha_b$
6	$R_b$	0	$90^\circ$	$360^\circ - \alpha_b$

Table 3.3: Nominal D-H parameters of  ${}^B T_{0j}$  ( $j=1,2,\dots,6$ ) of Stewart platform

According to Everett and Lin [1986], two types of equations are required for modeling of a manipulator with closed loops: (1) the open-loop transformations, which relate the end-effector to the world coordinate frame; (2) the closed-loop transformations which contain the closed-loop constraint equations. Both types of equations are contained in Equation (3.7). It becomes more clear that Equation (3.7) can be also interpreted as closed-loop constraint equations if it is written as:

$${}^w T_{0i} T_{1i} T_{2i} T_{3i} T_{4i} T_{5i} T_{6i} T_{pi} ({}^w T_{0ij} T_{1j} T_{2j} T_{3j} T_{4j} T_{5j} T_{6j} T_{pj})^{-1} = I$$

$$i, j = 1, 2, \dots, 6, i \neq j \quad (3.8)$$



Figure 3.4a is an example of closed-loop constraints. Figure 3.4b shows its equivalent loop. The equation for the equivalent loop can be easily obtained by manipulating Equation 3.8.

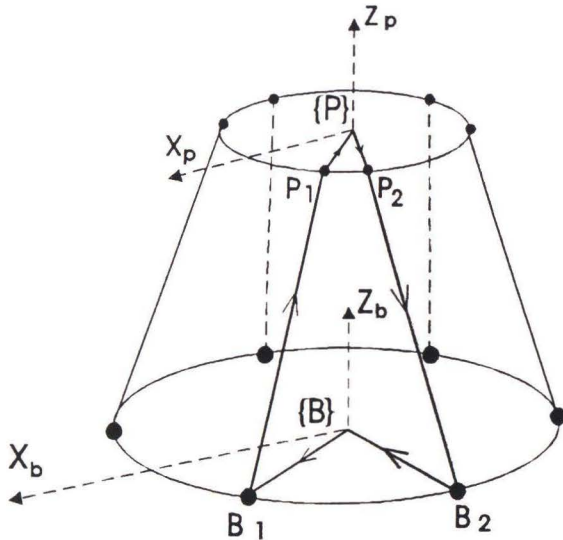


Figure 3.4a

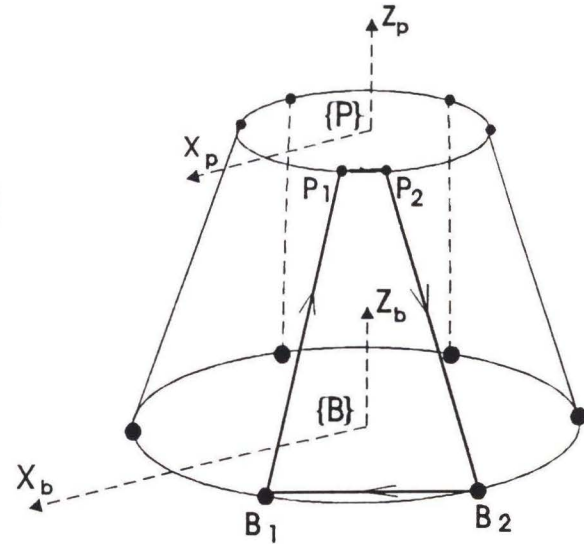


Figure 3.4b

Figure 3.4 An example of the closed-loop constraint

In summary, the proposed accurate model of Stewart platform accommodates all manufacturing and assembly errors and all information for the kinematic analysis. Also, the accurate model is compatible with the conventional one. It will be shown in the next chapter that if the nominal parameters (in the Table 3.1 and 3.3) are used, the forward and inverse kinematics solutions of this model are identical to the solutions of the conventional model.

## **CHAPTER 4**

### **STEWART PLATFORM ACCURACY**

The accuracy of a manipulator is one of the major concerns in the manipulator design and applications. This chapter discusses the accuracy problem of the Stewart platform. Section 4.1 provides algorithms for solving the forward and inverse kinematics of the accurate kinematic model of Stewart platform. These are used to evaluate the accuracy of a Stewart platform with specified manufacturing tolerances and assembly errors. Section 4.2 investigates the effects of different manufacturing tolerances on the platform accuracy. Concluding remarks are given in Section 4.3.

#### **4.1 Kinematic Analysis of the Accurate Model**

##### **4.1.1 Forward Kinematics**

In order to evaluate the accuracy of Stewart platform and to investigate the effects of the different errors on the platform accuracy, it is necessary to compute the pose of the end-effector from the measured link lengths, based on the accurate model which takes into account all platform manufacturing and assembly tolerances.

This requires the solution of the general forward kinematic problem for the accurate model.

The general forward kinematic problem can be stated as follows: Given the actual link length vector  $\mathbf{d}^a$ , the nominal parameters  $\mathbf{u}^n$  and the actual parameters  $\mathbf{u}^a$ , find the actual end-effector pose  $\mathbf{x}^a$ . Since there is no closed form solution for the forward kinematics of a general Stewart platform even for the nominal case [Nanua, Waldron and Murthy, 1990], a numerical method is used to solve this problem.

The Gauss-Newton least square algorithm can be used effectively to solve the nonlinear optimization problem with a objective function of summation of squares [Gill, Murray and Wright, 1981]. The algorithm adopted here is based on this method by which the following cost function:

$$Q(\mathbf{x}) = \sum_{j=1}^6 [d_j^a - |\phi_j(\mathbf{x}, \mathbf{u})|]^2 \quad (4.1)$$

is minimized by choosing  $\mathbf{x}$ , where  $\phi_j(\mathbf{x}, \mathbf{u})$  is the  $j^{\text{th}}$  joint-link train inverse kinematics solution for  $d_j$  ( $d_j$  is measured from the minimum length of the link and therefore  $d_j > 0$ ). If the nominal parameters,  $\mathbf{u}^n$ , are used,  $\phi_j(\mathbf{x}, \mathbf{u}^n)$  has an analytic solution given by Equation (4.6, 4.9), see next section. The resulting  $\mathbf{x}$  from minimizing the cost function is taken as the solution of the nominal forward kinematics problem. If the accurate model is applied,  $\phi_j(\mathbf{x}, \mathbf{u}^a)$  has to be obtained numerically by solving the general inverse kinematics problem (as described in the next section and Chapter 6), and then the obtained  $\mathbf{x}$  is taken as the solution for the general forward kinematics problem.

The problem is solved following these steps ( $k$  is the iteration index):

1. Make an initial guess of  $\mathbf{x}$ .
2. Using  $\mathbf{x}$ , perform the general inverse kinematics for each joint-link train and obtain an estimation for all link lengths  $\mathbf{d}_k$ .
3. Compute the cost function  $Q_k = |\mathbf{d}^a - \mathbf{d}_k|$ .
4. Check the termination condition,  $Q_k < \epsilon$ . If satisfied, then  $\mathbf{x}^a = \mathbf{x}_k$  and stop the program. Otherwise continue with step 5.
5. Calculate the cost function gradient,  $\nabla Q(\mathbf{x})$ , using finite difference operation.
6. Update the estimated  $\mathbf{x}_k$  by  $\mathbf{x}_{k+1} = \mathbf{x}_k + \Delta \mathbf{x}_k$ , where  $\Delta \mathbf{x}_k = -[\nabla Q(\mathbf{x})]^{-1}(\mathbf{d}^a - \mathbf{d}_k)$ .
7. Repeat from step 2.

There are several remarks regarding the above procedure.

- 1) The initial guess in step 1 can be made as follows:

$$\mathbf{x} = [0, 0, 0, 0, 0, d_{ave}] \quad (4.2)$$

where  $d_{ave}$  is the average length of the six links.

- 2) The method of formulating the gradient matrix  $\nabla Q(\mathbf{x})$  is described below. Denote  $f_j = d_j - \phi_j(\mathbf{x}, \mathbf{u})$ , then the gradient  $\nabla Q(\mathbf{x})$  can be obtained by

$$\nabla Q(\mathbf{x}) = \begin{bmatrix} \frac{\partial f_1}{\partial x_1} & \frac{\partial f_1}{\partial x_2} & \cdots & \frac{\partial f_1}{\partial x_6} \\ \frac{\partial f_2}{\partial x_1} & \frac{\partial f_2}{\partial x_2} & \cdots & \frac{\partial f_2}{\partial x_6} \\ \frac{\partial f_6}{\partial x_1} & \frac{\partial f_6}{\partial x_2} & \cdots & \frac{\partial f_6}{\partial x_6} \end{bmatrix} \quad (4.3)$$

Since functions  $\phi_j$  and  $f_j$  ( $j=1,2,\dots,6$ ) is can only be obtained by numerical methods for the accurate model, the partial derivative of each function  $f_j$  with

respect to the  $i^{\text{th}}$  element of the pose vector have to be computed by difference method. It means that each iteration involves 36 general inverse kinematics solutions of the accurate model.

- 3) Simulation studies show that the Gauss-Newton least square algorithm is very effective in solving the forward kinematics problems of Stewart platform both for the conventional model and for the accurate model. The solution converges to the true value after 4-5 iterations using this method. As a comparison, it takes more than one hundred iterations for the convergence if the descend method [Avreil 1976] is applied.
- 4) Simulation studies verified that if the nominal parameters (the parameters listed in the Table 3.1 and 3.3) are used in the forward kinematics of the accurate model, the result is identical to the solution of the forward kinematics of the conventional model. It indicates that the accurate model is compatible with the conventional model, and the conventional model is a special case of the accurate model, or an accurate model with the nominal parameters.

#### 4.1.2 Inverse Kinematics

The general inverse kinematic problem can be stated as follows: Given the actual platform pose,  $\mathbf{x}^a$ , the nominal parameters  $\mathbf{u}^n$  and the actual parameters  $\mathbf{u}^a$ , find the actual joint variables  $\mathbf{v}^a$  (including  $\mathbf{d}^a$  and  $\boldsymbol{\theta}^a$ ).

Although inverse kinematics problem solution is trivial for a conventional model (as given by Equation 2.2), it is not simple for the accurate model. The method employed in this study to solve Stewart platform inverse kinematics is to obtain the **solution of the inverse kinematic problem of each joint-link train**, treated

as a 2R-P-3R serial robot with two additional homogeneous transformations. For most serial industrial robots, analytical solutions for the nominal inverse kinematic problem do exist although these solutions are not necessarily unique. However, in this particular case, i. e. for the nominal model of a joint-link train of a Stewart platform, the analytical solution not only exists but is also unique. The uniqueness of the solution is due to the physical constraints introduced by the ball and the U-joints. For example, joint angle  $\theta_1$  (see Figure 4.1), the angle between axes  $X_0$  and  $X_1$ , can vary only within the range of  $0^\circ < \theta_1 < 180^\circ$ . Similar constraint is applied to  $\theta_2$ ,  $\theta_5$  and  $\theta_6$ . (Refer Figure 2.2 and 3.2). However, there is no angle limitation for  $\theta_4$  (rotational angle of the ball-joint about the Z axis).

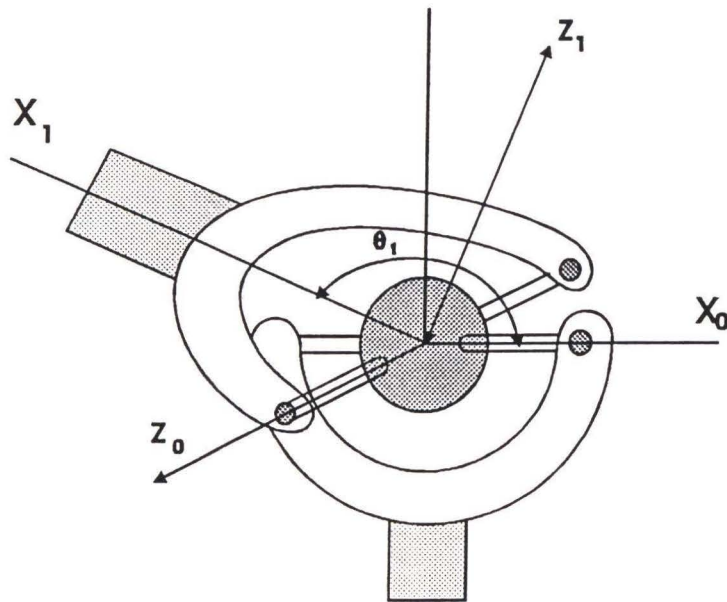


Figure 4.1 Range of a rotary joint

The analytical inverse kinematic solution of a joint-link train of the accurate model with nominal parameters is given as follows.

From Equation (3.4) one can obtain

$${}^0\mathbf{T}_6 = \mathbf{T}_1\mathbf{T}_2\mathbf{T}_3\mathbf{T}_4\mathbf{T}_5\mathbf{T}_6 = (\mathbf{T}_0)^{-1} {}^B\mathbf{T}_p(\mathbf{T}_p)^{-1} \quad (4.4)$$

The right side of the equation is known. Let  ${}^0\mathbf{T}_6 = \{{}^0\mathbf{R}_6, {}^0\mathbf{q}_6\}$ ,  ${}^B\mathbf{T}_p = \{\mathbf{R}, \mathbf{q}\}$  and  $\mathbf{T}_p = \{\mathbf{R}_p, \mathbf{q}_p\}$ . From equation (3.1) and (4.4), one can obtain

$${}^0\mathbf{R}_6 = \mathbf{R}_0^T \mathbf{R} \mathbf{R}_p^T \quad (4.5)$$

$${}^0\mathbf{q}_6 = \mathbf{R}_0^T (\mathbf{R} \mathbf{p} + \mathbf{q}_p - \mathbf{b}) \quad (4.6)$$

where superscript T stands for the transpose of matrix.  ${}^0\mathbf{q}_6$  is can also be written as

$${}^0\mathbf{q}_6 = \mathbf{q}_1 + \mathbf{R}_1\mathbf{q}_2 + \mathbf{R}_1\mathbf{R}_2\mathbf{q}_3 + \mathbf{R}_1\mathbf{R}_2\mathbf{R}_3\mathbf{q}_4 + \mathbf{R}_1\mathbf{R}_2\mathbf{R}_3\mathbf{R}_4\mathbf{q}_5 + \mathbf{R}_1\mathbf{R}_2\mathbf{R}_3\mathbf{R}_4\mathbf{R}_5\mathbf{q}_6 \quad (4.7)$$

The nominal parameters,  $\mathbf{q}_1, \mathbf{q}_2, \mathbf{q}_4, \mathbf{q}_5, \mathbf{q}_6 = 0^\circ$ ,  $\alpha_1, \alpha_2, = 90^\circ$ . Substituting these values in Equation (4.7), yields

$${}^0\mathbf{q}_6 = [d_3 \cos\theta_1 \sin\theta_2, d_3 \sin\theta_1 \sin\theta_2, -d_3 \cos\theta_2]^T \quad (4.8)$$

${}^0\mathbf{q}_6$  is known from (4.6). Let  ${}^0\mathbf{q}_6 = [{}^0\mathbf{q}_{61}, {}^0\mathbf{q}_{62}, {}^0\mathbf{q}_{63}]$ . Since the range of the rotational angle of joints  $\theta_1$  and  $\theta_2$  is limited between  $0^\circ$  and  $180^\circ$ , the following expressions can be solved for directly:

$$d_3 = |{}^0\mathbf{q}_6| = \sqrt{{}^0q_{61}^2 + {}^0q_{62}^2 + {}^0q_{63}^2} \quad (4.9)$$

$$\theta_2 = \arccos\left(-\frac{{}^0q_{63}}{d_3}\right) \quad (4.10)$$

$$\theta_1 = \arccos\left(-\frac{{}^0q_{61}}{d_3 \sin \theta_2}\right) \quad (4.11)$$

${}^0\mathbf{R}_6$  can be written as

$${}^0\mathbf{R}_6 = \mathbf{R}_1 \mathbf{R}_2 \mathbf{R}_3 \mathbf{R}_4 \mathbf{R}_5 \mathbf{R}_6 \quad (4.12)$$

we have

$$(\mathbf{R}_1 \mathbf{R}_2 \mathbf{R}_3)^{-1} {}^0\mathbf{R}_6 = \mathbf{R}_4 \mathbf{R}_5 \mathbf{R}_6 \quad (4.13)$$

Since  $\alpha_3$  and  $\theta_3$  are given,  $\theta_2$  and  $\theta_1$  have been obtained from Equations (4.10, 4.11),  $\mathbf{R}_1$ ,  $\mathbf{R}_2$ ,  $\mathbf{R}_3$  can be computed. Note that  ${}^0\mathbf{R}_6$  is given by (4.5), so the left side of (4.13) is obtained. Let it be a 3x3 matrix  $\mathbf{M}$  with components  $m_{ij}$ . Left-multiplying  $\mathbf{M}$  by  $\mathbf{R}_4^{-1}$  yields

$$\mathbf{R}_4^{-1} \mathbf{M} = \mathbf{R}_5 \mathbf{R}_6 \quad (4.14)$$

The constant  $\alpha_4$ ,  $\alpha_5$  and  $\alpha_6$  are now substituted into the equation. Expanding it using the nominal constant parameters, one can obtain a set of equations which can be used to compute the joint variable  $\theta_4$  to  $\theta_6$ . The expressions for  $\theta_4$  to  $\theta_6$  are:



$$\theta_4 = \arctan 2\left(\frac{m_{21}}{m_{12}}\right) \quad (4.15)$$

$$\theta_5 = \arccos(-m_{32}) \quad (4.16)$$

$$\theta_6 = \arccos\left(-\frac{m_{31}}{\sin\theta_5}\right) \quad (4.17)$$

Since  $\theta_5$  and  $\theta_6$  are less than  $180^\circ$  and greater than  $0^\circ$ , these are uniquely determined.

Comparing Equations (4.6, 4.9) with Equation (2.3), one can see that if the nominal parameters are used, the solution of the link length of the accurate model is identical to that of the conventional model. However, if the accurate model is used, the other passive joint variables can be obtained. The analytic solution of the passive rotary joint variables provides insight of the joint motion. Furthermore, the solution is necessary for solving the inverse kinematics problem of the general accurate model.

Although a unique analytical solution of the inverse kinematics problem for an accurate model with nominal parameters exists, it may be impossible to obtain an analytical solution for the inverse kinematics problem of an accurate model with actual or general parameters. A numerical solution is inevitable, which is similar to solving inverse kinematics problem of serial manipulator with actual or identified parameters. Solution for the accurate model of Stewart platform with general parameters is obtained by **solving the general inverse problem of each joint-link train**. The model-based Newton-Raphson method is employed to solve this problem. The detailed procedure for the algorithm will be given in Chapter 6, Section 6.2.

## 4.2 Effect of Manufacturing Tolerances on the Platform Accuracy

This section investigates the effect of the following factors on the platform accuracy: 1) Manufacturing tolerances of the U and ball joints; 2) Installation errors of the U-joints and ball joints; and 3) Measurement offsets of the link actuators. The study is performed by simulation of a particular platform having the following dimensions :  $R_b=3$  feet,  $R_p=1$  foot; link length ranges between 4.5 to 7.5 feet,  $\alpha_b=30^\circ$  and  $\alpha_p=15^\circ$ . The values for the manufacturing errors or D-H parameters deviations, are given as follows:

1. Manufacturing tolerance for both U-joints and ball joints (D-H parameters):

$$|\Delta d| < 0.004 \text{ inch}, |\Delta a| < 0.004 \text{ inch and } |\Delta \alpha| < 0.1^\circ .$$

2. Installation errors of the ball joints on the moving plate (tolerances):

$$|\Delta p_x| , |\Delta p_y| \text{ and } |\Delta p_z| < 0.012 \text{ inch.}$$

3. Installation errors of the U-joints on the base (D-H parameters):

$$|\Delta a| < 0.24 \text{ inch}, |\Delta \alpha| < 1^\circ \text{ and } |\Delta d| < 0.12 \text{ inch.}$$

4. Offsets of the link actuators:

$$|\delta d| < 0.024 \text{ inch.}$$

The above values are all realistic figures related to a physical platform currently under construction at Florida Atlantic University. The selection of large tolerance (about a quarter of inch) on the base is due to the fact that the base is constructed from welded members. The tolerance of the plate is much smaller than that of the base since the plate is made by machine tools. The errors used in the simulation were randomly selected according to uniform distribution within the above ranges.

The effects of the above errors on the pose accuracy of the platform were investigated one by one following the procedure below:

1. A random error vector within the range specified above was added to the corresponding nominal parameters.
2. A set of desired pose trajectories,  $\mathbf{x}^n$ , within the workspace was specified.
3. The six joint lengths variables were computed by the nominal inverse kinematics.
4. The actual pose trajectory  $\mathbf{x}^a$  was obtained by the general forward kinematics using the parameters assigned in step 1.
5. The pose error was computed from  $\mathbf{x}^n$  and  $\mathbf{x}^a$ .

The results presented in Figures 4.2-4.4 illustrate the following errors: 1) platform pose translation errors  $dx$ ,  $dy$  and  $dz$  along the X, Y and Z axes respectively; 2) The norm of the translation error  $dl$ ; and 3) Orientation errors  $dR$ ,  $dP$  and  $dY$  about the Z, Y and X axes respectively.

Figure 4.2 compares the translation error norm,  $dl$ , for the above four tolerance error sources. As expected the tolerances on the platform base caused significantly larger errors than those due to the other error sources. To further investigate the effects of the base tolerances, the translation and orientation errors were calculated and are shown in Figure 4.3. As shown, the value of the translation error reached a maximum of about 1 inch and the orientation error a maximum of about 5 degrees. Moreover, the orientation errors change sign along the trajectory which cause a 'rocking' motion.

Since the pose error is being determined by all individual tolerances, which may sometimes cancel one another and sometimes accumulate, the simulation program was executed again for the general case where all manufacturing errors exist. The results of this run are shown in Figure 4.4.

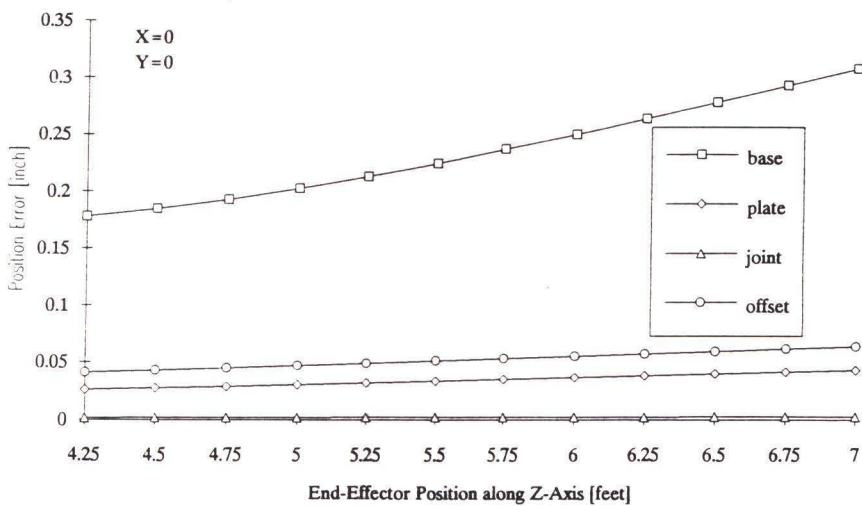
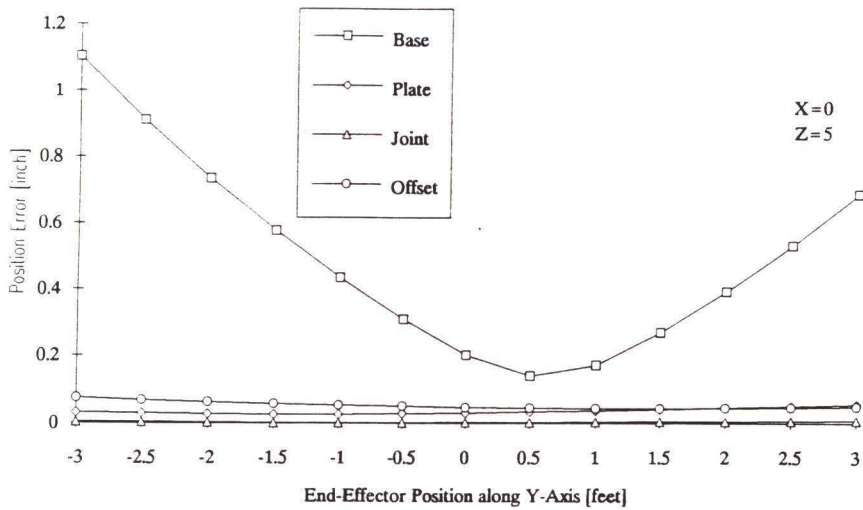
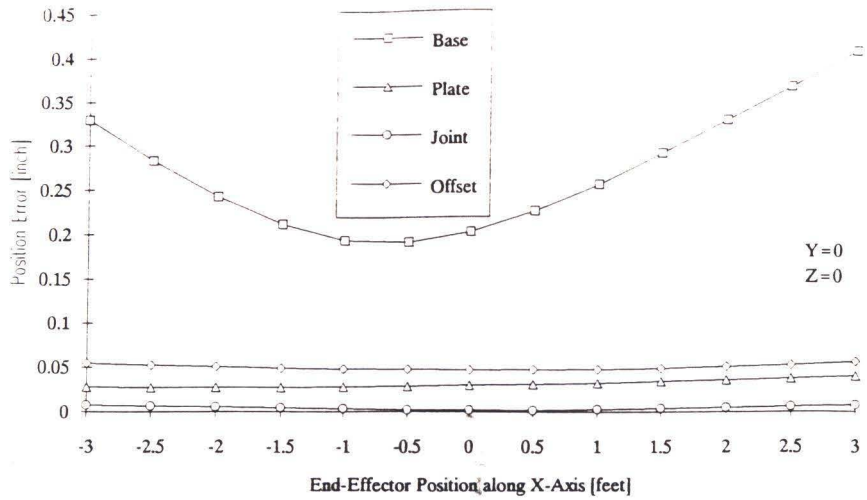
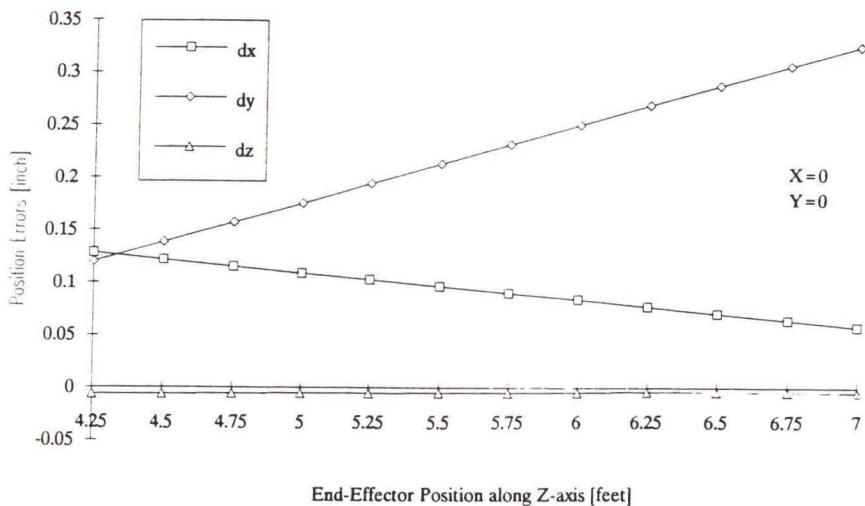
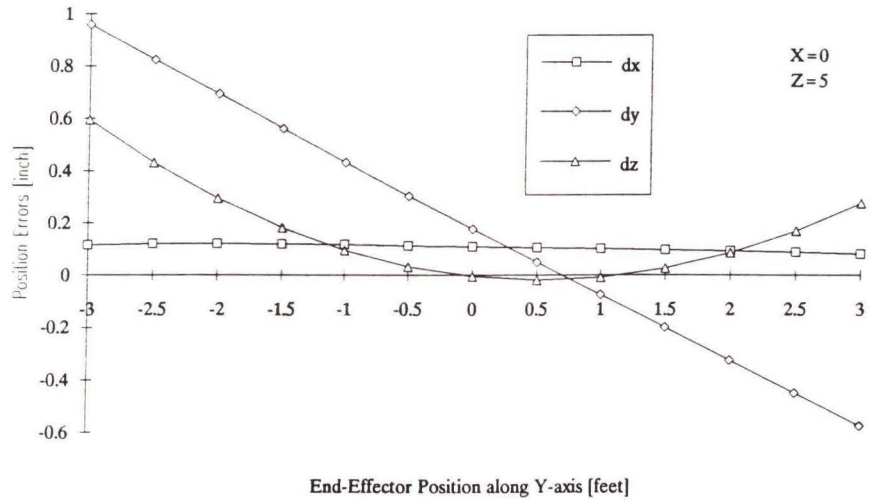
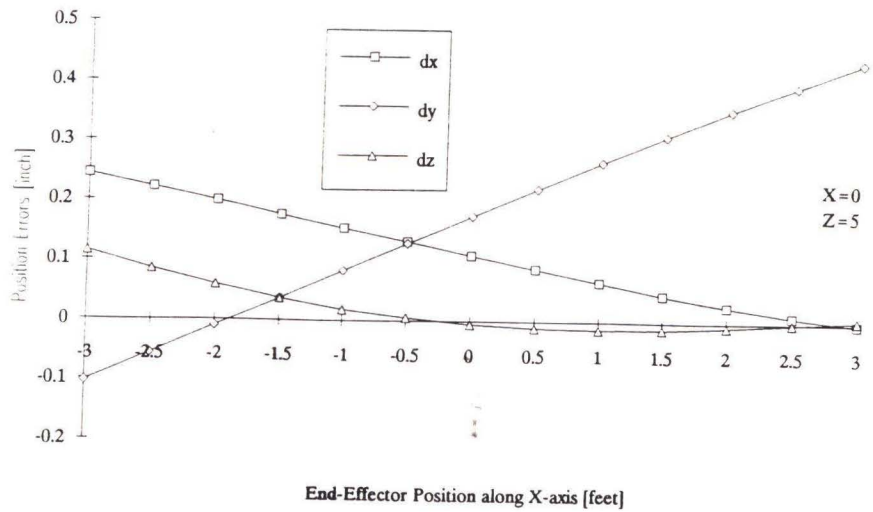


Figure 4.2 Platform maximum position error due to different manufacturing errors



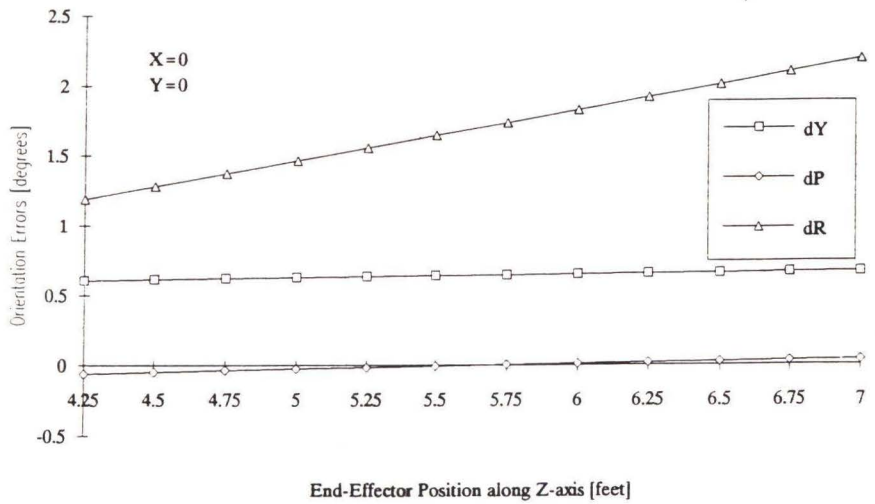
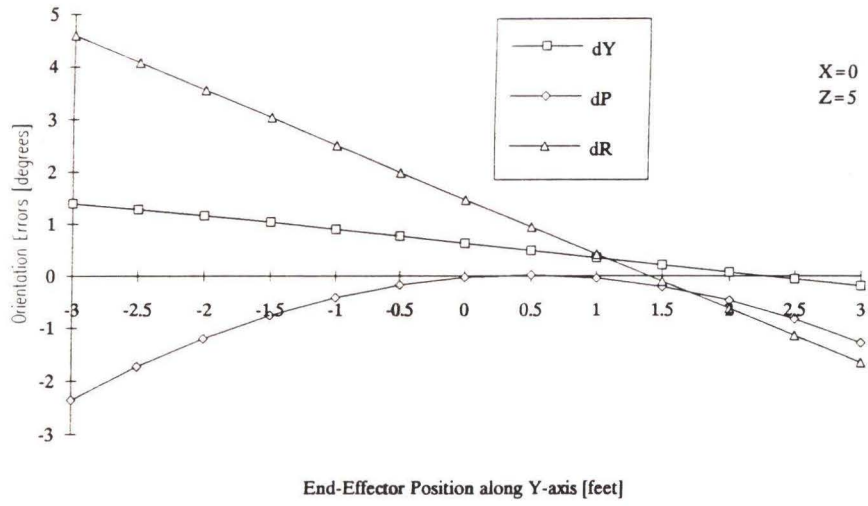
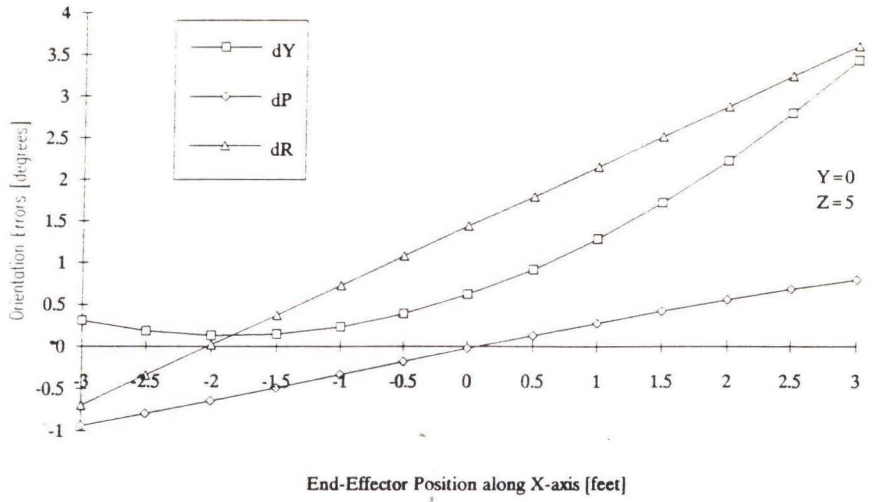
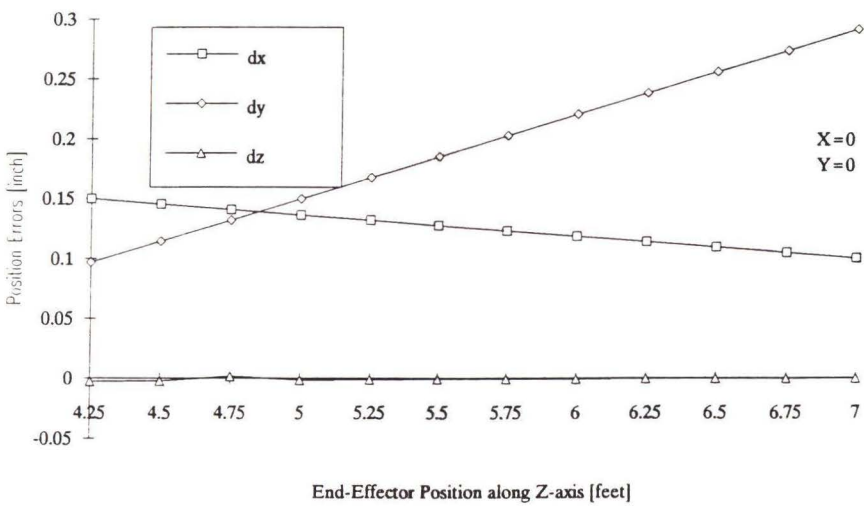
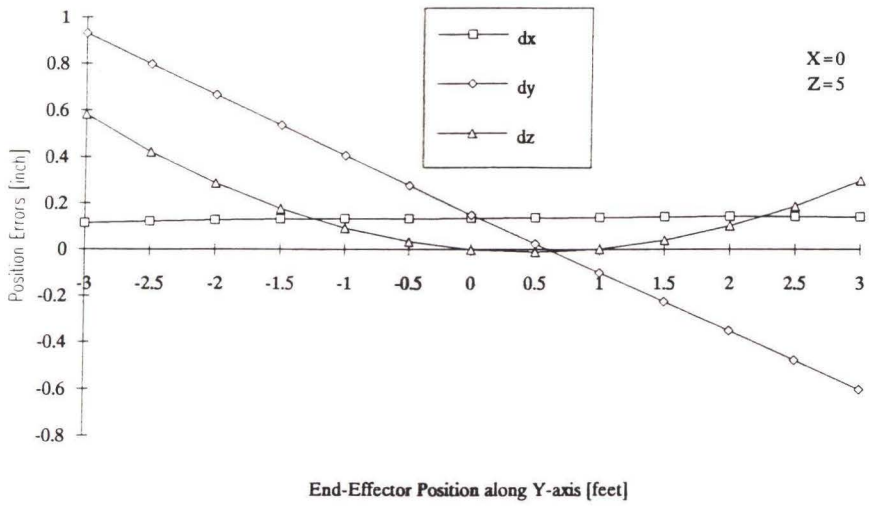
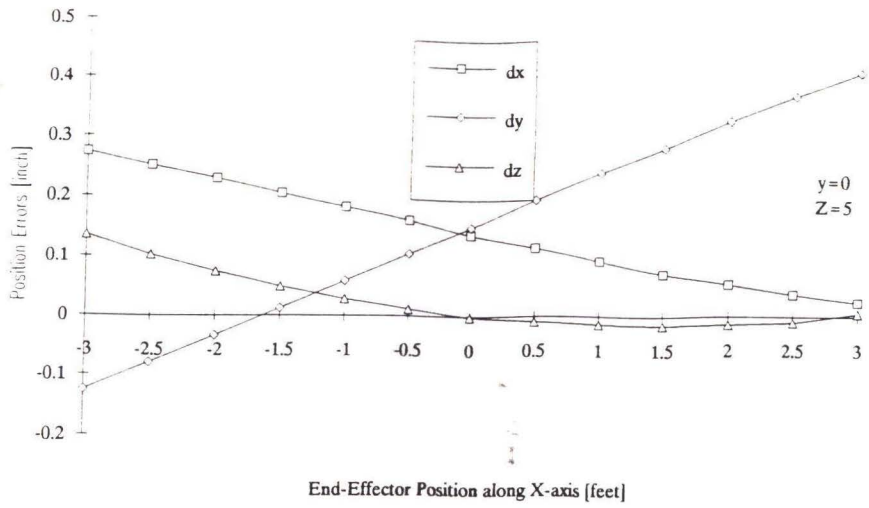


Figure 4.3 Platform pose error due to base tolerance



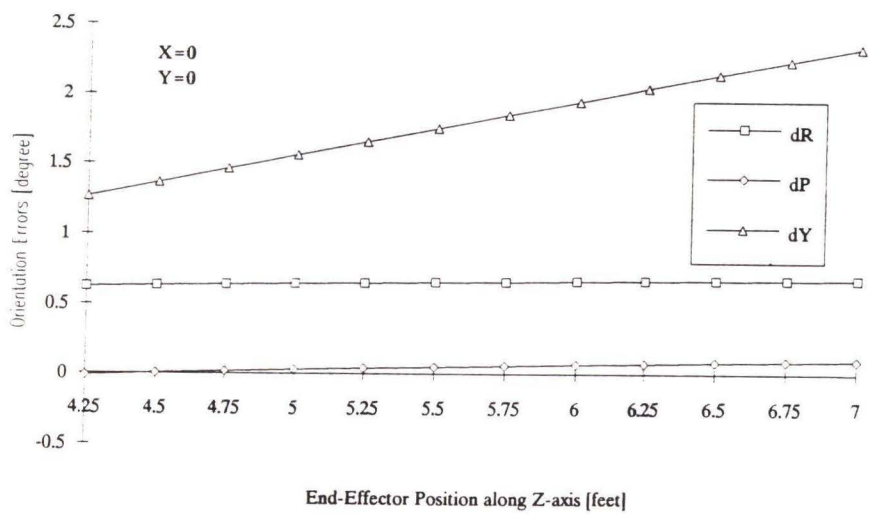
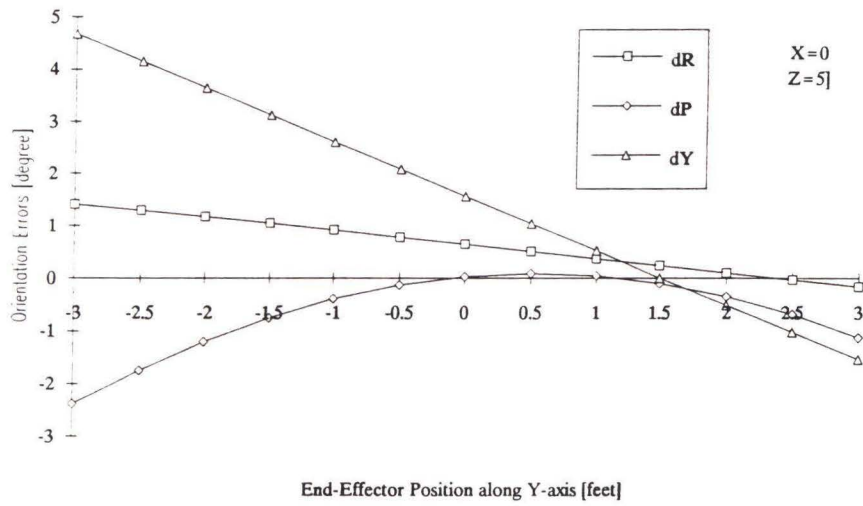
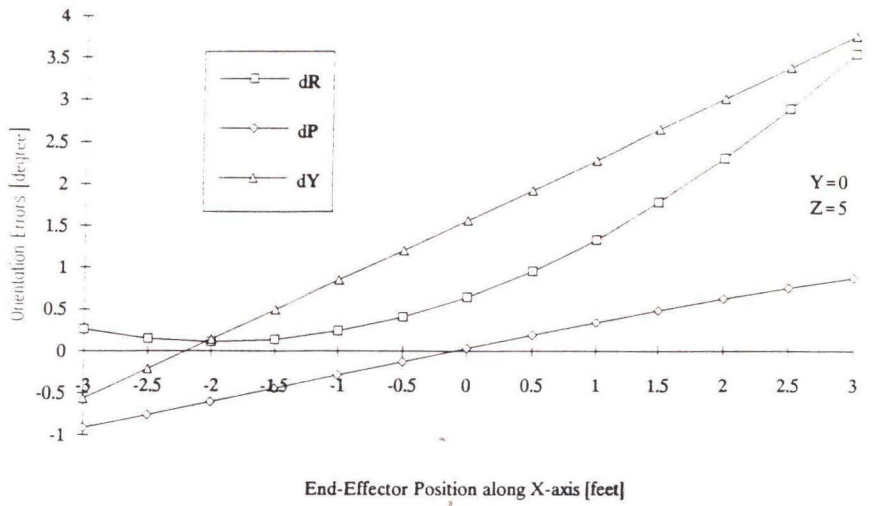


Figure 4.4 Platform pose error due to all manufacturing errors



The following conclusions can be obtained from these simulation results:

1. The order of magnitude of the pose error is in the same as that of the corresponding tolerances. For example, the tolerances specified for the fabrication of the base, caused errors in the location of U-joints in order of magnitude of 1/4" which resulted in pose errors in the order of magnitude of 1".
2. If realistic manufacturing tolerances are considered, the accuracy of the Stewart platform has the same order of magnitude as that of a serial manipulator with similar nominal dimensions.
3. The maximum pose errors always occur at the workspace boundary. If a high accuracy is expected, it is suggested that work area should be around the platform center.
4. The effect on the platform accuracy of manufacturing errors of the joints connecting actuators to both base and plate is negligible compared to the other manufacturing errors. In most cases it is reasonable to neglect these errors.

### **4.3 Concluding Remarks**

The algorithms for solving the forward kinematics problem of the accurate model are developed and applied in the accuracy analysis. The accuracy of a Stewart platform with specified manufacturing tolerances and installation errors is evaluated. On the other hand, the model and algorithms can be used to specify the machining tolerance and allowable assembly errors to obtain a desired accuracy of a Stewart platform. The effects of manufacturing tolerances on the platform accuracy are investigated. Simulation results indicate that the claim that parallel manipulators are more accurate is not substantiated. Moreover, the fabrication of a

large structure, to be used as a base for the platform, might have a major contribution to the platform error due to its poor tolerances.

# CHAPTER 5

## KINEMATIC CALIBRATION

An error-model based approach for the kinematic calibration of a Stewart platform is presented in this chapter. An introduction on the calibration of parallel manipulators and Stewart platform is given in Section 5.1. Section 5.2 presents parameter identification algorithm and focuses on the error model construction and the computation of the identification Jacobian matrix. Simulation results presented in Section 5.3 demonstrate the effectiveness of the approach for both conventional or accurate model. Also, simulated measurements, which will include realistic noise figures, are provided to show the effectiveness of the proposed calibration approach for the practical applications. Concluding remarks are given in the last section.

### 5.1 Introduction to Calibration of Stewart Platform

It is shown in Chapter 4 that the accuracy of a Stewart platform is in the same order of magnitude as that of a serial manipulator that has relatively the same nominal dimensions. The degradation in accuracy is mainly due to manufacturing tolerances used to construct the platform, manifested as deviations between the nominal kinematic parameters of the platform model and the actual ones. Since the

platform's controller determines the length of the actuators according to the nominal model, the resulting pose of the platform is inaccurate. One way to enhance the platform's accuracy is by kinematic calibration which is a process by which the actual kinematic parameters are identified and then used to modify the kinematic model used by the controller. Thus, the controller will use more accurate model and as a result the accuracy of the platform will be improved.

Similar to the serial manipulator calibration process, the calibration process of the Stewart platform consists of four steps: 1) Construction of the platform kinematic error model; 2) Measurement of the platform pose with respect to a reference frame as well as its joint variables (link lengths for Stewart platform); 3) Identification of the inaccurate kinematic parameters in the model; and 4) Compensation of the pose error based on the identified model.

Two different models: conventional model and accurate model, have been presented in the previous chapters and will not be repeated in detail in this chapter. Neither will the measurement techniques be discussed here since these are same as these used for serial manipulator calibration. Accuracy compensation problem will be discussed in Chapter 6. This chapter presents an error-model based kinematic parameter identification approach and focuses on the error model construction which is the central issue for the method. A detailed procedure is given to use numerical methods to compute the identification Jacobian matrix that relates the robot pose errors to the kinematic parameters errors. Both this approach and Zhuang and Roth's approach [1991] solve unconstrained non-linear optimization problems. In both cases, the actual ball joint centers need not be coplanar. However, the proposed approach can obtain global optimal solution. Furthermore,

it is easy to be implemented and can be applied on both conventional model and accurate model for the parameter identification.

It should be mentioned that the calibration discussed in this chapter is based on the assumption that the pose of the end-effector of Stewart platform is a function of only the joint variables, joint parameters and the kinematic dimensions. In other words, it is assumed that the manipulator is perfectly rigid and the joints and plates have no compliances and no friction. These assumptions are much closer to the truth compared to the serial manipulator kinematic calibration since the parallel manipulators' structure is relatively simpler and much more rigid than that of serial manipulators.

## 5.2 Parameter Identification

### 5.2.1 Problem Statement

The kinematic parameter identification problem can be stated as follows: Given the measured links length and measured platform pose, for  $j$  different platform poses, estimate the kinematic parameters which define the transformation between the two. The minimum number of measured poses,  $j_{\min}$ , depends on the number of parameters needed to be identified. Since measurement noise does exist, the parameters are identified using least square techniques and therefore  $j$  should be larger than  $j_{\min}$ .

For the conventional model, the errors of ball joints and U-joints and the assembly errors of joints with actuators are neglected. The parameters that need to be identified are the positions of U-joints on the base,  $\mathbf{b}_i$ , and the position of ball

joints on the plate,  $\mathbf{p}_i$ ,  $i=1,2,\dots,6$ , as shown in Figure 2.1. Similar to the parameter identification problem of a serial robot manipulator, for each active actuator, there is an offset that also needs to be identified. An offset is a constant or a difference between the joint reading and its actual value. Since each vector  $\mathbf{b}_i$  or  $\mathbf{p}_i$  has three elements, the total number of the parameters which need to be identified is 42.

As shown in Chapter 3, for each joint-link train of an accurate model of Stewart platform, there are 22 kinematic parameters including a link offset. Altogether there are 132 parameters that need to be identified for an accurate model.

### 5.2.2 Error-Model Based Approach and Identification Procedure

Error-model based identification method is widely applied for serial robot manipulator calibration [Hayati and Mirmirani 1982,1984,1985; Mooring and Tang 1984; Veitshegger and Wu, 1988; Roth 1988; Mooring, Roth and Driels, 1991]. Error-model based parameter identification method uses an iterative linear least square optimization algorithm. First, the robot pose vector can be expressed as a function of the parameter vector  $\mathbf{u}$  (with given joint variable vector  $\mathbf{v}$ ):

$$\mathbf{x} = \mathbf{f}(\mathbf{u}) \tag{5.1}$$

where the function  $\mathbf{f}$  stands for the forward kinematics of the robots.

Differentiating Equation (5.1) yields the identification Jacobian  $\mathbf{J}$ :

$$\mathbf{J} = \mathbf{dx}/\mathbf{du} = \mathbf{df}(\mathbf{u})/\mathbf{du} \tag{5.2}$$

For serial manipulators, the forward kinematics is straightforward and can generally be expressed in a closed analytical form. In order to apply the least square to the parameter estimation, it is a common practice to derive an error model by linearizing the manipulator kinematic model. Therefore, the identification Jacobian,  $J$ , is expressed analytically [Wu, 1984; Hayati, 1985; Veitshegger and Wu, 1988; Roth 1988; Mooring, Roth and Driels, 1991]. Figure 5.1 is a block diagram for parameter identification of serial robot manipulators using an error-model based approach. Since the nominal kinematic parameters are in general known from the design specifications, and the actual parameters are often in the neighborhood of their nominal parameters, the least square algorithm is easily applied in the

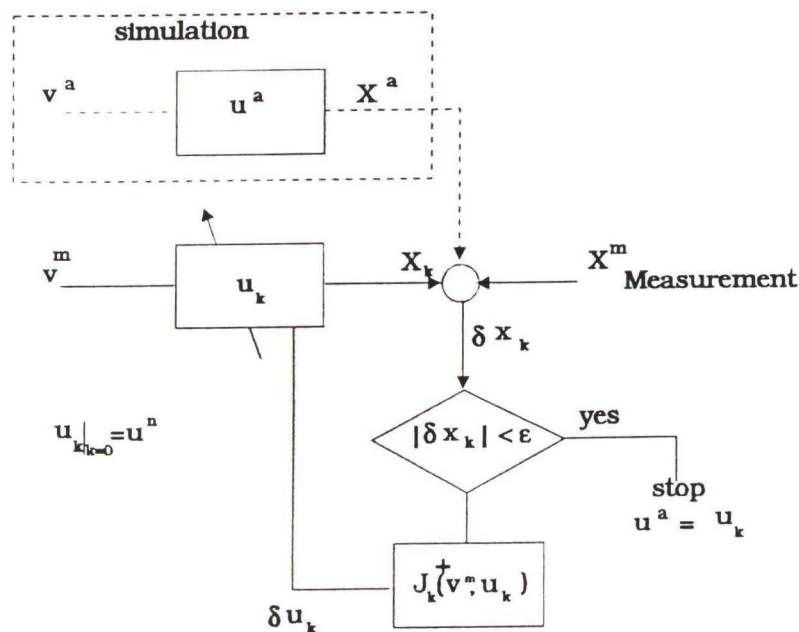


Figure 5.1 Flowchart of the kinematic parameter identification procedure for serial manipulators

estimation processes. As shown, in each iteration,  $k$ , a pose error vector,  $\delta \mathbf{x}$ , defined as the difference between the measured pose transformation matrix,  $\mathbf{X}^m$ , and the pose calculated by  $\mathbf{f}(\mathbf{u}_k, \mathbf{v}_j^m)$ , where  $\mathbf{v}_j^m$  is the measured joint variables at pose  $j$ ,  $\mathbf{X}_k$ , is used to update the parameter vector using the parameter identification Jacobian  $\mathbf{J}(\mathbf{u}_k, \mathbf{v}_j^m)$ .

The procedure for parameter identification of serial manipulators using standard least square estimation is briefly summarized as follows:

- 1) The pose transformation matrix,  $\mathbf{X}_k$  is calculated by  $\mathbf{f}(\mathbf{u}_k, \mathbf{v}_j^m)$ , where  $\mathbf{f}$  represents the forward kinematics of the serial manipulator,  $\mathbf{v}_j^m$  is the measured joint variables at pose  $j$ , and  $\mathbf{u}_k$  is the kinematic parameters vector ( $k$  is an iteration index). As first step, the nominal parameters,  $\mathbf{u}^n$  is used.
- 2) A pose error,  $\delta \mathbf{x}_k$ , defined as the difference between the measured pose,  $\mathbf{X}^m$ , and  $\mathbf{X}_k$ .
- 3) The Jacobian  $\mathbf{J}_k(\mathbf{u}_k, \mathbf{v}_j^m)$  is calculated.
- 4) The kinematic parameters vector is updated by  $\mathbf{u}_{k+1} = \mathbf{u}_k + \delta \mathbf{u}_k$ , where the correction term  $\delta \mathbf{u}_k = \mathbf{J}_k^+ \delta \mathbf{x}_k$ , where  $\mathbf{J}_k^+ = (\mathbf{J}_k^T \mathbf{J}_k)^{-1} \mathbf{J}_k^T$ .
- 5) The procedure defined by steps 2 through 5 is repeated until  $\delta \mathbf{x}$  is sufficiently small. Then the result of  $\mathbf{u}$  is used to represent the actual values of the kinematic parameters.

The approach is adopted for the parameter identification of Stewart platform and the similar procedure, as shown in Figure 5.2, is used. The identification procedure is given as follows:

- 1) Obtain  $s$  measurements of the platform poses  $\mathbf{X}_j^m$  ( $j$  is pose index,  $j=1,2,\dots,s$ ) within the platform workspace (see Chapter 2 for determining whether a pose is within the workspace) and the corresponding link lengths  $\mathbf{d}_j^m$ .



- 2) Let the initial parameter vector be  $\mathbf{u}_{k|k=0} = \mathbf{u}^n$ , where  $\mathbf{u}^n$  is the known nominal kinematic parameters vector and  $k$  is an iteration index.
- 3) Compute the platform pose  $\mathbf{X}_{j,k}$  using  $\mathbf{d}_j$  and  $\mathbf{u}_k$  by solving the platform forward kinematics problem.
- 4) Calculate the pose error vectors  $\delta \mathbf{x}_k$  from  $\mathbf{X}_{j,k}^m$  and  $\mathbf{X}_{j,k}$ .
- 5) Use the norm of  $\delta \mathbf{x}_k$  as termination condition. If  $|\delta \mathbf{x}_k| < \epsilon$ , then the identified parameter  $\mathbf{u}^a = \mathbf{u}_k$  and stop the program. Otherwise continue to step 6.
- 6) Compute the identification Jacobian  $\mathbf{J}_k$ .
- 7) Determine a correction vector for  $\mathbf{u}_k$  given by  $\delta \mathbf{u}_k = [(\mathbf{J}_k^T \mathbf{J}_k)^{-1} \mathbf{J}_k^T] \delta \mathbf{x}_k$ .
- 8) Update  $\mathbf{u}_k$  by  $\mathbf{u}_{k+1} = \mathbf{u}_k + \delta \mathbf{u}_k$  and go back to step 3.

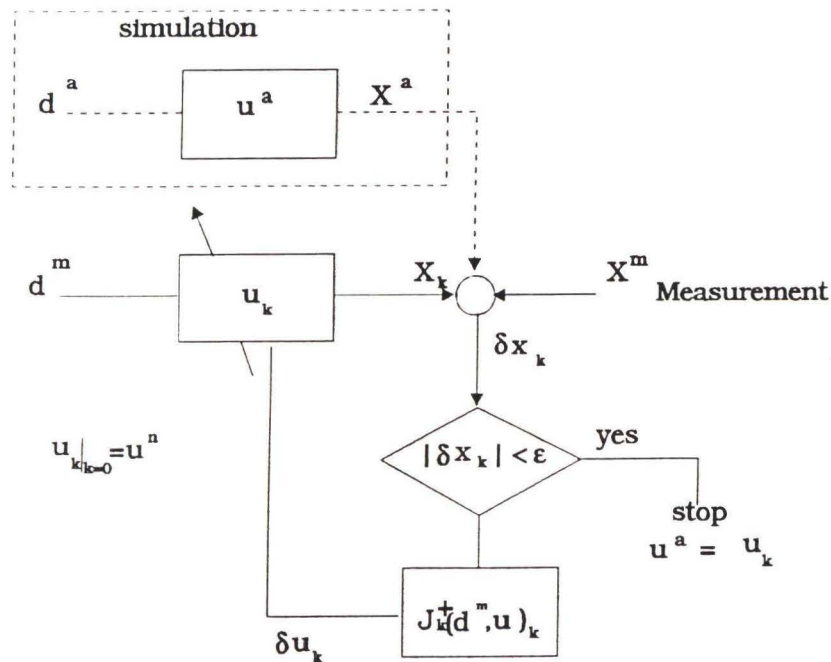


Figure 5.2 Flowchart of the kinematic parameter identification procedure for Stewart platform

The algorithm and procedure for forward kinematics solution in step 3 can be found in Chapter 4, Section 4.1. The computation of  $\delta\mathbf{x}_k$  in step 4 and the formulation of the identification Jacobian matrix in step 6 are discussed in the following section where the iteration index  $k$  is omitted for clarity.

### 5.2.3 Jacobian Formulation

The major issue in parameter identification by error-model based approach is the formulation of the identification Jacobian matrix. The identification Jacobian of Stewart platform cannot be obtained by the method used for serial manipulators. Since there is no analytical expression for the forward kinematics of the platform, it may be difficult to use the first order differentiation approach to obtain the analytical form of the identification Jacobian of Stewart platform. A step by step systematic approach is presented here to obtain the identification Jacobian of Stewart platform.

The identification Jacobian,  $\mathbf{J}$ , relates a differential pose vector,  $\delta\mathbf{x}$ , to a differential change of the kinematic parameter vector,  $\delta\mathbf{u}$ :

$$\delta\mathbf{x} = \mathbf{J} \delta\mathbf{u} \quad (5.3)$$

where  $\delta\mathbf{x}$  is a  $6s \times 1$  vector ( $s$  is the total number of measurement for the parameter identification) which can be expressed by:

$$\delta\mathbf{x} = [\delta\mathbf{x}_1^T, \delta\mathbf{x}_2^T, \dots, \delta\mathbf{x}_s^T]^T \quad (5.4)$$

where:  $\delta \mathbf{x}_j$  ( $j = 1, 2, \dots, s$ ) is a 6x1 error vector given by  $\delta \mathbf{x}_j = (\delta \mathbf{r}_j^T, \delta \mathbf{p}_j^T)_j^T$

$\delta \mathbf{r}_j$  is a 3x1 orientation error vector.

$\delta \mathbf{p}_j$  is a 3x1 position error vector.

The pose error vector at the  $j^{\text{th}}$  measurement,  $\delta \mathbf{x}_j$  can be obtained by the error matrix  $\Delta \mathbf{X}_j$  which is given by

$$\Delta \mathbf{X}_j = \mathbf{X}_j^{-1} d\mathbf{X}_j \quad (5.5)$$

where:  $\mathbf{X}_j$  - A 4x4 homogeneous pose transformation matrix, obtained by solving the platform forward kinematics problem.

$$d\mathbf{X}_j = \mathbf{X}_j^m - \mathbf{X}_j.$$

$\mathbf{X}_j^m$  - The measured platform pose transformation matrix.

Denote  $\Delta \mathbf{X}_j = \{\Delta \mathbf{R}_j, \Delta \mathbf{p}_j\}$  where  $\Delta \mathbf{R}_j$  is a anti-skew 3x3 orientation error matrix and  $\Delta \mathbf{p}_j$  is a 3x1 translation error vector. Then  $\delta \mathbf{p}_j = \Delta \mathbf{p}_j$ , and  $\delta \mathbf{r}_j$  can be computed from  $\Delta \mathbf{R}_j$  by

$$\delta \mathbf{r}_j \mathbf{S} = \Delta \mathbf{R}_j \quad (5.6)$$

where  $\mathbf{S}$  is a cross operator defined as follows:

$$\begin{bmatrix} a_1 \\ a_2 \\ a_3 \end{bmatrix} \mathbf{S} = \begin{bmatrix} 0 & -a_3 & a_2 \\ a_3 & 0 & -a_1 \\ -a_2 & a_1 & 0 \end{bmatrix} \quad (5.7)$$

The Jacobian is composed of s sub-Jacobian matrices  $\mathbf{J}_1, \dots, \mathbf{J}_s$  :

$$\mathbf{J} = [\mathbf{J}_1, \mathbf{J}_2 \dots \mathbf{J}_s]^T \quad (5.8)$$

For each measurement j,  $\mathbf{J}_j$  is defined as

$$\delta \mathbf{x}_j = \mathbf{J}_j \delta \mathbf{u} \quad (j = 1, 2, \dots, s) \quad (5.9)$$

where  $\mathbf{J}_j$  is a  $6 \times m$  submatrix where m is the number of parameters needed to be identified. It can be obtained by

$$\mathbf{J}_j = [\mathbf{j}_{1j}, \mathbf{j}_{2j}, \dots, \mathbf{j}_{mj}] \quad (5.10)$$

where  $\mathbf{j}_{ij}$ ,  $i = 1, 2, \dots, m$ , is a  $6 \times 1$  vector represents the partial derivative of the pose vector  $\mathbf{x}_j$  with respect to the  $i^{\text{th}}$  parameter  $u_i$ . It can be obtained numerically by a perturbation method as follows:

$$\mathbf{j}_{ij} = \delta \mathbf{x}_{ij} / \delta u_i \quad (5.11)$$

where  $\delta u_i$  is an appropriate small change in the parameter  $u_i$ . The  $6 \times 1$  error vector  $\delta \mathbf{x}_{ij}$  is obtained from the transformation matrices  $\mathbf{X}_j(\mathbf{u})$  and  $\mathbf{X}_j(\mathbf{u} + \delta \mathbf{u}_i)$ , just as the  $\delta \mathbf{x}_j$  is obtained from  $\mathbf{X}_j(\mathbf{u})$  and  $\mathbf{X}_j^m$ . Note that  $\delta \mathbf{u}_i$  is a  $m \times 1$  vector all elements of which are zeros except for the  $i^{\text{th}}$  element which has the value of  $\delta u_i$  ( $\delta \mathbf{u}_i = [0, \dots, 0, \delta u_i, 0, \dots, 0]^T$ ). In other words, the perturbation matrix  $\mathbf{X}_j(\mathbf{u} + \delta \mathbf{u}_i)$  is the forward

kinematics solution using the parameter vector with its  $i^{\text{th}}$  element perturbed. In summary, the Jacobian can be expressed as following  $6s$  by  $m$  matrix:

$$\mathbf{J} = \begin{bmatrix} \frac{\delta x_{11}}{\delta u_1} & \frac{\delta x_{21}}{\delta u_2} & \dots & \frac{\delta x_{m1}}{\delta u_m} \\ \frac{\delta x_{12}}{\delta u_1} & \frac{\delta x_{22}}{\delta u_2} & \dots & \frac{\delta x_{m2}}{\delta u_m} \\ \vdots & \vdots & \ddots & \vdots \\ \frac{\delta x_{1s}}{\delta u_1} & \frac{\delta x_{2s}}{\delta u_2} & \dots & \frac{\delta x_{ms}}{\delta u_m} \end{bmatrix} \quad (5.12)$$

It can be seen from Equations (5.8) to (5.12) that the computation of the identification Jacobian involves a great number of platform forward kinematics solutions for the conventional and the accurate models. Both are solved numerically, therefore the parameter identification procedure is computationally intensive. For the accurate model, the general forward kinematics solution which involves a numbers of general inverse kinematics solutions which are also obtained numerically, takes considerable computer time. Therefore, a powerful computer is a must to perform the parameter identification for the accurate model.

### 5.3 Simulation Studies

A simulation study was performed in order to verify the above algorithm. In this study a platform with the following dimensions:  $R_b = 3$  feet,  $R_p = 1$  foot, and links with length ranges between 4.5-7.5 feet, was used. The following uniformly distributed random errors were imposed on the nominal parameters:

1. Position error of the U-joints at the base:

$$|\Delta b_x| < 0.24 \text{ inch}, |\Delta b_y| < 0.24 \text{ inch}, |\Delta b_z| < 0.12 \text{ inch}.$$

2. Position error of ball joints on the moving plate:

$$|\Delta p_x| < 0.012 \text{ inch}, |\Delta p_y| < 0.012 \text{ inch}, |\Delta p_z| < 0.012 \text{ inch}.$$

3. Link offset:  $|\Delta d| < 0.024 \text{ inch}$ .

4. Manufacturing tolerance for both U-joints and ball-joints (D-H parameters):

$$|\Delta d| < 0.004 \text{ inch}, |\Delta a| < 0.004 \text{ inch and } |\Delta \alpha| < 0.1^\circ.$$

Four different cases were investigated:

Case 1: The results in Chapter 4 indicate that the contribution of the joints manufacturing tolerances have a minor effect on the platform pose error. Therefore, a conventional model in which these parameters were not considered can be used. In this model, the number of parameters that have to be identified is 42. In this case 8 pose measurements were used (one more than the minimum required) and it was assumed that there is no measurement noise (the measurement of the platform pose is accurate). Figure 5.3 shows the

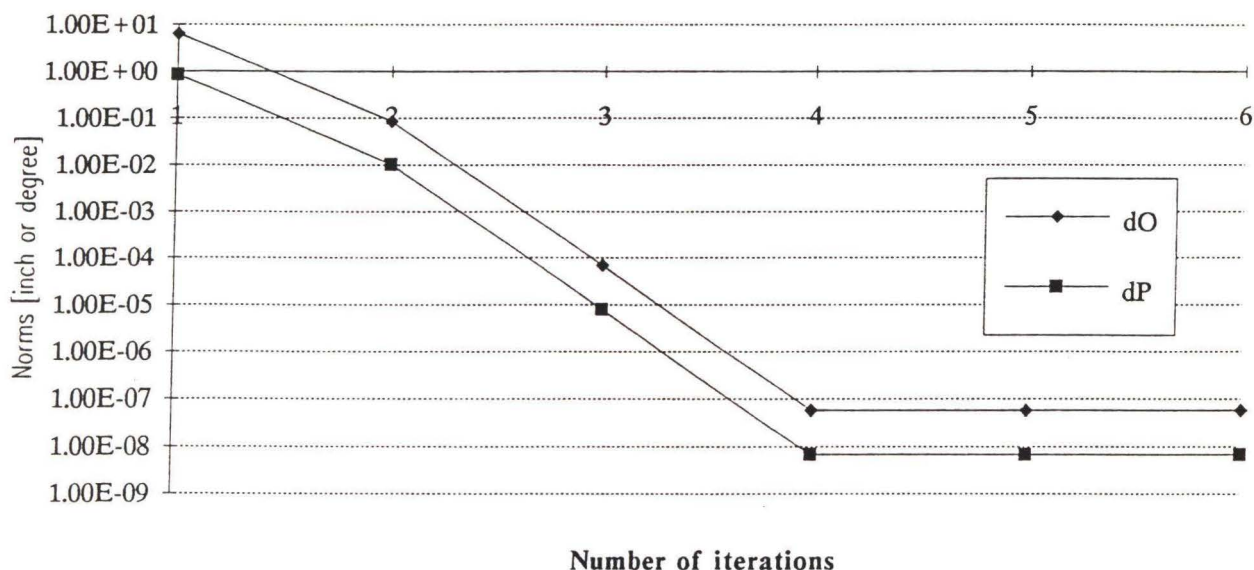


Figure 5.3 Convergence of the pose error vector norm versus iteration number

convergence of the pose error norm as function of the number of iterations of the identification procedure. The pose error, which is a 6x1 vector, was divided into translation and orientation errors the norm of which are shown in the figure. As shown, initially the translation error is about 0.8 inch and the orientation error is about  $8^\circ$ . After only 4 iterations both errors were practically reduced to zero.

**Case 2:** This case is the same as the previous one but a uniformly distributed random noise was added to the pose measurement in order to simulate measurement errors which are inevitable in practical calibration measurements. The magnitudes of the measurement errors used in the simulation were adopted from experimental results obtained by using a theodolite as a measuring device. These errors are: 1) Pose position measurement error of  $\pm 0.0024$  inch; and 2) Pose orientation error of  $\pm 0.0285$  degree. Since the measurements are contaminated by noise, more pose measurements are required in order to improve the identification from 'Least Squares' point of view. As before, the parameters error vector has 42 elements: 24 elements due to errors in the location of the U-joint at the base; 24 elements due to errors in the location of the Ball-joint at the plate; and 6 elements describing the links offsets. Figure 5.4 illustrates the convergence of the norm of the three sets of parameter errors (base, plate and offset) as function of the number of measured poses. As expected better identification results are obtained as the number of measured poses increases. However, very little improvement can be achieved once the number of measured poses exceeds a certain limit (about 20 in this case). To be more specific, Figure 5.5 provides the initial and the final (after identification)

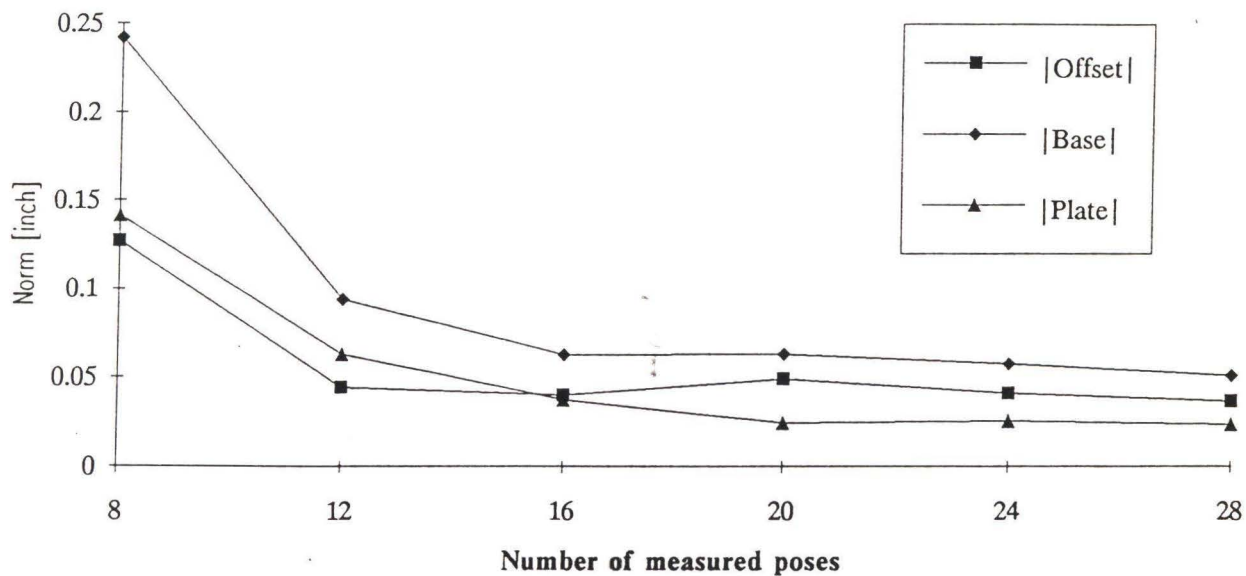


Figure 5.4 Convergence of the parameter error vector norm (Case 2)

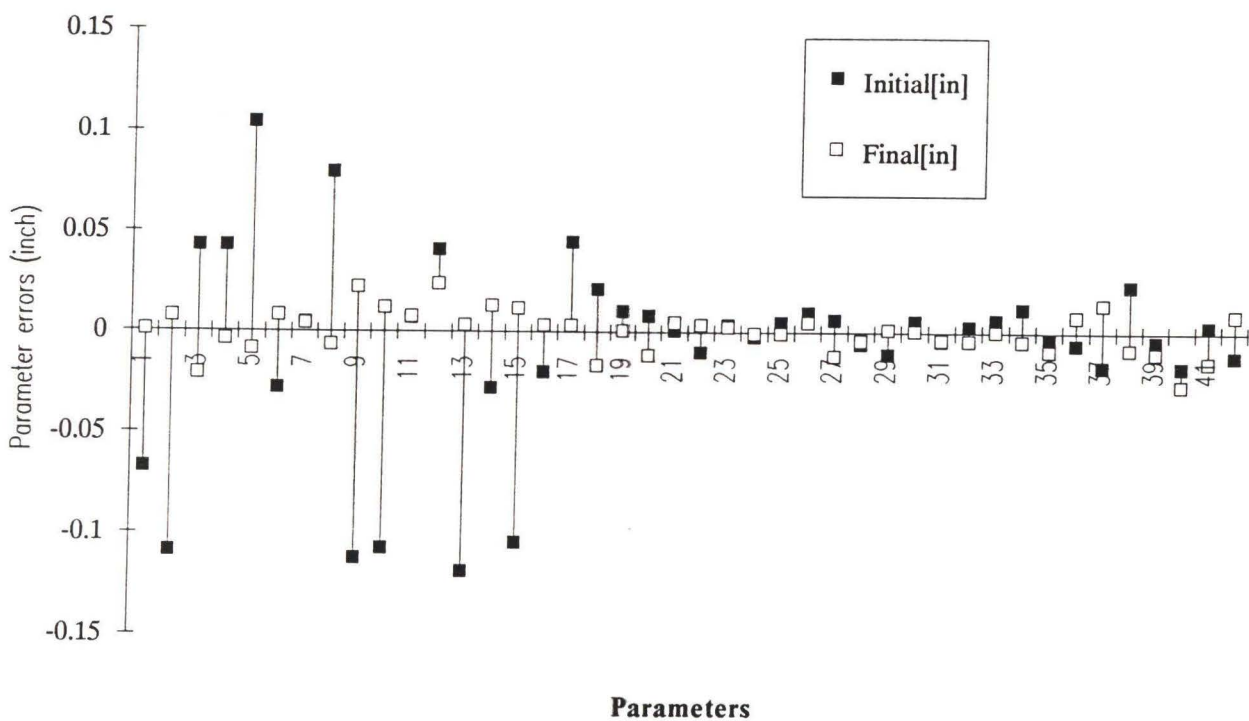


Figure 5.5 Initial and final values of kinematic parameter errors (Case 2)



values of the parameters errors for the case of 28 measured poses and 4 iterations of the identification algorithm.

The initial values are given by the difference between the actual and the nominal values while the final values are given by the difference between the actual and the identified values. As shown the large errors, mainly due to the errors in the location of the U-joint on the base, were reduced substantially, while small initial errors were slightly reduced or even increased a little bit due to the least square averaging effect. It should be emphasized that the errors cannot be eliminated, even with large number of measurements, due to the existing measurement errors.

**Case 3:** This case is the same as the case 2 but it is assumed that a more accurate measurement system is employed. The uniformly distributed random measurement noise are much smaller and within the following range: 1) Pose position measurement error of  $\pm 0.00024$  inch; and 2) Pose orientation error of  $\pm 0.00285$  degree. Similar to Figure 5.4, Figure 5.6 illustrates the convergence of the norm of the three sets of parameter errors as function of the number of measured poses. Again, better identification results are obtained as the number of measured poses increases. Since in this case the measurement noises are only one tenth in magnitude compare to that in case 2 and much smaller than the errors of both ball joints, U-joints and link offsets, the identified parameters are much closer to the actual ones. The norm of the errors between the identified and actual parameter vectors is one order of magnitude smaller than the error in case 2. Figure 5.7 shows initial and final (after identification) values of the parameters errors for the case of 28 measured poses. The details of the values of the nominal, actual and identified parameters for Case 2 and Case 3 are

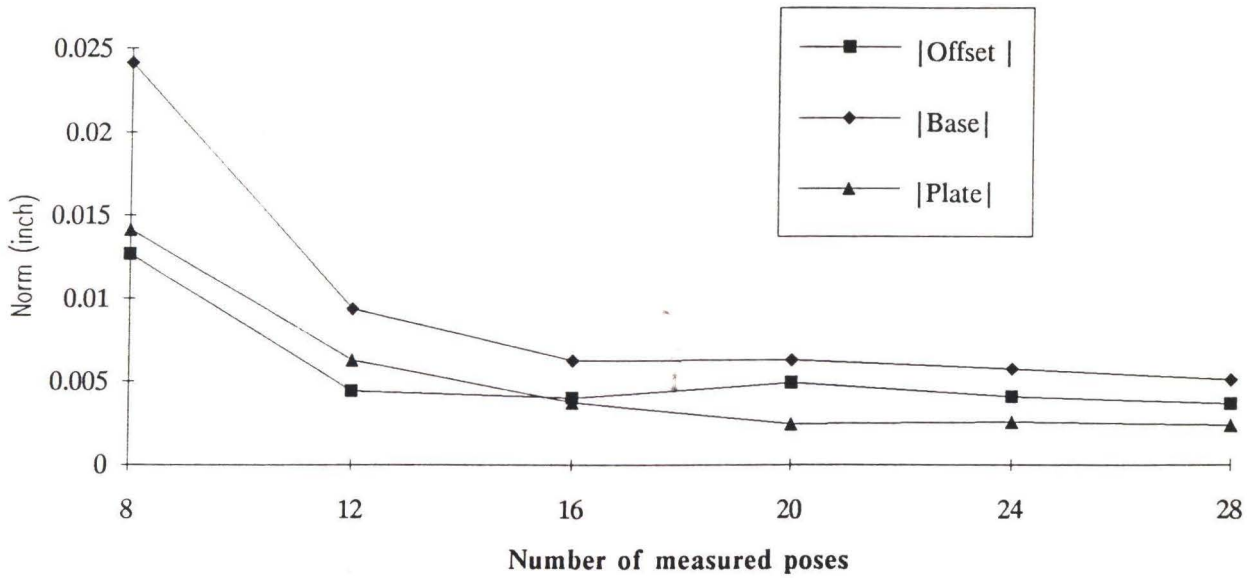


Figure 5.6 Convergence of the parameter error vector norm (Case 3)

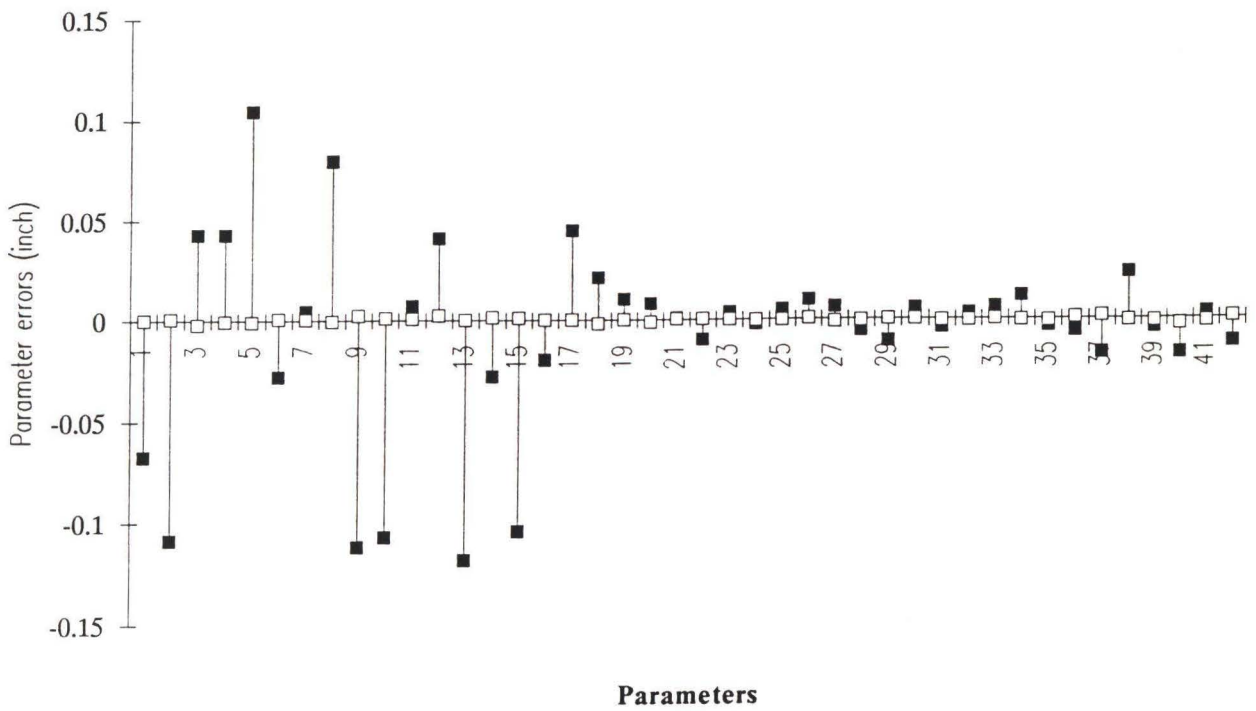


Figure 5.7 Initial and final values of kinematic parameter errors (Case 3)

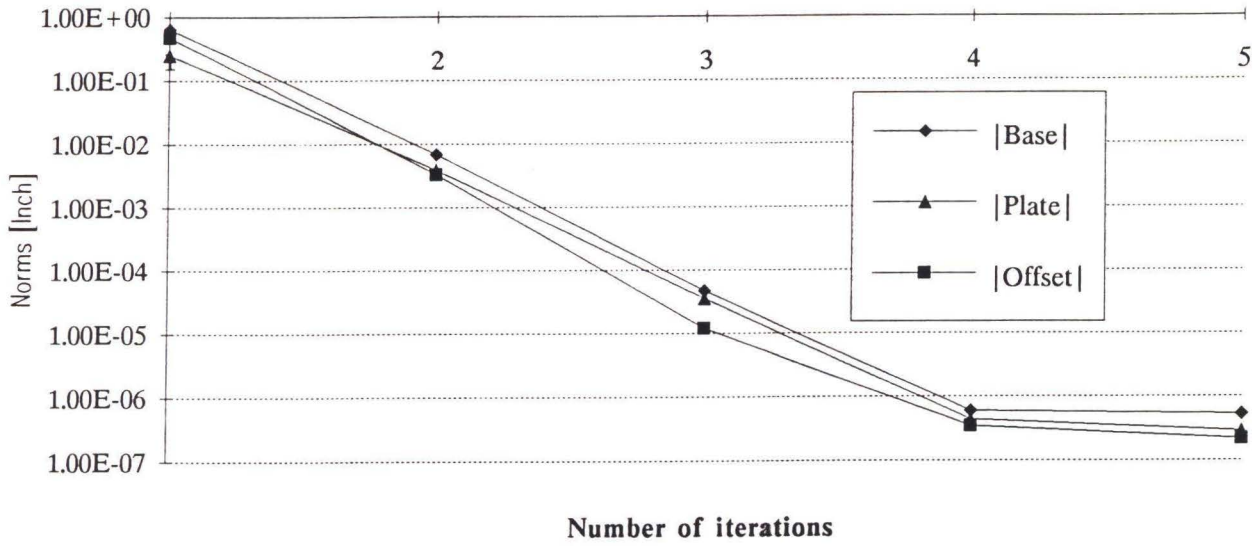


Figure 5.8 Convergence of the parameter error vector (Case 4)

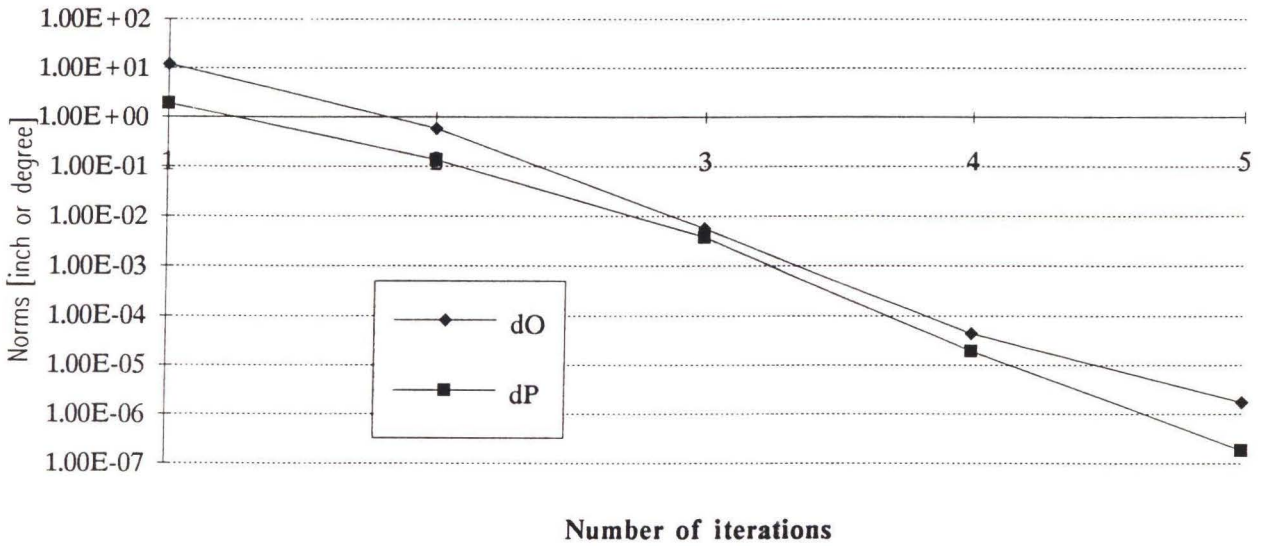


Figure 5.9 Convergence of the pose error vector (Case 4)

shown in Appendix C. It is interesting to note that the accuracy of the identified parameters (which can be represented by the difference between the actual parameters and the identified parameters) are ten times better than that in case 2.

**Case 4:** In this case the accurate model, which includes 132 parameters, was simulated and used to identify the above 42 parameters, assuming that the other parameters are accurate. This simulation was performed in order to verify the effectiveness of the algorithm and therefore no measurement noise was included and only 8 measured poses were used. Figure 5.8 shows that the parameters converge to their true value after 4 iterations and Figure 5.9 shows that as a result the pose error is essentially eliminated. Similarly, one can choose any other subset of the above 132 parameters to identify.

## 5.4 Computational Issue

It has been pointed out that the parameter identification algorithm involves a great number of general forward kinematic solutions. An efficient, fast-convergent forward kinematics solution is essential. The Gauss-Newton least square method introduced in Chapter 4 can obtain forward kinematic solution in the accuracy of  $10^{-8}$  within 4-5 iterations. Nevertheless, the proposed identification algorithm is computationally intensive for the parameter identification of the accurate model and has to be performed on a powerful computer for practical implementation. If  $m$  parameters have to be identified, and  $s$  measured poses are used, the forward kinematics problem, which is also solved iteratively by numerical methods, has to be solved  $s(m+1)$  times for each iteration of the identification algorithm. For example,

if 42 parameters in the accurate model are being identified using 8 measured poses (as in Case 4), 344 forward kinematics solutions have to be obtained for each identification iteration. For this case, about 10-11 hours of SUN 3/260 CPU time are needed (The program is written in MATLAB). It means that it takes about 40-50 hours of CPU time for complete the identification procedure which might require 4-5 iterations. Assume that all 132 parameters need to be identified and the measurement configuration  $s$  equals 40, then the identification Jacobian matrix will have a dimension of 240 by 132, and there will be 5,320 general forward kinematics solutions to be solved for each iteration. However, if the conventional model is used, the computational time for the forward kinematic solution is much reduced, and the CPU time is reduced to about one and half hours for each iteration of the identification of 42 parameters.

## 5.5 Concluding Remarks

An algorithm for the identification of the kinematic parameters of a Stewart platform has been presented and verified through simulations. The algorithm can be applied to both the conventional and the accurate models. The accuracy of the identified parameters is approximately inversely proportional to the measurement noise level. In general, measurement noise should be much smaller than parameter errors to be identified. If the measurement accuracy cannot be at least 1-2 orders of magnitude higher than the manufacturing tolerances of the errors of the joints, it is suggested that the conventional model be used so that the cost of the measurement and computation can be substantially reduced and the same accuracy can be achieved.

# CHAPTER 6

## ACCURACY COMPENSATION

This chapter discusses the accuracy compensation problem of Stewart platform. Section 6.1 presents a compensation algorithm for the proposed accurate model. Section 6.2 provides simulation results that demonstrate the accuracy improvement achieved after compensation. The simulation uses the identified parameters obtained from Case 2, Chapter 5, in which realistic measurement noise is taken into account.

### 6.1 Compensation Procedure

Design of a robot accuracy compensator is the final stage of a calibration task. Accuracy compensation is a process by which robot pose errors are compensated through corrections of the nominal joint variables. For parallel manipulator such as Stewart platform, the problem is to find the 'correct' link lengths for a specified platform pose based on the identified kinematic parameters.

The accuracy compensation problem is identical to the inverse kinematics problem using the kinematic model with the identified kinematic parameters.

For the conventional model of a Stewart platform, in which only errors of the joint locations and link offsets are considered, the implementation of the compensation is straightforward. The inverse kinematics problem is solved by Equation (2.1) in which the **identified values of  $b_i$  and  $p_i$**  are used. Then the identified link offsets are added to resulted link lengths,  $d$ . These values are used to drive the platform to the required position.

The compensation procedure for the accurate model is not so simple and it has to be implemented numerically. It is mentioned in Chapter 4, section 4.2 that for an accurate model, the inverse kinematics solution of Stewart platform can be obtained **by solving the inverse kinematics problems of each joint-link train one by one**. This problem is similar to the problem of solving the inverse kinematics of a six degree freedom, 2R-P-3R serial manipulator. Similar to carefully designed industrial serial manipulators, a joint-link train has parallel or orthogonal axes and the analytical solution for the inverse kinematics can be obtained. However, after parameter identification, these axes are not exactly parallel or orthogonal and do not necessary intersect. These deviations invalidate the assumption on which the analytic inverse kinematics equations can be applied.

Newton-Raphson algorithm is applied for solving inverse kinematics of each joint-link train of the accurate model. Denote the vector  $\mathbf{v}_j$  as joint variable vector of the  $j^{\text{th}}$  joint-link train (recall that the joint variables in each joint-link train are  $\theta_1, \theta_2, d_3, \theta_4, \theta_5, \theta_6$ ), and the vector  $\mathbf{u}_j$  as parameters of the  $j^{\text{th}}$  joint-link train. The problem can be mathematically stated as follows:

Given the desired platform pose  $\mathbf{x}^a$ , the **joint-link train forward kinematics model**  $\mathbf{x}_j = f_j(\mathbf{v}_j, \mathbf{u}_j^a)$   $j=1,2\dots 6$ , and its nominal inverse kinematics model  $\mathbf{v}_j = g_j(\mathbf{x}^a, \mathbf{u}_j^n)$ , find  $\mathbf{v}_j^a$ , such that  $\mathbf{x}^a = f_j(\mathbf{v}_j^a, \mathbf{u}_j^a)$ .

As an initial guess for  $\mathbf{v}_j$ , the nominal inverse kinematics of the platform can be used. The solution of the nominal value for  $\mathbf{v}_j$  is provided in Section 4.2.

The problem is solved, for each joint-link train separately, as follows (the subscription  $j$  is omitted for clarity and  $k$  is the iteration index) by Newton-Raphson algorithm:

1. Make an initial guess of  $\mathbf{v}|_{k=0}$ , using the nominal model of the joint-link train  $\mathbf{v}|_{k=0} = \mathbf{g}(\mathbf{x}^a, \mathbf{u}_j^n)$ .
2. Compute an estimated platform pose  $\mathbf{x}_k = \mathbf{f}(\mathbf{v}_k, \mathbf{u}_j^a)$ .
3. Obtain a pose error vector  $\delta\mathbf{x}_k$  from  $\mathbf{x}_k$  and  $\mathbf{x}^a$ .
4. Compute a correction term  $\delta\mathbf{v}_k = \mathbf{J}_k^{-1} \delta\mathbf{x}_k$ , where  $\mathbf{J}_k$  is the joint-link train Jacobian which can be formulated from the nominal joint-link train model.
5. Update the estimated  $\mathbf{v}_k$  by  $\mathbf{v}_{k+1} = \mathbf{v}_k + \delta\mathbf{v}_k$ .
6. Check whether the termination condition,  $|\delta\mathbf{x}_k| < \epsilon$ , is satisfied. If so, then  $\mathbf{v}^a = \mathbf{v}_k$  and stop the program. Otherwise go to step 2.

The active joint variable vector,  $\mathbf{d}$ , can be retrieved from the six joint-link variable vector,  $\mathbf{v}_1 - \mathbf{v}_6$ .

The approach for the formulation of the joint-link train Jacobian in step 4 can be a differential method or vector cross product method. These methods can be found in the robotics text books by Paul [1981], Craig [1986] or Schilling [1990].

It is worth pointing out that this algorithm, similar to the algorithms used in serial manipulator compensation, is computationally time consuming. Therefore, it will be very difficult to apply it in real-time controllers. In this regards, the conventional model with identified parameters can be used in real-time controls, and an example of accuracy improvement after compensation is shown in the next section.



## 6.2 Accuracy Improvement After Compensation

Simulation studies were carried out in order to investigate the accuracy improvement after accuracy compensation. If no measurement noise is considered and the identified parameters are exactly the same as their actual values (as in Case 1 and Case 4 of section 5.3), the manipulator will be driven to the desired pose without any error. However, the identified parameters must have some deviation from the actual values due to the noise in the measurement process. In the following simulations, the nominal, identified and accurate parameters, are the same as these in Case 2 of section 5.3 and are listed in the appendix C, are used. Recall that the realistic measurement noise is included in Case 2 for the parameter identification of the conventional model. Again, the compensation does not require the time consuming numerical algorithm and can be implemented in real-time controls.

The platform accuracy before and after compensation is investigated and compared by the following procedure:

1. A set of poses (20 different poses),  $\mathbf{x}^a$ , was randomly selected within the platform workspace.
2. The joint lengths variables,  $\mathbf{d}^i$  and  $\mathbf{d}^n$  are computed by the inverse kinematics using the identified parameters,  $\mathbf{u}^i$ , and the nominal parameters,  $\mathbf{u}^n$ , respectively.
3. The poses after compensation,  $\mathbf{x}^i$ , were obtained by the forward kinematics using the actual parameters  $\mathbf{u}^a$  and  $\mathbf{d}^i$ , and the poses before compensation,  $\mathbf{x}^n$ , were obtained by the forward kinematics using  $\mathbf{u}^a$  and  $\mathbf{d}^n$ .
4. The pose errors after the compensation is computed from  $\mathbf{x}^a$  and  $\mathbf{x}^i$ . The pose errors before compensation is computed from  $\mathbf{x}^a$  and  $\mathbf{x}^n$ .

The results presented in figures 6.1-6.3 compare the pose error before and after parameter identification and compensation. Figure 6.1 compares the translation error norm before and after compensation. As shown, the values of the errors before compensation are in the range of 0.2 - 0.9 inch and after compensation, the values were reduced to the range of 0.01-0.06 inch. Figure 6.2 compares the pose position error elements dx, dy and dz respectively and Figure 6.3 compares the pose orientation error elements dR, dP and dY respectively. The maximum position error along one direction is less than 0.03 inch and the maximum angle error is less than 0.3 degree after compensation. Recall that the position and orientation measurement pose errors are  $\pm 0.0024$  inch and 0.00285 degree. If higher pose accuracy is required, the parameters have to be identified with high accuracy. In order to achieve this, measurement noise during the calibration phase must be further suppressed. Simulation result shows that the measurement error must be at least one order of magnitude smaller than the expected pose accuracy.

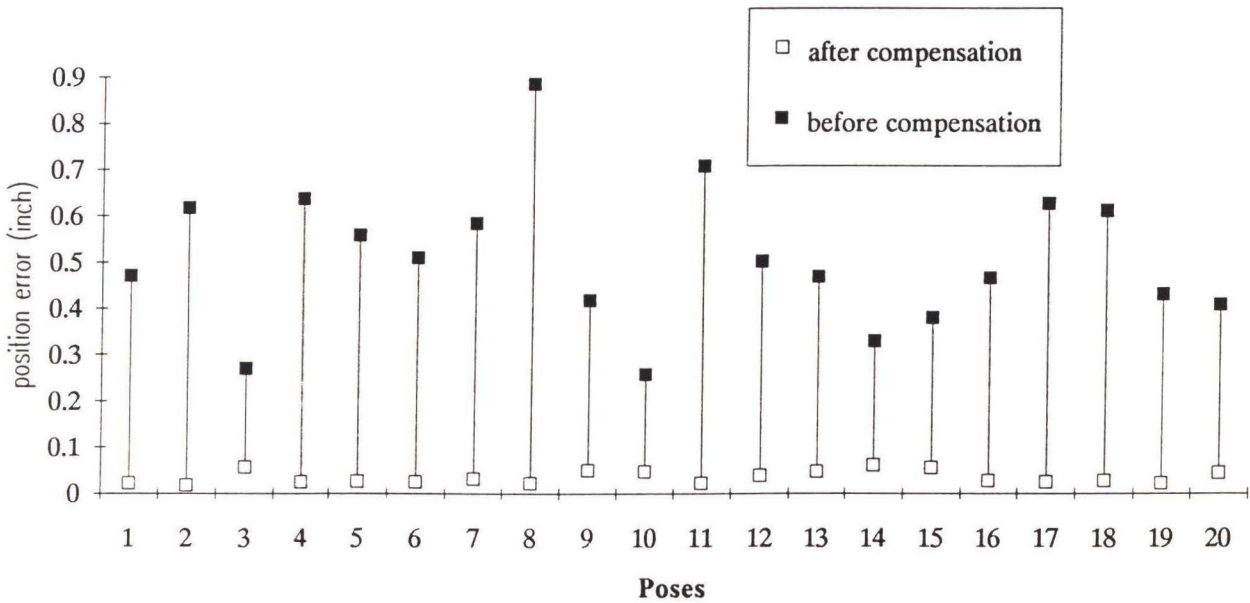


Figure 6.1 Comparison of the translation error before and after compensation

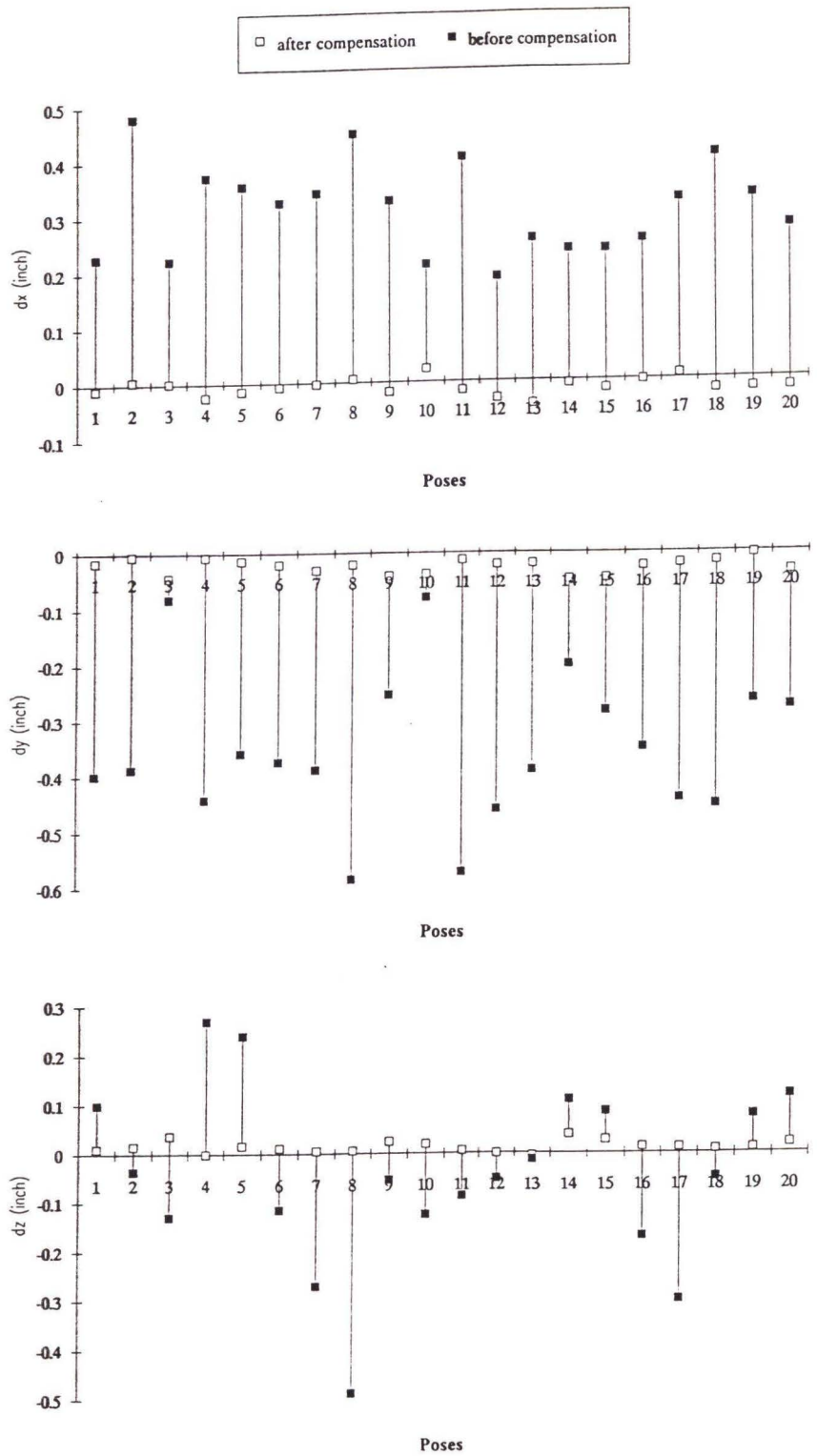


Figure 6.2 Comparison of the position error components before and after compensation

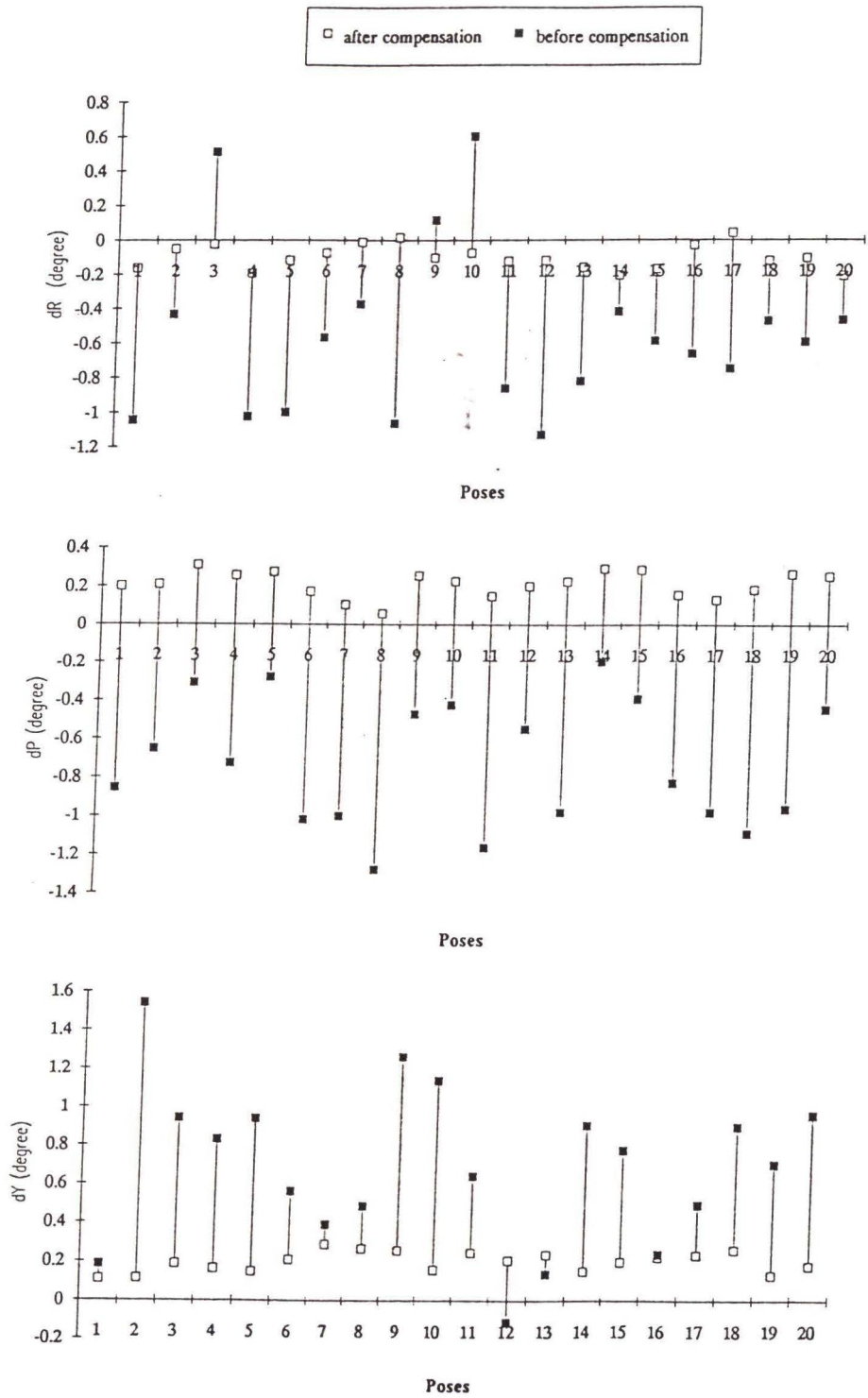


Figure 6.3 Comparison of the orientation error components before and after compensation

## CHAPTER 7

### CONCLUSIONS

Several issues related to a typical parallel manipulator - Stewart platform are addressed in this dissertation. First, the workspace of the platform is analyzed in detail. Second, the accuracy of the platform is evaluated using the proposed accurate model and the forward kinematics algorithm. Third, a calibration strategy is developed to enhance the platform accuracy. The simulation results and conclusions provide guidelines how to increase the workspace and how to enhance the accuracy of Stewart platform.

The contributions of the dissertation are as follows:

1. An algorithm for determination of the workspace of Stewart platform has been developed considering all kinematic constraints that exist in a practical Stewart platform, that is, link length limitations, range of joint angles, and link interferences. Explicit constraint equations are derived.
2. The effects of platform dimensions, actuator's strokes and the kinematic constraints on the workspace and the dexterity of Stewart platform have been analyzed using the proposed criterion of workspace volume. The results have manifested the major and minor effects on the workspace and provided a guide for the selection of joints, actuators and platform dimension in order to maximize the workspace in the design of Stewart platform.

3. An accurate kinematic model of Stewart platform that accommodates various manufacturing and installation errors has been developed. This can be used in platform accuracy analysis and in those applications where very high accuracy is required. Algorithms for forward and inverse kinematics solutions of the accurate kinematic model have been developed. The accuracy of Stewart platform with specified manufacturing tolerances has been evaluated and the effects of realistic manufacturing tolerances on platform accuracy have been investigated revealing the major error sources of the platform. It is concluded that the accuracy of Stewart platform is in the same order of the magnitude as that of a serial manipulator with similar dimensions.
4. An error-model based approach for the kinematic calibration of Stewart platform has been developed and parameter identification algorithm has been explored. A detailed procedure of formulating the identification Jacobian has been presented and the accurate compensation problem has been solved. Simulations for the kinematic calibration have been performed considering realistic measurement noise. The results have shown that the accuracy of Stewart platform can be significantly improved after the calibration.

The following issues related to Stewart platform are suggested for further investigation:

1. One of the major research topics on Stewart platform is to find an analytical solution for the forward kinematics problem. It seems impossible to obtain closed analytical solutions for a general Stewart platform. However, it may be possible to obtain closed form solutions in some special cases, or for a platform with some kind of constraints. One of the major constraints, which exist in most

practical Stewart platform but has not been considered by researchers, is the rotary joint angle limitation.

2. It remains to investigate singularity problems of Stewart platform. Although the singularity at a particular configuration of Stewart platform can be determined, it is impractical to examine the singularity for all reachable points by checking the determinant of the manipulator Jacobian or the dependency of screws of joint axes for every point. Development of an effective algorithm to determine all singular points within the workspace would be meaningful.
3. The observability of the kinematic parameters is normally defined in terms of the identification Jacobian of the linearized error models. Since no analytical solution for the forward kinematic problem is available, the formulation of the Jacobian is based on the difference method. An open research topic is how to determine the singularity of the identification Jacobian, and how to infer about possible unobservable status.
4. It is necessary to perform experimental studies on the calibration of Stewart platform in order to verify the proposed procedure. To do this, an accurate measuring system is a necessity. Practical measurement methods to be performed on the factory floor need to be developed.
5. The simulation studies of the parameter identification of all 132 parameters of the accurate model considering measurement noise need to be completed. The author's programs for parameter identification are written in MATLAB. These programs can be transferred to other computer languages, such as C. Then the simulation can be run on a supercomputer which usually does not support MATLAB.

## APPENDIX A

### Computation of the Coordinates of the Intersections of Link Vectors and Their Common Normal

Assume the link vectors  $l_i = {}^B p_i - b_i$ ,  $l_{i+1} = {}^B p_{i+1} - b_{i+1}$  where  $n_i$  is their common normal. The points  $c_i$  and  $c_{i+1}$  are the intersection points of  $n_i$  with  $l_i$  and  $l_{i+1}$  respectively. As shown in figure A1,  $S_1$  is a plane determined by  $n_i$  and  $l_{i+1}$  and its normal vector  $m_i$  is given by the cross product of  $n_i$  by  $l_{i+1}$  as given as follows:

$$m_i = n_i \times ({}^B p_{i+1} - b_{i+1}) \quad (A.1)$$

Let the plane  $S_2$  be parallel to  $S_1$  and the point  ${}^B p_i$  on plane  $S_2$ . The distance from the point  $b_i$  to  $S_1$ ,  $|d-b_i|$ , and the distance from  $b_i$  to  $S_2$ ,  $|e-b_i|$ , are given by:

$$|(b_{i+1}-b_i) \cdot m_i| \quad (A.2)$$

and

$$|({}^B p_i - b_i) \cdot m_i| \quad (A.3)$$

Since the triangles  $b_i {}^B p_i e$  and  $b_i c_i d$  are similar, the following equation is valid:



$$\frac{\mathbf{c}_i - \mathbf{b}_i}{{}^B\mathbf{p}_i - \mathbf{b}_i} = \frac{(\mathbf{b}_{i+1} - \mathbf{b}_i) \cdot \mathbf{m}_i}{({}^B\mathbf{p}_i - \mathbf{b}_i) \cdot \mathbf{m}_i} \quad (\text{A.4})$$

or

$$\mathbf{c}_i = \frac{(\mathbf{b}_{i+1} - \mathbf{b}_i) \cdot \mathbf{m}_i}{({}^B\mathbf{p}_i - \mathbf{b}_i) \cdot \mathbf{m}_i} ({}^B\mathbf{p}_i - \mathbf{b}_i) + \mathbf{b}_i \quad (\text{A.5})$$

Similarly, the intersection point  $\mathbf{c}_{i+1}$  is given by

$$\mathbf{c}_{i+1} = \frac{(\mathbf{b}_i - \mathbf{b}_{i+1}) \cdot \mathbf{m}_{i+1}}({}^B\mathbf{p}_{i+1} - \mathbf{b}_{i+1}) \cdot \mathbf{m}_{i+1} ({}^B\mathbf{p}_{i+1} - \mathbf{b}_{i+1}) + \mathbf{b}_{i+1} \quad (\text{A.6})$$

Where  $\mathbf{m}_{i+1}$  is given by the cross product of  $\mathbf{n}_{i+1}$  by  $\mathbf{l}_i$  as given as follows:

$$\mathbf{m}_i = \mathbf{n}_{i+1} \times ({}^B\mathbf{p}_i - \mathbf{b}_i) \quad (\text{A.7})$$

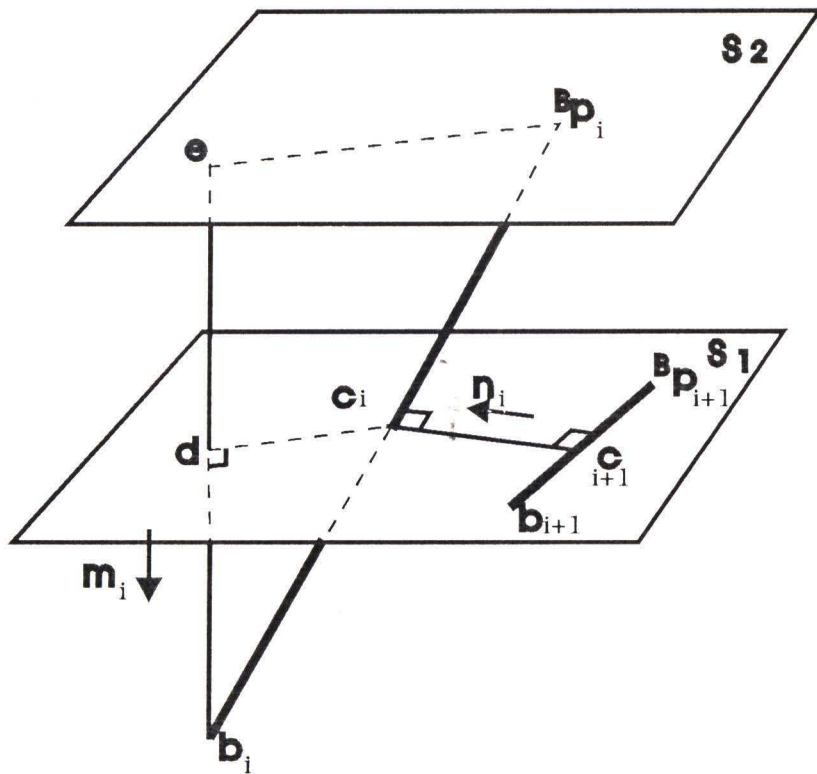


Figure A.1 Intersections of link vectors and their common normal

## APPENDIX B

### Flow Chart of the Program to Compute Workspace Volume And Boundary

The flow chart of the program which computes the workspace volume and boundaries of Stewart platform is shown in Figure B.1 and B.2. Related description can be found in Chapter 2, Section 2.2. A few symbols in the flow chart are explained as follows.

1.  $\Delta R$  - The increment of the radius
2.  $R_{\max}$  - The maximum search radius.
3.  $\Delta\gamma$  - The increment of the polar angle,  $\Delta\gamma = 2^\circ$ .
4.  $S$  - A flag used to indicate the previous point's status. If it is within the workspace,  $S=1$ , otherwise  $S=0$ .
5.  $C$  - The number of the boundary points during a search in a whole plane.
6.  $Z_r$  - A predetermined pose value in Z direction.

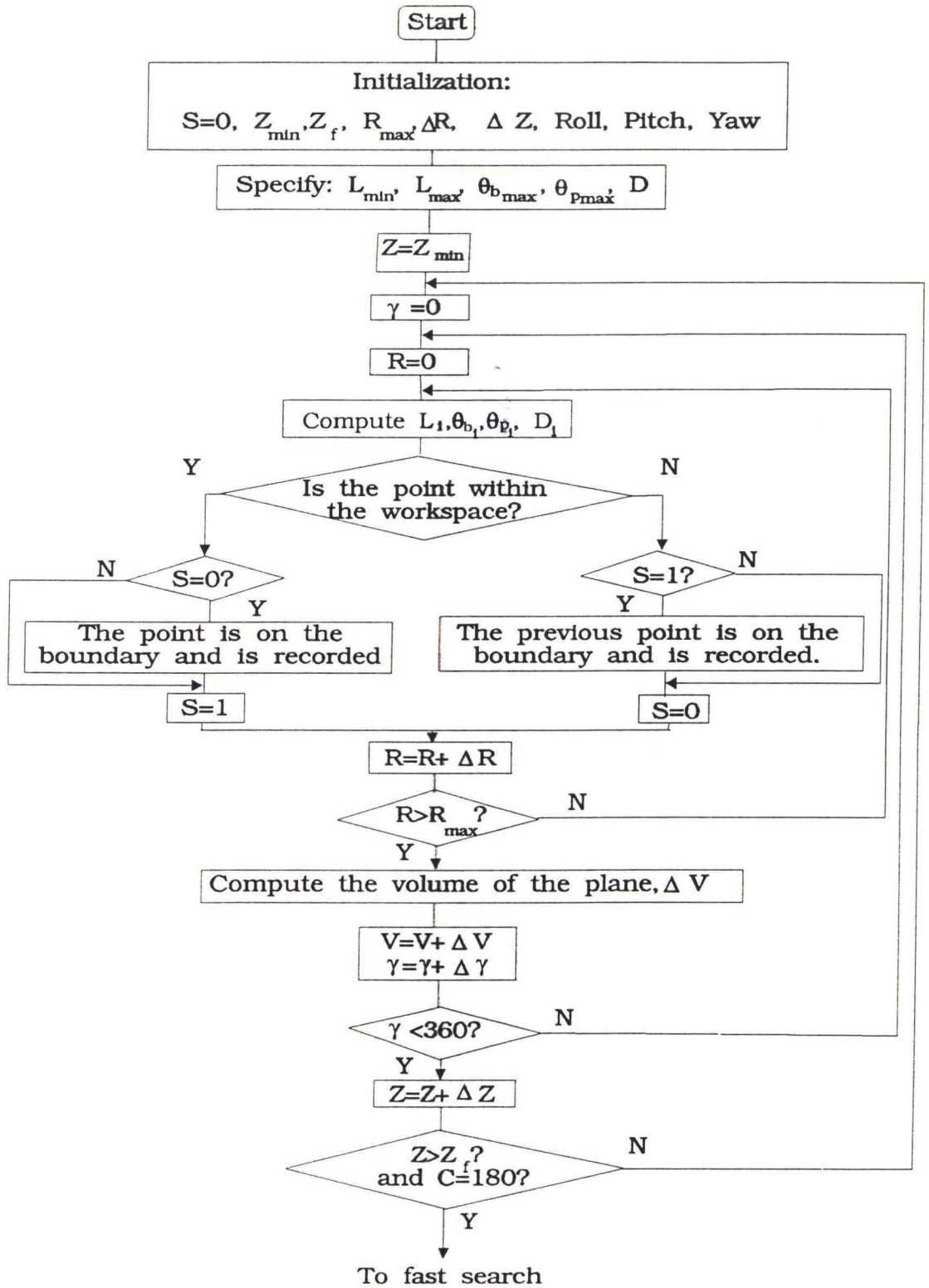


Figure B.1 Flow chart for workspace computation

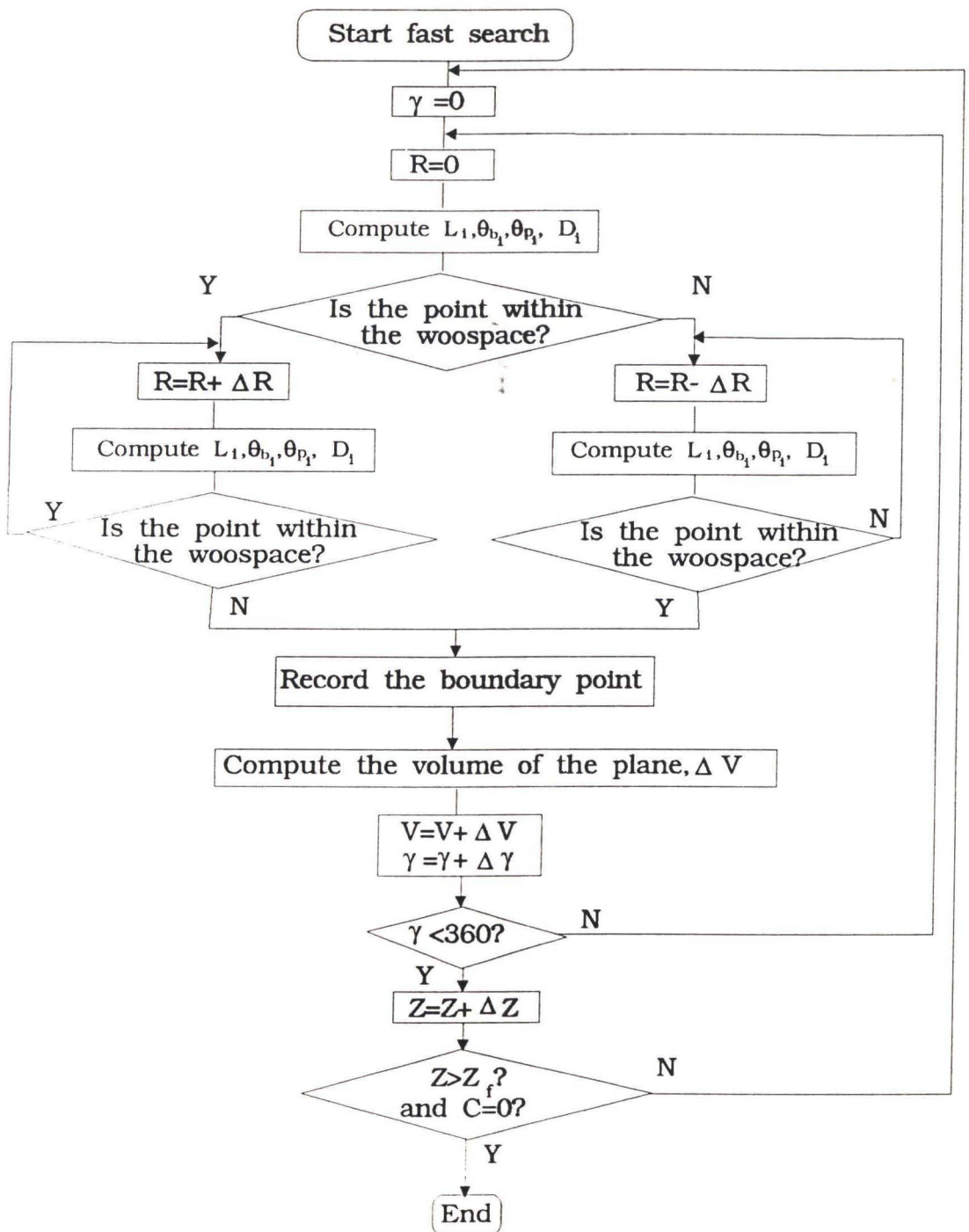


Figure B.2 Flow chart of the fast search algorithm

## APPENDIX C

### Nominal, Actual and Identified Parameters Used in the Simulation Studies

Following table shows the nominal, actual, two set of the identified parameters (corresponding Case 2 and Case 3 in Chapter 5), and the initial and two set of final errors.

Nominal - Nominal parameters (feet).

Actual - Actual parameters (feet).

Iden1 - First set of identified parameters (feet), corresponding to Case 2.

Iden2 - Second set of identified parameters (feet), corresponding to Case 3.

A-N - Difference between actual and nominal parameters (feet).

A-Id1 - Difference between actual and fist set of identified parameters (feet).

A-Id2 - Difference between actual and second set of identified parameters (feet).

Initial - Difference between actual and nominal parameters (inch).

Final1 - Difference between actual and fist set of identified parameters (inch).

Final2 - Difference between actual and second set of identified parameters (inch).

	Nominal[ft]	Actual[ft]	Iden1[ft]	A-N[ft]	A-Id1[ft]	Initial[in]	Final1[in]	Iden2[ft]	A-Id2[ft]	Final2[in]
b1x	2.5980762	2.592455	2.592387	-0.00562	6.85E-05	-0.06745	0.000822	2.592449	6.8E-06	8.16E-05
b1y	1.5	1.490941	1.490312	-0.00906	0.000629	-0.10871	0.007549	1.490878	6.28E-05	0.000754
b1z	0	0.003577	0.005318	0.003577	-0.00174	0.042928	-0.02088	0.003751	-0.00017	-0.00209
b2x	0	0.003586	0.003887	0.003586	-0.0003	0.043031	-0.00361	0.003616	-3E-05	-0.00036
b2y	3	3.008694	3.00941	0.008694	-0.00072	0.104327	-0.00859	3.008766	-7.2E-05	-0.00086
b2z	0	-0.00233	-0.00302	-0.00233	0.000689	-0.02796	0.008268	-0.0024	6.89E-05	0.000827
b3x	-2.598076	-2.59769	-2.59806	0.000388	0.00037	0.00466	0.004444	-2.59773	3.71E-05	0.000445
b3y	1.5	1.506619	1.507137	0.006619	-0.00052	0.079432	-0.00621	1.506671	-5.2E-05	-0.00062
b3z	0	-0.00931	-0.01116	-0.00931	0.001852	-0.1117	0.022222	-0.00949	0.000185	0.002221
b4x	-2.598076	-2.60701	-2.60802	-0.00893	0.001016	-0.10717	0.012192	-2.60711	0.000102	0.001219
b4y	-1.5	-1.49941	-1.50005	0.000594	0.000639	0.007128	0.00767	-1.49947	6.39E-05	0.000767
b4z	0	0.003423	0.001433	0.003423	0.00199	0.041076	0.023885	0.003224	0.000199	0.002387
b5x	0	-0.00985	-0.01012	-0.00985	0.000276	-0.11815	0.003309	-0.00987	2.76E-05	0.000331
b5y	-3	-3.00233	-3.00342	-0.00233	0.001086	-0.02798	0.013038	-3.00244	0.000109	0.001303
b5z	0	-0.00866	-0.00964	-0.00866	0.000976	-0.10396	0.011717	-0.00876	9.75E-05	0.00117
b6x	2.5980762	2.596426	2.596152	-0.00165	0.000274	-0.0198	0.00329	2.596399	2.74E-05	0.000329
b6y	-1.5	-1.49626	-1.49653	0.003735	0.000269	0.044826	0.003228	-1.49629	2.69E-05	0.000323
b6z	0	0.00178	0.003167	0.00178	-0.00139	0.021354	-0.01665	0.001918	-0.00014	-0.00166
p1x	-0.965926	-0.96506	-0.96512	0.000861	5.28E-05	0.010331	0.000634	-0.96507	5.28E-06	6.34E-05
p1y	-0.258819	-0.25813	-0.25716	0.000692	-0.00096	0.008308	-0.01158	-0.25803	-9.6E-05	-0.00116
p1z	0	5.39E-05	-0.00036	5.39E-05	0.000414	0.000646	0.004964	1.24E-05	4.15E-05	0.000497
p2x	0.2588191	0.258003	0.2577	-0.00082	0.000303	-0.00979	0.003641	0.257973	3.03E-05	0.000363
p2y	-0.965926	-0.96562	-0.96583	0.000308	0.000216	0.003694	0.002592	-0.96564	2.16E-05	0.000259
p2z	0	-0.00017	-0.00013	-0.00017	-4.1E-05	-0.00202	-0.00049	-0.00016	-4E-06	-4.8E-05
p3x	0.7071068	0.707509	0.70754	0.000402	-3E-05	0.004829	-0.00036	0.707512	-3.1E-06	-3.7E-05
p3y	-0.707107	-0.70629	-0.7067	0.000821	0.000411	0.009848	0.004935	-0.70633	4.11E-05	0.000493
p3z	0	0.000524	0.001506	0.000524	-0.00098	0.006293	-0.01177	0.000622	-9.8E-05	-0.00118
p4x	0.7071068	0.706632	0.706959	-0.00048	-0.00033	-0.0057	-0.00393	0.706664	-3.3E-05	-0.00039
p4y	0.7071068	0.706202	0.706082	-0.00091	0.00012	-0.01086	0.00144	0.70619	1.2E-05	0.000144
p4z	0	0.000472	0.000405	0.000472	6.75E-05	0.005666	0.00081	0.000465	6.84E-06	8.2E-05
p5x	0.258819	0.258476	0.258798	-0.00034	-0.00032	-0.00412	-0.00387	0.258508	-3.2E-05	-0.00039
p5y	0.9659258	0.966191	0.966527	0.000265	-0.00034	0.003183	-0.00402	0.966225	-3.4E-05	-0.0004
p5z	0	0.000513	0.000472	0.000513	4.08E-05	0.006154	0.000489	0.000509	4.16E-06	5E-05
p6x	-0.965926	-0.96494	-0.96459	0.000982	-0.00035	0.011785	-0.00425	-0.96491	-3.5E-05	-0.00042
p6y	0.2588191	0.25855	0.259305	-0.00027	-0.00076	-0.00323	-0.00907	0.258625	-7.6E-05	-0.00091
p6z	0	-0.00051	-0.00117	-0.00051	0.000664	-0.00607	0.007971	-0.00057	6.65E-05	0.000798
off1	0	-0.00141	-0.00258	-0.00141	0.001176	-0.01689	0.014114	-0.00152	0.000117	0.00141
off2	0	0.001933	0.002621	0.001933	-0.00069	0.023199	-0.00826	0.002002	-6.9E-05	-0.00083
off3	0	-0.00036	0.000488	-0.00036	-0.00085	-0.00438	-0.01023	-0.00028	-8.5E-05	-0.00102
off4	0	-0.00143	0.000754	-0.00143	-0.00219	-0.01719	-0.02625	-0.00121	-0.00022	-0.00262
off5	0	0.00026	0.001472	0.00026	-0.00121	0.003115	-0.01455	0.000381	-0.00012	-0.00145
off6	0	-0.00099	-0.0017	-0.00099	0.000709	-0.0119	0.008502	-0.00106	7.08E-05	0.000849

Table C.1 Nominal, Actual and identified parameters and the errors

## REFERENCES

- [1] Avreil, M., Nonlinear Programming: Analysis and Methods, Prentice-Hall, 1976
- [2] Craig, J. J., Introductions to Robotics: Mechanics and Control, Addison Wesley, 1986
- [3] Dagalakis, N.G., Albus, J.S., Wang, B.L. and Lee, J.D., "Stiffness Study of a Parallel Link Robot Crane for Shipbuilding Applications," Proc. of the 7th Int. Conf. on Offshore Mechanics and Arctic Engineering, Houston, Texas, Feb. 1988, pp. 29-37.
- [4] Denavit, J. and Hartenberg, R. S., "A Kinematic Notation for Lower-Pair Mechanisms Based on Matrices," Transaction of ASME Journal of Applied Mechanics, 22(2): June 1955 , pp. 215-221.
- [5] Durfee, W.K., Idris, H.R. and Dubowsky, S., "Real-time Control of the Vehicle Emulation System," Proceedings of ACC Conference, Boston, MA, pp. 2057-2058, 1991.
- [6] Everett, L. J., Driels, M., and Mooring, B. W., " Kinematic Modelling for Robot Calibration," Proc. of IEEE Int. conf. on Robotics and Automation, 1987, pp. 183-189.
- [7] Fichter, E. F., "A Stewart Platform-Based Manipulator: General Theory and Practical Consideration," Journal of Robotic Research, Summer 1986, pp. 157-182.



- [8] Fichter, E. F., and McDowell, E. D., "A Novel Design of a Robot Arm," ASME Int. Computer Technology Conference, San Francisco, 1980, pp. 250-256.
- [9] Griffis, M., and Duffy, J., "A Forward Displacement Analysis of A Class of Stewart Platform," Journal of Robotic Systems. 1989, pp. 703-720.
- [10] Gill, P. E., Murray, W. and Wright, M. H., Practical Optimization, Academic Press, 1981
- [11] Gosselin, C., "Determination of the Workspace of 6-DOF Parallel Manipulators", ASME Journal of Mechanical Design, Vol. 112, September 1990, pp. 331-336.
- [12] Hayati, S., and Mirmirani, M., "A Software for Robot Geometry Parameter Estimation," Assembly Automation, Vol. 2, No. 4, Nov. 1982
- [13] Hayati, S., and Mirmirani, M., "Puma 600 Robot Arm Geometric Calibration," Proc. of IEEE Intl. Conf. on Robotics, Atlanta, Georgia, March 1984
- [14] Hayati, S., and Mirmirani, M., "Improving the Absolute Position Accuracy of Robot Manipulator," Journal of Robotic Systems, Vol. 2(4), 1985, pp. 397-413.
- [15] Hoffman, R. and Hoffman, M. C., "Vibration Models of an Aircraft Simulation Motion Systems," in Proc. 5th World Congress for the Theory of Machines and Mechanisms, 1979, pp. 603-606.
- [16] Huang, M. Z., "On the Kinematics of Parallel-chain Platform Manipulator," Proc. of The Fourth Annual Conference on Recent Advance in Robotics, Boca Raton, Florida, May 1991, pp. 251-256.
- [17] Huang M. Z., and Gautam A., "An Algorithm for On-Line Compensation of Geometric Errors in Industrial Robots," Proc. 3rd Conf. on Recent Advance in Robotics, May 1989, FAU, Boca Raton, FL. pp. 174-177.

- [18] Huang, M. Z., and Masory O., "A Simple Method for Automatic Identification of Manipulator Kinematic Parameters," ASME Conf. on Design Automation, 1990
- [19] Hunt, K. H., "Structural Kinematic of In-Parallel-Actuated Robot-Arms," ASME Journal of Mechanisms, Transmissions, and Automation in Design, Vol. 105, Dec.1983, pp. 705-711.
- [20] Landsburger, S.E. and Sheridan, T.B., "A New Design For Parallel Link Manipulators," IEEE Proc. System Man and Cybernetics Conf., Tuscon, Arizona, Nov. 1985, pp. 812-814.
- [21] Lee, J. et al, "Computer Simulation of a Parallel Link Manipulator," J. Robotics & Computer Integrated Manufacturing, Vol. 5, No. 4,1989, pp. 333-342.
- [22] Lee, K. M. and Shah, D. K., "Kinematic Analysis of a Three-Degree-of-Freedom In-Parallel Actuated Manipulator", IEEE Journal of Robotics and Automation, Vol. 4, N0. 3, June 1988, pp. 354-360.
- [23] Masory, O. and Wang, J., "Workspace Evaluation of Stewart Platform," Proc. of ASME Conference, Sept. 1992, Scottsdale, Arizona.
- [24] McCallion, H. and Truong, P. D., "The Analysis of a Six Degree of Freedom Work Station for Mechanized Assembly," Proc. 5th World Congress for the Theory of Machines and Mechanisms, 1979, pp. 603-606.
- [25] McCallion, H., Johnson, G. R. and Phan, D.T., "A Compliance Device for Inserting a Peg Into a Hole," The Industrial Robot, June 1979
- [26] Mooring, B. W., "The Effect of Joint Axis Misalignment on Robot Position Accuracy," Proceedings of the 1983 ASME Computers in Engineering Conference, August 1983, pp. 151-155.

- [27] Mooring, B. W. and Tang G. R., : " An Improved Method for Identifying the Kinematic Parameters in a Six Axis Robot," Proc. Intl Comput. in Eng. Conf. Exhibit. August, Las Vegas, Nevada, 1984, pp. 79-84.
- [28] Mooring, B. W., and Padavala, S. S., "The Effect of Kinematic Model Complexity on Manipulator Accuracy," IEEE International Conference on Robotics and Automation, 1989, pp. 593-598.
- [29] Mooring, B. W., Roth, Z. S. and Driels M., The Fundamentals of Robot Calibration, John Wiley & Sons, 1991
- [30] Nanua, P., Waldron, K. J. and Murthy, V., "Direct Kinematic Solution of a Stewart Platform," IEEE Transaction on Robotics and Automation, Vol. 6, No.4, Aug. 1990, pp. 438-443.
- [31] Nguyen, C. C. and Pooran, F.J., "Kinematic Analysis and Workspace Determination of a 6 DOF CKCM Robot End-Effector," Elsevier Science Publishers B.V. 0378-3804/89, 1989, pp. 283-294
- [32] Paul, R. P., Robot manipulators: Mechanics, Programming and Control, Cambridge, Mass., MIT Press, 1981
- [33] Powell, I.L., "The Kinematic Analysis and Simulation of the Parallel Topology Manipulator," Marconi Review, XLV(226):121-138, 3rd quarter 1982.
- [34] Roth, Z. S., Mooring, B. W. and Ravani, B., "An Overview of Robot Calibration," IEEE J. Robotics and Automation, Vol. 3, No.5, Oct. 1987, pp. 377-385.
- [35] Roth, Z. S., "Robot Calibration: The Identification Phase, Lecture Notes on Manipulator Calibration," IEEE intl. Conf. on Robotics and Automation, Philadelphia, PA, April 1988

- [36] Schilling, R. J., Fundamentals of Robotics, Analysis and Control, Prentice Hall, Inc., 1990
- [37] Sheridan, T.B., "Human Supervisory Control of Robot Systems," Proc. Int. Conf. on Robotics and Automation, San Francisco, California, Apr. 1986, pp. 802-812.
- [38] Stewart, D., "A Platform With Six Degree of Freedom," Proceedings of the Institution of Mechanical Engineering, Vol. 180, Part 1, No. 15, 1965-66, pp. 371-386.
- [39] Sugimoto, K., "Kinematics and Dynamics Analysis of Parallel Manipulators by Means of Motor Algebra," ASME J. of Mechanisms, Transmissions, and Automation in Design, Vol. 109, 1987, pp. 3-7.
- [40] Sugimoto, K. and Okata, T., "Compensation of Position Errors Caused by Geometric Deviations in Robot System," Robotics Research: the Second International Symposium, MIT Press, Cambridge, MA, 1985 pp. 231-236.
- [41] Veischegger, W. K. and Wu, C., "Robot Accuracy Analysis," IEEE 1985 proceedings of International Conference on Cybernetics & Society, pp. 425-430.
- [42] Veischegger, W. K. and Wu, C. H., "Robot Calibration and Compensation," IEEE J. Robotics Automation, Vol. 4, No. 6, Dec. 1988, pp. 643-656.
- [43] Vuskovic M. I., "Compensation of Kinematic Errors Using Kinematic Sensitivities," Proc. of th IEEE Intl. Conf. on Robotics and Automation, Arizona, May 1989, pp. 745-750.
- [44] Waldron, K. J. and Hunt, K.H., "Series-Parallel Dualities in Actively Coordinated Mechanisms," 4th Int. Symp. Robotics Research, edited by R.C. Bolles & B. Both, 1987 pp.175-180.

- [45] Wu, C. H., "A Kinematic CAD Tool For the Design and Control of a Robot Manipulator," Int. J. Robotics Research, Vol. 3, No.1, 1984, pp. 58-67.
- [46] Yang, D. C. H. and Lea, T.W., "Feasibility Study of a Platform Type of Robot Manipulators From a Kinematic Viewpoint", ASME Journal of Mechanism, Transmissions, and Automation in Design, Vol. 106, June 1984, pp. 191-198.
- [47] Zhuang, H., Hamano, F. and Roth, Z., " Optimal Design of Robot Accuracy Compensation," Proc. of th IEEE Intl. Conf. on Robotics and Automation, Arizona, May 1989, pp.751-756.
- [48] Zhuang, H. and Roth, Z., "A Method for Kinematic Calibration of Stewart Platforms," ASME Annual Winter Meeting, Atlanta, GA, 1991, pp. 43-48.
- [49] Zhuang, H. and Roth, Z., "A United Approach to Kinematic Modeling, Identification And Compensation for Robot Calibration," Control and Dynamic System, Vol. 39, 1991 by Academic Press Inc., pp. 71-127.

